The design of TACN-based molecular systems for different supramolecular functions

Journal Name

ARTICLE

The design of TACN-based molecular systems for different supramolecular functions

Eleonora Macedi,[a,b] Andrea Bencini,*[a] Claudia Caltagirone*[c] and Vito Lippolis*[c]

Abstract text goes here. The abstract should be a single paragraph that summarises the content of the article

Introduction

The creation of functions at the molecular level is one of the main goal of supramolecular chemistry [1]. In this respect, "coordinatively unsaturated" metal complexes of macrocyclic ligands have proven worthwhile for assembling functional supramolecular compounds with a variety of potential applications in chemistry, biology and medicine: from recognition and sensing of a guest substrate to functional and structural models of biomolecules and diagnostic and therapeutic agents [1-9].

Macrocyclic ligands, in particular polyaza-macrocycles, have been extensively considered as core components of functional supramolecular compounds because they can both be easily functionalised at the secondary N-donors, which is useful for their implementation in supramolecular systems, and they can afford kinetically and thermodynamically stable metal complexes living one or more coordination sites on the metal centre free to be occupied by more weakly bound ligands, which is instrumental to confer the desired function(s) to the final supramolecular platform [1-10].

1,4,7-triazacyclononane (TACN, [9]aneN$_3$) is a 12-membered ring whose basic coordination chemistry with main group and transition metal ions has been widely studied over the last forty years, affording a series of mono- and poly-nuclear complexes with interesting properties in which the macrocyclic moiety serves as a tridentate face-capping group, allowing variation of the donor array at the remaining coordination sites of a coordinated metal ion [10,11]. Furthermore, during the years, versatile synthetic methodologies have also been refined for a sequential symmetric and non-symmetric functionalization of the secondary N-donors of TACN with a plethora of coordinating groups, thus allowing the preparation of a wide array of functionalized TACN derivatives [7,10,12-14].

All this has brought researchers in the last 15 years to use TACN as the key component in the construction of TACN-based supramolecular systems featuring a wide variety of potential practical applications.

In this review, we will highlight the most significant achievements in the TACN-based design of supramolecular systems. A great attention will be devoted to show how the use of TACN is convenient for the purposes of the desired supramolecular functions.

1. Recognition and sensing supramolecular functions.

The great success of TACN in the development of supramolecular systems featuring a great variety of functions, has been determined by its peculiar coordination properties [11] and, most of all, by the presence in the literature of well tested synthetic methodologies which allow symmetric and non-symmetric functionalization of this macrocycle at the three nitrogen atoms to form mono-, di- and tri-substituted TACN derivatives of the form RTACN, R$_2$TACN, R$_3$TACN, but also R^{1}R^{2}TACN, R^{1}R$^2_2$TACN, R^{1}R^{2}R^{3}TACN, with the pendant arms bearing different functional groups [7,10,12-14]. Ligands of this type can confer remarkable stability upon metal centres, adapting to their preferred coordination geometries and

a. Dipartimento di Chimica "Ugo Schiff", Polo Scientifico, Università degli Studi di Firenze, Via della Lastruccia 3, 50019 Sesto Fiorentino, Firenze, Italy

b. Department of Pure and Applied Sciences, University of Urbino, P.zza Rinascimento 6, I-61029 Urbino, Italy.

c. Dipartimento di Scienze Chimiche e Geologiche, Università degli Studi di Cagliari, S.S. 554 Bivio per Sestu, 09042 Monserrato(CA), Italy.

* Corresponding authors E-mail: andrea.bencini@unifi.it, ccaltagirone@unica.it, lippolis@unica.it

oxidation states and allowing the interaction with exogenous species at the coordination site(s) left free by the polydentate assembly. Multi-TACN systems can also be easily assembled to accommodate two or more metal centres in close proximity [7,10,12,13], thus offering good starting models for different supramolecular functions. In this first section, the most significant TACN-based systems featuring selective recognition and sensing properties will be reviewed, dividing them according to the number of TACN units present.

### 1.1 Receptors and sensors featuring one TACN unit.

Metal complexes of mono-TACN systems assembled by mono- or bis-functionalization of the triaza macrocycle with pendant arms of different complexity bearing donor groups, can be very useful to develop chemical sensors, especially for neutral and anionic target species. In fact, the resulting four- and five-coordinated metal complexes, respectively, offer the possibility of binding small molecule at the coordinatively unsaturated metal centre, which can be detected spectroscopically.

One such case is represented by the tetradentate ligand L1, which was initially reported together with L2 as a selective fluorescent chemosensor for Zn^{2+} [15].

Both ligands featuring one and three 2-quinolylmethyl pendant arms, respectively, in fact, are not emissive over the pH range 2.0-12.0 in MeCN/H_2O (1:1 v/v) and H_2O media at 25 °C, due to a photoinduced electron transfer (PET) process from the nitrogen donor atom(s) of the macrocyclic moiety to the excited state of the quinoline fluorogenic fragment(s). A significant chelation enhancement of fluorescence (CHEF) effect (λ_{ex} = 316 nm, λ_{em} = 380 nm) is observed for both ligands in the presence of Zn^{2+} in the pH range 3.0-10.0 (both in MeCN/H_2O (1:1 v/v) and H_2O media) with the maximum effect at about pH 7.0 (MOPS buffer) (a smaller CHEF effect was also observed on adding Cd^{2+} to both ligands, $I_{rel}(Zn^{2+})/I_{rel}(Cd^{2+})$ = 4). This CHEF effect, determined by the formation of the corresponding 1:1 $[ZnL]^{2+}$ complexes (L = L1, L2) featuring the three aliphatic nitrogen donors coordinated to the metal centre, is not observed in the presence of other metal ions such as Cu^{2+}, Hg^{2+} and Pb^{2+} [15]. A similar optical selectivity for Zn^{2+} was observed by Mikata and co-workers for the structural analogue of L2 featuring three 6-methoxy-2-quinolylmethyl pendant arms (λ_{ex} = 341 nm, λ_{em} = 420 nm) [16]. On the other hand, [9]aneN$_3$ functionalized with three 1-isoquinolylmethyl moieties exhibits minimal fluorescence enhancement upon zinc(II) binding [16].

However, the tetradentate L1 can only partially fulfil the coordination sphere of a metal centre such as copper(II), which prefers a penta- or hexa-coordinated environment. Therefore, strong binding of anionic species to the free coordination site(s) of the metal centre would in principle allow a colorimetric detection of the anions even by naked eye. In fact, the complex $[Cu(L1)](BF_4)_2 \cdot MeCN$ (1) can be easily obtained as a blue powder by reacting $Cu(BF_4)_2 \cdot xH_2O$ with L1 in 1:1 molar ratio in MeCN [17]. This complex in MeCN and H_2O shows a broad d–d absorption band at 600 nm (ε = 106 $M^{-1} cm^{-1}$) and 634 nm (ε = 78 $M^{-1} cm^{-1}$), respectively, corresponding to a light blue colour.

Interestingly, in MeCN a colour change can be observed only upon addition of I$^-$ and CN$^-$, while in water only upon addition of CN$^-$. The other anions considered (F$^-$, Cl$^-$, Br$^-$, I$^-$, MeCO$_2^-$, PhCO$_2^-$, $H_2PO_4^-$, HSO$_4^-$, HCO$_3^-$, NO$_3^-$, N$_3^-$, CN$^-$, SCN$^-$ as nBu$_4$N$^+$ or nEt$_4$N$^+$ salts) did not affect the absorption spectrum of $[Cu(L1)]^{2+}$ in the two solvents [17,18].

L1 L2
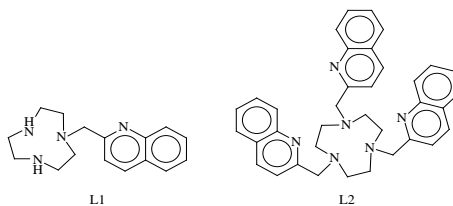
The addition of increasing amounts of I$^-$ to a light blue solution of 1 in MeCN causes a red-shift (about 30 nm) and an increase in the absorbance of the d-d transition of 1; furthermore, a new band is formed at 420 nm with a titration profile showing an inflection point in correspondence of the 1:1 I$^-$/1 molar ratio and a final green colour of the solution (Fig. 1a), from which the green complex [Cu(L1)I]I (2) can be isolated (Fig. 1b). No significant colour changes could be observed upon the addition of I$^-$ to an aqueous solution of 1.

The addition of increasing amounts of CN$^-$ to a light blue solution of 1 in MeCN only produces changes in the d-d absorption band: up to a 1:1 CN$^-$/1 molar ratio a blue-shift of the band and a slight increase in the absorbance is observed; further addition of CN$^-$ causes a more marked blue-shift of the band accompanied by a decrease of the absorbance up to a 2:1 CN$^-$/1 molar ratio, in agreement with the sequential formation of 1:1 and 2:1 CN$^-$/1 complexes (Fig. 2). The solution turns from light to dark blue and then pink. The addition of 1 equiv. of 1 to the pink solution of the 2:1 CN$^-$/1 reversibly restores the dark blue colour of the 1:1 CN$^-$/ $[Cu(L1)]^{2+}$ complex.

The X-ray crystal structure of the compound $[Cu(L1)CN]BF_4 \cdot \frac{1}{2}$ H_2O (3), isolated from a MeCN solution of 1 and n-Bu$_4$NCN, confirms the coordination of the cyanide anion to the metal centre in an overall penta-coordination environment (Fig. 2b). In H_2O, the d–d absorption band of 1 isosbestically blue-shifts from 634 to 575 nm up to the addition of 2 eq. of CN$^-$ and increases in the absorbance suggesting the formation of a 2:1 CN$^-$/$[Cu(L1)]^{2+}$ complex.

Figure 1. a) Titration curve following the absorbance at 420 nm of a MeCN solution of 1 upon addition of I$^-$, and colours of the solution at the beginning and at the end

of the titration; b) crystal structure of the cation complex [Cu(L1)I]+ in **2** showing the metal centre coordinated to the tetradentate L1 and an iodide anion. Figure 1a is reprinted from Ref. [18] with permission from Elsevier. Copyright © 2014.
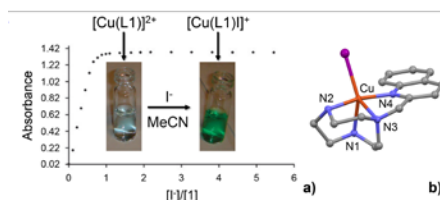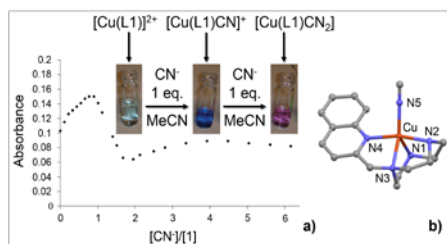

Figure 2. a) Titration curve following the absorbance at 585 nm of a MeCN solution of **1** upon addition of CN⁻, and colours of the solution after the addition of 1 and 2 equivs. of CN⁻; b) crystal structure of the cation complex [Cu(L1)CN]+ in **3** showing the CN⁻ anion coordinated to the metal centre together with the four N-donor atoms from L1. Figure 2a is reprinted from Ref. [18] with permission from Elsevier. Copyright © 2014.

In competitive experiments, both in MeCN and H₂O, in the presence at the same time of 1 or 2 equivs. of all anions considered (including I⁻), the colours observed are those for the formation of the 1:1 and/or 2:1 CN⁻/[Cu(L1)]²⁺ complexes and do not change in time. Therefore, the complex cation [Cu(L1)]²⁺ in **1** in MeCN is able to visually discriminate the presence of either I⁻ (in the absence of CN⁻, Fig. 1) or CN⁻ (also in the presence of I⁻, Fig. 2) among the other anions via different colour changes. Therefore, [Cu(L1)]²⁺ can be considered a ''solvent-based-dual'' sensor, because it is able to selectively sense CN⁻ in two different media, with ''double'' response in MeCN because it can distinguish two different anions (I⁻ and CN⁻) with different colours in this solvent. Adopting the Boolean logic language, it is possible to say that [Cu(L1)]²⁺ performs the logical OR operation if the nature of the sensed anions (I⁻, CN⁻) and the solvents (MeCN, H₂O) are considered as inputs and colour change as output (Fig. 3).

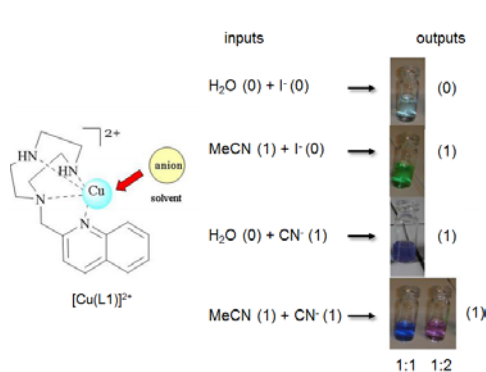Figure 3. Truth table of the OR operation performed by [Cu(L1)]²⁺ on solvents [H₂O (0), MeCN (1)] and anions (I⁻ (0); CN⁻ (1)] inputs. In the case of MeCN as solvent and CN⁻ as anion, two distinct colours can be observed depending on the **1**/CN⁻ molar ratio. Reprinted from Ref. [18] with permission from Elsevier. Copyright © 2014.

As a matter of fact, symmetric and non-symmetric functionalization of [9]ane₃ at the three nitrogen atoms to form tri-substituted TACN derivatives of the form R₃TACN, R¹R²₂TACN and R¹R²R³TACN, has been largely used to develop receptors for the selective sensing of metal cations, inorganic/organic anions and small neutral molecules [7,10,12-14]. The change of the donor groups present in the pendant arms allows to tune the selectivity properties of the resulting chemosensor.

Ligand L3 differs from L2 for the presence in the three pendant arms of a 5-chloro-8-hydroxyquinoline as the fluorogenic unit instead of a quinoline moiety. Analogously to L2, L3 shows a low intensity emission band in MeCN/H₂O 1:1 (v/v) at pH = 7.0 (1 M HEPES buffer) (λ_{ex}= 344 nm, λ_{em}= 500 nm) due to both an intramolecular photoinduced proton transfer (PPT) between the hydroxyl group and the quinoline nitrogen atom and a photoinduced electron transfer (PET) between the nitrogen atom of the macrocycle and the fluorogenic moiety.

Upon addition of increasing amounts of metal ions (Cu²⁺, Zn²⁺, Cd²⁺, Pb²⁺, Al³⁺, Hg²⁺, Co²⁺, Ni²⁺, Mn²⁺, Mg²⁺, K⁺, Ca²⁺, Ag⁺ and Na⁺) a CHEF effect was only observed in the presence of Cd²⁺ (Fig. 4a) and, to a lesser extent, in the presence of Zn²⁺ and Al³⁺ (Fig. 4b) [19].

A fluorescence intensity/molar ratio plot (Fig. 4c) suggested the formation of a 1:1 metal-to-ligand complex. This is also supported by variable pH fluorescence and potentiometric measurements on the system Cd²⁺/L3. Clearly, the chemical species responsible for the CHEF effect is the 1:1 complex [CdH₋₃L3]⁻, containing three deprotonated metal-bound hydroxyl groups (Fig. 4d).

Interestingly, in H₂O, L3 resulted quenched also in the presence of Cd²⁺, but the fluorescence emission in the presence of this metal ion in water could be restored by adding catanionic vesicles of a new formulation based on sodium bis(2-ethylhexyl)

sulfosuccinate, a traditional surfactant, and 1-dodecyl-3-methylimidazolium bromide, an ionic liquid, thus offering the possibility to detect this metal ion also in water. Furthermore, L3 resulted not toxic and able to detect Cd^{2+} in living Cos-7 cells in vitro [19].

When metal ions preferring coordination numbers higher than six are considered, coordinatively unsaturated metal complexes of mono-TACN systems able to bind and possibly sense anions and small neutral molecules can be obtained also with tri-substituted TACN derivatives featuring pendant arms bearing donor groups.
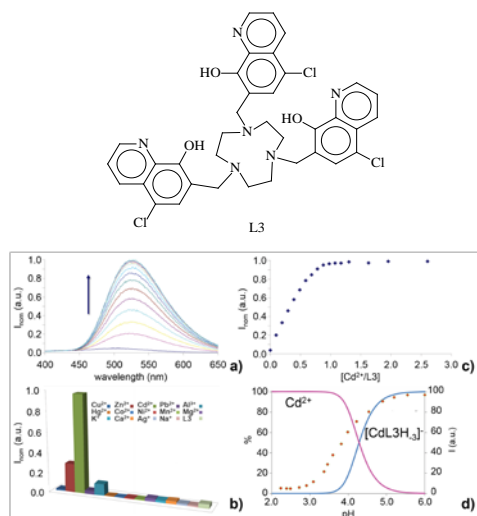

L3

Figure 4. a) Changes in the emission spectrum of L3 upon addition of increasing amounts of Cd^{2+}; b) normalized fluorescence emission of L3 upon addition of 1 equiv. of different metal ions; c) normalized fluorescence intensity/molar ratio plot for L3 upon addition of increasing amounts of Cd^{2+} (MeCN/H$_2$O 1:1 (v/v), pH = 7.0 (HEPES 1M), (λ_{exc} = 344 nm, λ_{em}= 530 nm); d) distribution diagram for the Cd^{2+}/L3 system (MeCN/H$_2$O 1:1 (v/v) in NH$_4$Cl 0.1 M, 25 ^{0}C) superimposed to spectrofluorimetric emission intensities at 530 nm at different pH values. Adapted from Ref. [19] with permission from The Royal Society of Chemistry.

This is the case of neutral lanthanide complexes [LnL4] (Ln = Sm (**4**), Eu (**5**), Lu (**6**)) obtained from the reaction of L4 with [Ln{N(SiHMe$_2$)$_2$}$_3$(THF)$_2$] (Ln = Sm, Lu) and [Eu{N(SiMe$_3$)$_2$}$_3$], respectively [20]. The single crystal X-ray diffraction analysis of **4-6** shows no THF molecules bound to the six-fold coordinated metal centres. The L4^{3-} ligand acts as a hexadentate chelator imposing a facial N$_3$O$_3$ donor set and a distorted trigonal anti-prismatic coordination environment at the metal centres. The metal ions are located below the trigonal plane of the three aryloxide donors with the smaller lutetium being more shielded in **6** than the bigger samarium and europium in **4** and **5**, respectively; therefore, small molecules fitting into the cone-

type ligand arrangements of **4-6** is still to be expected with a reduced redox activation by the lanthanide complexes, as instead observed for analogous uranium(III) complexes [21].

In fact, treatment of **4-6** with CO, CO$_2$ and O$_2$ does not lead to any reaction as contrary to what observed in the case of [UL4] [21]; however, the exposure of **4** and **5** to gaseous SO$_2$ at room temperature in THF results in an immediate colour change from almost colourless (**4**) or yellow (**5**) to red-orange (Fig. 5). This behaviour was demonstrated, also by X-Ray diffraction analyses, to be determined by the formation of the SO$_2$-bridged complexes [(LnL4)$_2$(μ,η^1, η^1-SO$_2$)] (Ln = Sm (**7**), Ln = Eu (**8**), Fig. 5) showing an absorption band at 408 nm (**7**) and 398 nm (**8**) in the UV/Vis spectra of THF solutions.
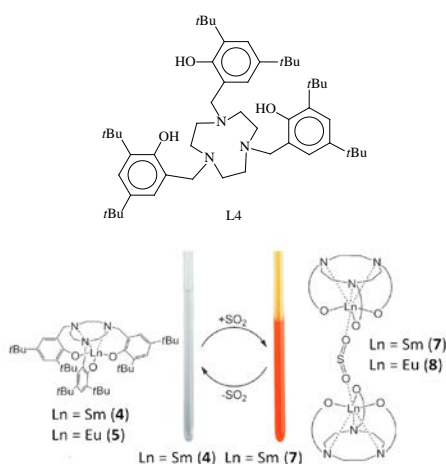

L4

Figure 5. Reversible formation of [(LnL4)2(μ,η1, η1-SO2)] (Ln = Sm (**7**), Ln = Eu (**8**)) complexes by reaction of [LnL4] (Ln = Sm (**4**), Ln = Eu (**5**), respectively) with SO2 in THF, with colour change in the case of **4**. Adapted from Ref. [20] with permission from John Wiley and Sons. Copyright © 2012.

The lutetium complex **6** does not give any reaction with SO$_2$, presumably because the small Lu^{3+} in the complex is sterically too encumbered to provide a suitable coordination site for SO$_2$. The formation of complexes **7** and **8**, which are the first lanthanide complexes coordinated to SO$_2$, is also reversible as SO$_2$ is released slowly at room temperature to afford the starting complexes **4** and **5**, respectively.

[9]aneN$_3$ based tris-aryloxide ligands have also been used to construct luminescent oxygen sensitive lanthanide complexes [22-25]. In particular, L5 has proved to be an effective sensitizer of the f-f emission of Tb^{3+} and Dy^{3+} lanthanide cations in complexes [TbL5(THF)] (**9**) and [DyL5(THF)] (**10**), respectively, under N$_2$ [23,25]. In both complexes, the coordination polyhedron of the seven-coordinated lanthanide cations can be described as a monocapped octahedron in which the oxygen atom of the coordinated THF caps the triangular face formed by the three aryloxide donors of the L5^{3-} ligand. The asymmetric

environment of the lanthanide(III) ions promotes a f-f transition and, therefore, provides high quantum yields for complexes **9** and **10** under N_2.

As regards **9**, the luminescent spectrum in THF, under N_2 (λ_{ex} = 300 nm), shows the typical seven bands due to the $^5D_4 \rightarrow {}^7F_J$ transitions [J = 6 (490), 5 (547), 4 (588), 3 (622), 2 (653), 1 (673) and 0 (679 nm)] with an efficient intramolecular energy transfer from the phenolate moieties to the Tb^{3+} ion. The quite high luminescent quantum yield, Φ, was determined to be 0.91 (quinine bisulfate in 0.5 M H_2SO_4 as reference) with an emission lifetime, τ, of 840 μs, under N_2 in THF. The luminescence of **9** is reversibly quenched by oxygen (Φ = 0.054, τ = 40 μs with a Stern-Volmer quenching constant, K_{SV}, of 8300 M^{-1}) and no degradation of the complex is observed for at least 10 cycles of alternating changes in the oxygen concentration (under air (21%)) and N_2 (0%) (Fig. 6) [23].

L5
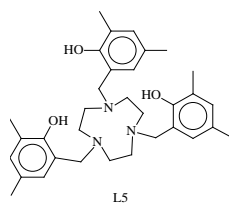
A similar behaviour is observed for **10**, which shows in THF under N_2 (λ_{ex} = 300 nm) the typical four bands luminescence spectrum determined by the $^4F_{9/2} \rightarrow {}^6H_J$ f-f transitions (J = 15/2, 13/2, 11/2, 9/2) of the Dy^{3+} ion (Φ = 0.050, τ = 17.7 μs). Also the luminescence intensity of **10** is oxygen sensitive (Φ = 0.011, τ = 4.1 μs, K_{SV} 305 M^{-1}) and reversibly responds to alternating O_2 and N_2 exposures [25]. Interestingly, a luminescent colorimetric oxygen sensor has been developed by embedding **9** and its analogous Sm^{3+} complex [SmL5(THF)] (**11**) in polystyrene film (PS). The latter shows four bands in the luminescence spectrum in THF under N_2 corresponding to the $^4G_{5/2} \rightarrow {}^6H_J$ [J = 5/2 (566), 7/2 (606), 9/2 (647) and 11/2 (716 nm), respectively] transitions of the Sm^{3+} ion and is oxygen insensitive (Φ = 0.010, τ = 12.2 μs) [26]. The relative luminescence intensities of each band in the spectra of **9** and **11** embedded in PS under N_2 are similar to those found in THF in the same conditions, including the behaviour to cycles of alternating N_2 and O_2 exposures. The system consisting of both **9** and **11** together in polystyrene film shows a very interesting reversible luminescent green-yellow-red response under N_2-air-O_2 exposures, respectively (Fig. 7) [26], with a ratiometric response for the I_{547}/I_{647} luminescence intensities ratio (R) and a non-linear Stern-Volmer plot (R_0/R vs. $[O_2]$) in the O_2 concentration range of 0 to 100%.

Recently, Parker and coworkers have reported a series of highly emitting Eu^{3+} complexes featuring TACN as the core ligand structure. In particular, coordinatively unsaturated complexes based on heptadentate ligands featuring pyridyl-alkynylaryl groups as emission sensitizers, have been prepared and proved to reversibly bind and selectively sense anions such as carboxylates, bicarbonate, lactate and citrate in aqueous media [27].

These complexes show emission spectra particularly sensitive to the coordination environment of the Eu^{3+} centre. In particular, the electric-dipole allowed transitions (ΔJ = 2 and ΔJ = 4, ca. 615 and 700 nm, respectively) are hypersensitive to ligand as contrary to the magnetic-dipole allowed transition (ΔJ = 1, ca. 590 nm) that is normally independent of the ligand environment.
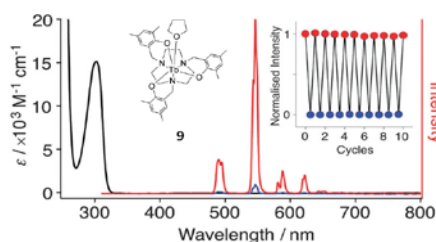

Figure 6. Uv-Vis absorption (black) and corrected luminescence spectra of **9** under N_2 (red) and air (blue) in THF at room temperature (λ_{ex} = 300 nm). The inset shows the reversible responses of the luminescence intensity of **9** (2.0×10^{-6} M, λ_{em} = 547 nm) to alternating air and N_2 exposures. Adapted from Ref. [23] with permission from The Royal Society of Chemistry.

In solution, the coordinated water molecule can be displaced by a range of added anions leading to emission intensity increases and a change in the spectral fingerprint of the Eu^{3+} complexes [27].

Interestingly, the ditopic, coordinatively unsaturated Eu^{3+} complex **12** bearing an alkyliminodiacetate group in the ligand L6, can be used for the selective ion pair recognition of zinc(II) and citrate anions in water by ratiometric luminescence signalling [28].

The emission and excitation spectral features and lifetime of complex **12** do not vary on changing the pH in the range from 4.5 to 7.5 and do not change in the presence of added anions (1000-fold excess) such as bicarbonate, citrate, lactate, acetate and phosphate in water at pH 7.4 (295 K). This is in contrast with the properties of the mono-*N*-methyl complex [EuL6^a]$^{3+}$ (**13**) (L6^a is the analogue of L6 but featuring a methyl group instead of the alkyliminodiacetate group) for which anion addition was found to lead to major changes in emission lifetime and emission band intensities [28].

Addition of $ZnCl_2$ (10 μM to 10 mM) to **12** also does not lead to any significant change in emission or excitation intensity nor in spectral form. However, the emission spectral profile of **12** changes on adding oxy-anions in the presence of $ZnCl_2$ (beyond a threshold concentration, 0.3 mM for citrate and an order of magnitude higher for lactate/acetate), notably in the hypersensitive ΔJ = 2 and ΔJ = 4 transitions around 615–625 nm and 680–700 nm, respectively (Fig. 8).

The strongest binding is observed for zinc and citrate (log K = 3.9, pH 7.4) with a selectivity following the order citrate > lactate/acetate/bicarbonate and nearly identical variations in the europium(III) complex emission spectra. Presumably, the 1:1 complex formed between 12 and Zn^{2+}, with the divalent

metal ion bound to the iminodiacetate moiety, allows the oxo-anions binding to the Eu^{3+} centre in a common coordination mode and the consequent modulation of the emission spectrum.
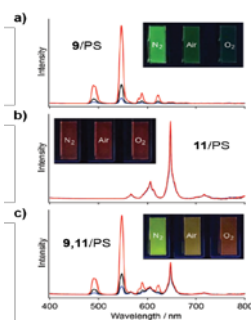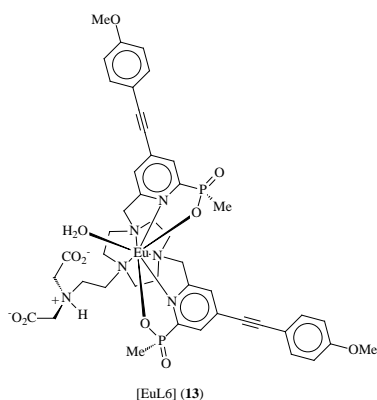

Figure 7. Luminescence spectra [under N_2 (red), air (black) and O_2 (blue), λ_{ex} = 300 nm] of (a) **9**/PS, (b) **11**/PS and (c) **9,11**/PS. Insets: luminescent colour of the sensor slides (20.0 × 7.0 mm) under N_2, air and O_2. Adapted from Ref. [26] with permission from The Royal Society of Chemistry.

[EuL6] (**13**)

A racemic mixture of Eu^{3+} complexes such as 12 can exhibit a net Circularly Polarized Luminescence (CPL) signal when chiral anions bind the metal centre to afford diastereoisomeric complexes of different relative stability. The intensity of the induced CPL signal would depend on the binding selectivity and conformational rigidity of the diastereoisomeric complexes, on the emission timescale.

In this respect, Parker and co-workers prepared the dicationic complex 14 as a probe for *O*-phosphono-aminoacids and related hexapeptides *via* a selective emission and CPL signalling [29]. In 14, the steric demand at the Eu^{3+} centre created by the *N*-benzyl moiety of the ligand L7, supported by the absence of metal coordinated solvent in water or methanol solution, would disfavour the chelation of anions with a small bite angle (carbonate and simple carboxylate); at the same time, the

ammonium group at the *meta*-position of the *N*-benzyl moiety would electrostatically aid metal coordination of a phosphate group and stabilize the interaction *via* hydrogen bonding. Indeed, the complex cation 14 does not show any change in the spectral form in aqueous methanol following the addition of hydrogencarbonate, while exhibits a significant emission modulation and a binding constant of 4.2 (log K) with added hydrogenphosphate [29].
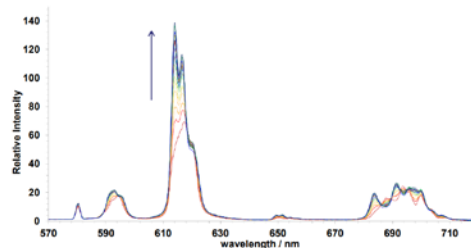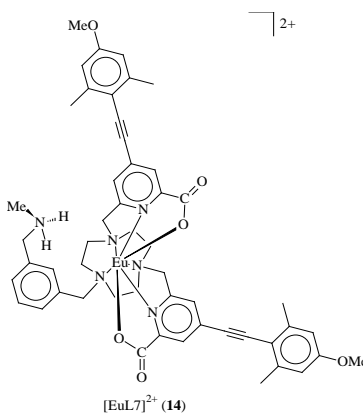

Figure 8. Changes in the emission spectrum of **12** (5 μM) as a function of added citrate in the presence of $ZnCl_2$ (10 mM; λ_{exc} = 332 nm, H_2O, pH 7.4). Reproduced from Ref. [28] with permission from The Royal Society of Chemistry.

[EuL7]$^{2+}$ (**14**)

A spectral form of the total emission spectrum similar to the case of inorganic phosphate was observed following the addition of phosphorylated Serine (Ser), Thyrosine (Tyr) and Threonine (Thr) (stability constant for binding each O-P-aminoacid was evaluated to be log K = 4.80) to a H_2O/MeOH (1:1 v/v) solution of 14 at pH 7.4 (HEPES buffer, 10 mM, λ_{exc} = 352 nm): major changes were observed in the hypersensitive ΔJ = 4 transitions and in the ΔJ = 1 manifold. Interestingly, a strong induced CPL signal was observed upon addition of O-P-Ser or O-P-Thr, with an emission dissymmetry value bigger for the latter [g_{em} (592.5 nm) = + 0.08]. No induced CPL signal could be recorded for the [14·O-P-Tyr] adduct probably because of a more remote position of the chiral centre in the O-P-Tyr

molecule with respect to the phosphate coordinating group [29].

Interestingly, an induced selective CPL response of 14 was recorded following the addition in MeOH of the hexapeptide Gly-Ala-Pro-O-P-Tyr-Lys-Phe (GAPY*KF), with a very high dissymmetry value [g_{em} (592.5 nm) = + 0.10] and opposite both in sign and form to that recorded for the peptide Gly-O-P-Ser-Pro-Phe-Lys-Phe (GS*PFKF) [g_{em} (592.5 nm) = - 0.04].

This underlines the importance of the chiral structure and the rigidity of the entire peptide bound to the lanthanide centre in determining the CPL response. An induced CPL signal of 14 similar to that observed with O-P-Ser or O-P-Thr and the phosphorylated hexapeptides (little activity observed in the ΔJ = 3 and ΔJ = 4 regions and a significant modulation in the ΔJ = 1 region) was recorded in MeOH [g_{em} (592.5 nm) = + 0.04] in the presence of oleoyl-L-α-lysophosphatidic acid (LPA) which significantly increases its levels (from 0.1-6.3 μM up to 40 μM) in ovarian cancer cells. The reached lower and upper limits of detection of LPA using 14 as a probe were 5 and 40 μM, respectively, thanks to a quite high stability constant of the formed adduct in MeOH (log K = 5.25). No induced CPL signal was recorded with other phospholipid species [29].

An interesting use of lanthanide complexes of TACN derivatives as chemosensors for metal cations has been reported by Platas-Iglesias, Tripier and co-workers [30]. They have synthesized the two heteroditopic ligands H_3L8 and H_3L9 featuring a DO3A unit ($H3DO3A$ = 1,4,7,10-tetraazacyclododecane-1,4,7-triacetic acid) linked to a TACN moiety by a 2,6-dimethylpyridine spacer. Eu^{3+} and Gd^{3+} form 1:1 complexes with the deprotonated form of both ligands following reaction in water and using NaOH as a base. In the complexes [Ln(L)] (15-18) (Ln = Eu^{3+}, Gd^{3+}; L = $L8^{3-}$, $L9^{3-}$), the Ln^{3+} ions are eight-coordinated by the ligands through the seven donor atoms of the DO3A unit and the N atom of the pyridyl linker with the absence of inner-sphere water molecules. Addition of Zn^{2+} causes significant changes in the electronic spectra of the complexes indicating the formation of both 1:1 and 2:1 [Ln(L)]/Zn^{2+} species without changes in the coordination sphere of the Ln^{3+} ions. In 1:1 complexes, the Zn^{2+} ion is coordinated within the TACN compartment with the twisted-square antiprismatic (TSAP) isomer of the cyclen ring prevailing in solution in the case of $L9^{3-}$ (see Fig. 9a). Interestingly, the Gd^{3+} complexes [GdZn(L9)]$^{2+}$ (19) shows a very weak emission band at 325 nm (λ_{exc} = 244 nm) due to a Photoinduced Electron Transfer (PET) process from the amine nitrogen atoms of the TACN moiety.

An enhancement of the fluorescence emission is observed in the presence of Zn^{2+} as a consequence of the coordination of this metal ion by the nitrogen atoms of the TACN moiety (Fig.s 9b and 9c). This "turn-ON" behaviour is not observed in the presence of other metal ions such as Ca^{2+}, Mg^{2+} and Cu^{2+} (Fig. 9d).

The idea of using metal complexes of TACN derivatives as optical chemosensors of either metal cations or anions has been elegantly used by Geng, Wang and co-workers. They have synthesized the neutral 2:1 ligand-to-metal copper(II) complex 20 featuring the ligand L10 in which a TACN moiety is functionalized with a BODIPY-based pendant arm [31].

The uncoordinated ligand is strongly emissive at 512 nm (λ_{exc} = 470 nm) with a quantum yield (Φ) of 0.316 in Tris-HCl buffer at pH 7.4. On the contrary, complex 20 is weakly emissive (Φ = 0.041) due to the quenching effect of the paramagnetic Cu^{2+} ion.
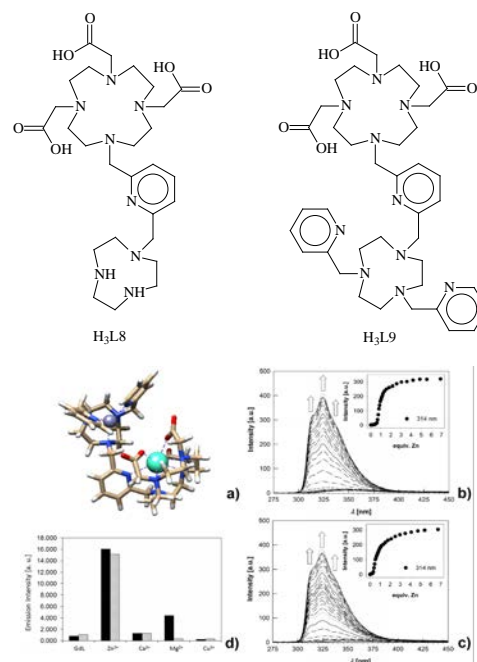

H₃L8   H₃L9

Figure 9. a) Optimized geometry of [GdZn(L9)]$^{2+}$ (19) at DFT level with the cyclen ring in the TSAP conformation; emission spectra of b) [Gd(L8)] (17) and c) [Gd(L9)] (18) (λ_{exc} = 244 nm) during the course of the titrations with Zn^{2+} in H_2O at pH 7.4 (insets show the emission intensity at 314 nm upon substrate addition); d) luminescence emission intensity of [Gd(L)] (17, 18) (L = $L8^{3-}$, black bars; L = $L9^{3-}$, grey bars) in the presence of an excess amount of different cations (7 equivs.) at pH 7.4. Reprinted from Ref. [30] with permission from John Wiley and Sons. Copyright © 2014.

Complex 20 was designed as turn-ON fluorescent chemosensor for biothiols such as Cysteine (Cys), Homocysteine (Hcy) and Glutathione (GSH), with the idea that these biomolecules would reduce the copper(II) centre to Cu^+, thus causing a recovery of the fluorescence emission.

Based on this strategy, the fluorescence response of 20 towards Cys, Hcy, GSH and various aminoacids, such as His, Glu, Arg, Lys, Glu, Thr, Tyr, Trp, Phe, Asp, Met and Ile was tested in Tris-HCl at pH = 7.4. A selective enhancement of the fluorescence emission intensity was only recorded in the presence of Hcy even in competitive conditions. This selectivity has been attributed to the ability of Hcy to form a kinetically stable complex with the

reduced form of 20 by imposing a six-membered chelate ring on the Cu$^+$ centre sandwiched by two L10 units, which can resist the oxidation of the molecular oxygen compared with the analogous complex with Csy featuring a five- membered chelate ring. Complex 20 has been applied for the determination of Hcy in human serum with a detection limit of 241.4 nM and for monitoring the activity of cystathionine β-synthase in vitro [31].


[Cu(L10)$_2$(Cl)$_2$] (**20**)
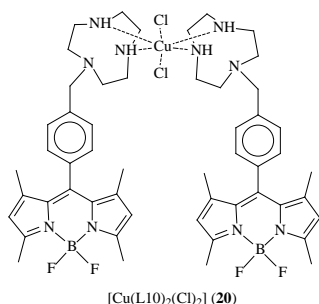
In the area of supramolecular host-guest chemistry, the design and development of the calix[6]aza-cryptand L11 is particularly interesting [32,33].

This funnel-shaped aza-ligand is formed through the introduction of three pyridine arms as spacers onto the small rim of a calix[6]arene, which assumes a cone conformation, and subsequently capping with a TACN unit. The TACN cap and the pyridine spacers provide an N$_6$-coordination core pre-organized by the covalent linkage to the calix small rim for a strong hemidirected coordination to Pb^{2+}. Indeed, Pb^{2+} is strongly bound to the N$_6$-core of L11, being resistant to heating in acidic and coordinating media. In the two structurally characterized complex cations [Pb(L11)H$_2$O]$^{2+}$ (21) and [Pb(L11)EtOH]$^{2+}$ (22) (Fig. 10) the three pyridine N-donors and the Pb^{2+} ion lie in one plane and the angles between them are close to 120°, leaving a gap in the coordination sphere opposite to the TACN moiety where either a water or an ethanol guest is placed. The Pb-N bond distances and the Pb···O interactions are indicative of an hemidirected geometry at the metal centre and the presence of a stereochemically active lone pair directed towards the cavity of the calix[6]arene moiety [33].

Solution studies confirm the host-guest behaviour of the [Pb(L11)]$^{2+}$ complex (23), with neutral guest molecules such as H$_2$O, EtOH and N-Me-formamide embedded in the cavity formed between the coordinated metal centre and the calix small rim and assuming positions that optimize stabilizing interactions with the aromatic walls [33].

The idea of tailor-made receptors for a selective metal cation coordination following a dimensional discrimination has been nicely applied by P. Beer and co-workers in the design of the bis-TACN N$_9$-azacryptand L12 [34]. This "Beer can" shaped ligand features two TACN units bridged by three pyridyl side arms; the nine N-donor groups are oriented towards the centre of the cage-like structure and are, therefore, pre-disposed for an in-cavity synergic metal complexation. The highly pre-organized

ligand can undergo slight conformational distortions in order to accommodate the cations Li$^+$, Na$^+$, K$^+$, Pb^{2+}; however, binding competition experiments revealed that L12 exclusively binds sodium and lead in the presence of potassium, zinc and calcium cations in methanol solution [34].
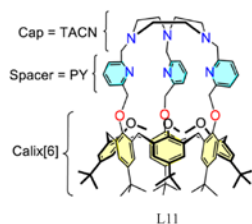
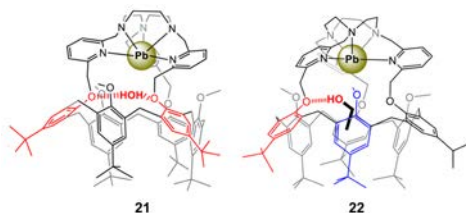Adapted with permission from Ref. [33]. Copyright © 2013, American Chemical Society.

Figure 10. XRD structures of [Pb(L11)H$_2$O]$^{2+}$ (21) and [Pb(L11)EtOH]$^{2+}$ (22). The coloured phenoxyl units are those involved in H- (red) and CH-π (blue) bonding with the exogenous guest (H$_2$O and EtOH). Adapted with permission from Ref. [33]. Copyright © 2013, American Chemical Society.

In the quest of enzyme-like artificial cavities, the cholesterol-armed TACN L13 has been synthesized to prove the possibility of a selective host-guest molecular interaction and recognition by mechanical adaptation in a dynamic media of the host conformation [35]. A Langmuir monolayer of L13 at the air-water interface has been subjected to mechanical structural modification by compression in the presence of Li$^+$ [the complexation at the TACN core reduces the collapse surface pressure (π) of the condensed phase of L13 keeping unchanged the limiting molecular area (A)] in the water phase. π/A isotherms are shifted to larger areas on increasing the guest concentration in the water subphase.

The shifts in molecular areas at various guest concentrations can be then converted into the binding constants of the guest to the monolayer of L13 at each surface pressure. In this way the authors have been able to differentiate the ribonucleosides uridine (U) and thymine (T), both of which possess identical H-bonding sites and a single methyl group difference in their structure [35].

Both increments in the molecular areas of L13 on changing the surface pressure on the Langmuir monolayer and the calculated binding constants clearly depend on the type of nucleoside in the water subphase in the absence and in the presence of LiCl

(Fig. 11) with a clear binding preference of U over T and ribonucleoside adenosine (A). Presumably, the hydrophobic methyl groups of T units are oriented in the air-phase and inserted between molecules of L13, thus reducing the strength of the host-guest interaction and disrupting the Langmuir layer of molecules of L13 [35].

The same L13 system and the same host-guest discrimination concepts based on the mechanical tuning of the host at a dynamic interfacial medium have been also used to selectively recognize ribonucletides monophospates [36].

L12

L13
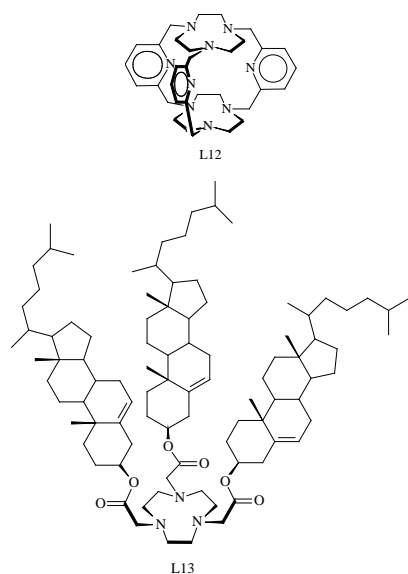
1.2 Receptors and sensors featuring two/three TACN units.

In the nineties, a variety of ligands containing two or more TACN units separated by different spacers, such as aliphatic chains or aromatic units, have been prepared and their coordination properties towards metal cations investigated [7,10,12,13]. More recently, a family of bis-TACN featuring heteroaromatic spacers and their metal complexes have been proposed for the selective recognition and sensing of anions.
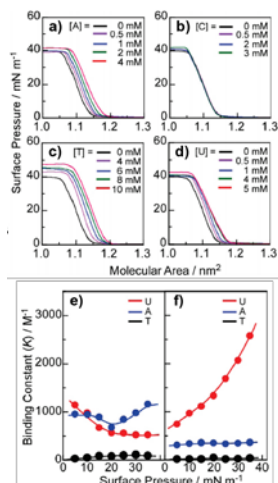

Figure 11. a-d) π/A isotherms (20 °C) of L13 with LiCl (10 mM) in the presence of adenosine, A (a), cytidine, C (b), 5-methyluridine (thymine analogue), T (c); uridine, U (d); e, f) Binding constants of U, A, and T to L13 at various surface pressures at 20 °C without LiCl (e) and with LiCl (10 mM) (f). Adapted with permission from Ref. [35]. Copyright © 2010, American Chemical Society.

For example, ligands L14-L16 were designed following the idea of a rational incorporation of different binding sites for multiple non-covalent interactions with the anion guest, within clefts or cavities geometrically configured to fit the stereochemical requirements and size of the anionic group to achieve the best possible host-guest "complementarity" in aqueous media under specific pH conditions.

In fact, L14-L16 can easily give charged polyammonium cations in aqueous solutions; at the same time, the two TACN units face each other at a distance that depends on the heteroaromatic spacer and on their degree of protonation, thus creating pseudocavities where the anion guests can fit, according also to their dimensions.

The binding selectivity towards halogenide anions observed for L14 and L15 clearly confirms the fundamental idea that the strength of a host-guest interaction following a three-dimensional inclusion of the guest within the intramolecular cleft of a hollow receptor molecule, depends on the geometrical size/cavity fitting and binding complementarity of the two partners.

The stability constants determined potentiometrically for the formation of 1:1 complexes between different protonated species of L14 and L15 with halogenide anions show that L15 interacts only with Cl⁻, while in the case of L14 an interaction with all halogenide anions is observed, with a marked high affinity for Br⁻ over F⁻, Cl⁻ and I⁻. In both cases, the host-guest

interaction requires, to be observed, that both ligands are at least diprotonated [37].

A plot of the overall percentages of the complexed anions ($\Sigma(H_xL14A)^{x-1}$; A = F⁻, Cl⁻, Br⁻ or I⁻) *vs.* pH for a competitive system containing L14 and the four different halogenide anions in equimolecular ratio (Fig. 12) clearly points out that bromide is selectively complexed over a wide pH range (a bromide percentage greater than 80% is complexed for pH < 8) and only minor amounts (less than 7%) of the F⁻, Cl⁻ or I⁻ complexes are formed.

Considering that L14 contains a larger cavity than L15, selective complexation of Cl⁻ by L15 and of Br⁻ by L14 represents a clear case of dimensional recognition of spherical anions.

The different distances between the two TACN units, determined by the rigid spacers, is also at the base of the observed selectivity in inorganic phosphate anion recognition by L14-L16 in H₂O.
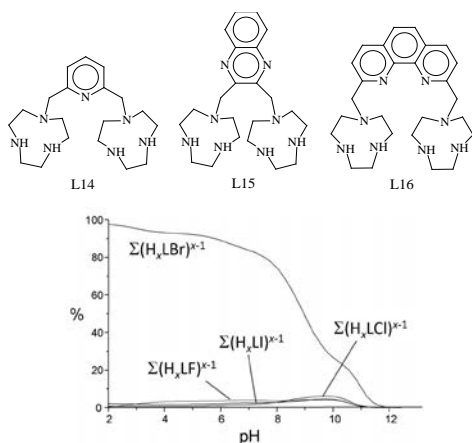

L14   L15   L16

Figure 12. Plots of the overall percentages of the L14 complexes with halogenide anions on changing the pH ($\Sigma(H_xLA)^{x-1}$; A = F⁻, Cl⁻, Br⁻ or I⁻; L = L14) in a competitive system containing L14 and halogenide anions in equimolecular ratio (10⁻³ M). Adapted from Ref. [37] with permission from The Royal Society of Chemistry.

The binding process has been studied by potentiometric, ¹H- and ³¹P-NMR measurements and modelling calculations; it is essentially driven by charge-charge and H-bonding interactions and depends almost exclusively on the spatial arrangement of the ammonium groups [38]. In fact, in L15 the two macrocyclic units are at a short distance from one another, generating a cleft where only a monophosphate can be conveniently hosted (Fig.s 13a-d). In the case of L16, the two TACN units, separated by the larger phenanthroline moiety, simultaneously act as a chelating anion unit for the longer phosphate chain of triphosphate to form a tight "chelate" complex. This structural arrangement is partially lost in the case of diphosphate, while the smaller monophosphate anion can interact with only a single TACN unit and, actually, it is not bound by this receptor in aqueous

solution (Fig.s 13). For L14, the selectivity is less pronounced, but a clear preference for diphosphate anions is evident for pH values higher than 5 [38].

A similar behaviour has been observed for compound L17, which features a 2,2'-methylene-*bis*-cresol moiety as spacer unit connecting two TACN moieties [39].
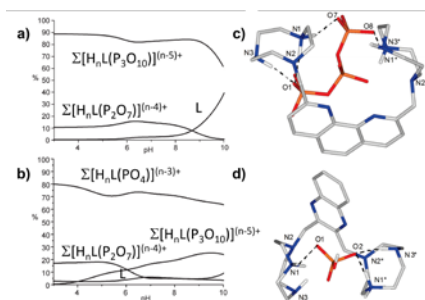

Figure 13. Plots of the overall percentages of the L16 (a) and L15 (b) complexed species with inorganic phosphate anions on changing the pH (L = L15, L16) in a competitive system containing the ligand and anions in equimolecular ratio (10⁻³ M); c) lowest-energy conformer of the adducts between (H₂L16)²⁺ and (P₃O₁₀)⁵⁻; d) lowest-energy conformer of the adducts between (H2L15)²⁺ and (HPO4)²⁻. Adapted with permission from Ref. [38]. Copyright © 2011, American Chemical Society.

L17
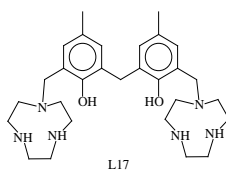
The heteroaromatic moieties in L14-L16 could play an "active" role in the binding process thanks to their ability to give π-stacking interactions with aromatic fragments. In fact, both L15 and L16 can bind ATP or ADP nucleobases via the simultaneous interaction of both TACN units with the anionic phosphate chain of these substrates. However, differently from inorganic phosphate binding, the recognition properties toward nucleotides displayed by L15 and L16 are mainly determined by the ability of the spacer to form π-stacked assemblies with adenine moiety. As a consequence, L16, which contains the most extended heteroaromatic unit, is a better nucleotide binder than L15, with a preference for ATP over ADP and inorganic triphosphate [38].

Both TACN units act cooperatively in the binding process of the phosphate anion, thanks to the clamp-like conformation assumed by the receptor. The most stable complexes are unusually formed at alkaline pH values in the range 8-10, where the receptor assumes a zwitterionic form, but contains up to four charged ammonium groups as potential binding sites for the anionic phosphate chains. The stability of the adducts

increases in the order diphosphate < triphosphate < ATP [39]. In the case of ATP, weak forces (edge to face π-stacking, C-H$\cdots\pi$ and N-H$\cdots\pi$ interactions) are also at work leading to a higher stability of the corresponding complexes with L17 [39].

Inorganic phosphate binding by bis-TACN derivatives can also be performed by their corresponding metal complexes and, depending on the nature of the spacer between the two macrocyclic units, the supramolecular system can also work as a selective optical chemosensor of the considered anions.

Potentiometric, ^{1}H-NMR and UV-Vis studies have demonstrated that L18 possesses a very low binding ability towards inorganic phosphate anions in water because in this solvent it assumes a *trans-trans* conformation which sets the two macrocyclic units to far from each other for an efficient substrate encapsulation [40,41].

Zn^{2+} binding by the terpyridine spacer unit of L18 at pH = 7.0 affords the complex $[ZnH_2L18]^{4+}$ (24) (the only species present in water solution at neutral pH) in which the coordinated ligand assumes a *cis-cis* conformation.

L18 (*trans-trans*)   L18 (*cis-cis*)
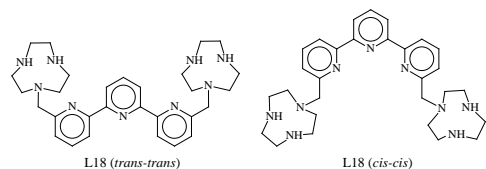
The Zn^{2+} complexation by L18 at pH = 7 is also accompanied by a selective enhancement of the fluorescent emission of the ligand at 355 nm (λ_{exc} = 279 nm) [40]. Differently from L18 in free form, its mononuclear Zn^{2+} complex shows a marked tendency to bind selectively the anion $(P_2O_7)^{4-}$ (DP) over $(PO_4)^{3-}$ (MP) and $(P_3O_{10})^{5-}$ (TP) in a wide pH range. For instance, at pH 7 the percentage of complexed DP is ca. 90%, while the percentages of MP and TP bound to the Zn^{2+} complex are ca. 2% and 8%, respectively (Fig. 14a) [40]. This recognition ability for DP can be reasonably ascribed to an optimal dimensional fitting of this anion within the cleft between the two TACN units, generated by the ligand conformational change upon Zn^{2+} binding.

Following DFT calculations, the DP anion results encapsulated within the cleft delimited by the two protonated TACN units in the minimized structure of the adduct $[ZnH_2L18(H_2O)_2(P_2O_7)]$ (25) and does not replace the water molecules in the coordination sphere of the metal; it prefers indeed to establish a hydrogen bonding network involving both the coordinated water molecules and the ammonium groups of the receptor (Fig. 14b) [40].

Interestingly, DP binding to the 1:1 Zn^{2+} complex of L18 causes a progressive quenching of the fluorescence emission at 355 nm. Therefore, L18 can selectively bind, via weak non-coordinative forces, and sense DP in water thanks to a conformational change in its structure exerted by Zn^{2+} coordination, thus behaving as an OFF-ON-OFF fluorescent switch on adding in sequence Zn^{2+} and DP (Fig. 15) [40].

The *bis*-TACN ligand L19, featuring an acridine spacer unit, can form both stable 1:1 and 2:1 metal-to-ligand complexes in solution with the metal cation(s) bound to a single TACN unit, being the two macrocyclic units too far to be simultaneously involved in a single metal ion coordination [41].
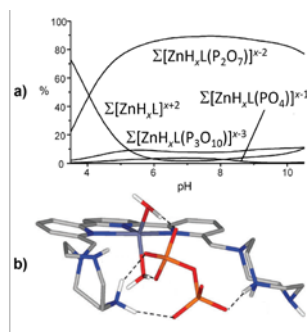

Figure 14. a) Plot of the overall percentages of L18 complexed species with inorganic phosphate anions on changing the pH (L = L18) in a competitive system containing the ligand and anions in equimolecular ratio (10^{-3} M); b) minimized structure of the adduct $[ZnH_2L18(H_2O)_2(P_2O_7)]$ (25). Adapted from Ref. [40] with permission from The Royal Society of Chemistry.
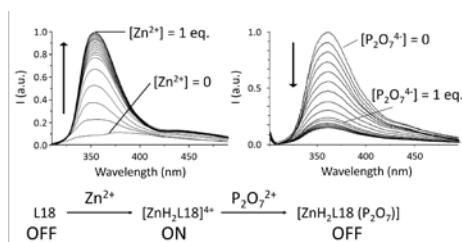

Figure 15. (left) Fluorescence emission spectra of L18 in H_2O at pH = 7.0 in the presence of increasing amounts of Zn^{2+} ([L18] = $1.0\ 10^{-5}$ M); (right) fluorescence emission spectra of the complex $[ZnH_2L18]^{4+}$ (24) in water at pH = 7.0 in the presence of increasing amounts of $(P_2O_7)^{4-}$.(λ_{exc} = 279 nm). Adapted from Ref. [40] with permission from The Royal Society of Chemistry.

A selective fluorescent enhancement of the fluorescent emission of L19 at 435 nm is observed upon formation of both mononuclear $[ZnHL19]^{3+}$ (26) and binuclear $[Zn_2(L19)]^{4+}$ (27) complexes in the pH ranges 5-9 and 7-11, respectively, in H_2O/EtOH (80/20 v:v), following an OFF-ON-OFF profile on changing the pH. The dizinc complex $[Zn_2(L19)]^{4+}$ (27) shows a marked binding affinity for the triphosphate anion $(P_3O_{10})^{5-}$ (TP) above pH 4 thanks to its fitting inside the metal-delimited cavity; no interaction is detected with other inorganic phosphate anions (Fig. 16a).

This thermodynamic selectivity is accompanied by a selective quenching of the fluorescence emission of a solution of $[Zn_2(L19)]^{4+}$ (27) in H_2O/EtOH (80/20 v:v), upon the $(P_3O_{10})^{5-}$ binding. Both ternary adducts with $(P_3O_{10})^{5-}$ and $(HP_3O_{10})^{4-}$ are basically not fluorescent

and, consequently, the sensing system is basically not emissive in the presence of TP at pH higher than 4 (Fig. 16b) [41].

Both L18 and L19 represent, therefore, unique cases of OFF-ON-OFF optical switches for inorganic phosphate anions based on a host-guest geometrical fit. The free ligands are not emissive, their Zn^{2+} complexes show a CHEF effect, the addition of phosphate anions restores the OFF emissive state of the ligands. The directional and space control of the interactions involved in the binding and signaling processes, and, therefore, the switching properties of the receptors are finely dependent on pH, on the number of Zn^{2+} coordinated ions and on the metal ion localization within the different binding sites of the two receptors.

The use of Zn^{2+} complexes of TACN derivatives for polyphosphate anions selective binding and sensing has been cleverly exploited by A.M. Bond and L. Spiccia in the design and development of ligand L20 [42]. It comprises two TACN units, each bearing a pyrene functionalized pendant arm, bridged by a ferrocene molecule.
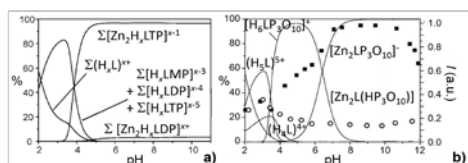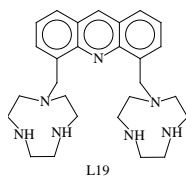

L19

Figure 16. a) Plot of the overall percentage of MP, DP and TP complexed by the dizinc complexes of L19 on changing the pH in H2O/EtOH (80/20 v:v, [L19]= [MP] = [DP] = [TP] = 1.0·10-3 M, [Zn^{2+}] = 2·10^{-3} M); b) normalized emission of the dizinc complexes of L19 at 435 nm in the absence (■) and in the presence (○) of 2 equivs. of TP at different pH values superimposed on the distribution diagram of the L19/Zn^{2+}/TP system in H2O/EtOH (80/20 v:v, [L19] = [TP] = 1.0 10^{-5} M, [Zn^{2+}] = 2.0·10^{-5} M). Adapted from Ref. [41] with permission from John Wiley and Sons. Copyright © 2016.

Addition of $(P_2O_7)^{4-}$ (DP) to a MeCN/Tris-HCl (1:9 v/v) buffer solution of the dizinc complex of L20 [Zn_2(L20)]$^{4+}$ (28), leads to a progressive decrease of the typical fluorescence emission of pyrene at ca. 404 nm and a simultaneous fluorescence enhancement at 475 nm with the formation of the 1:1 [Zn_2(L20)]$^{4+}$/DP adduct with a binding constant of 4.45 10^6 M^{-1} (the largest among evaluated binding constants of other inorganic and biologic polyphosphates, followed by those of ADT and ATP) [42]. These results were interpreted considering that the interaction of DP with the dizinc complex of L20 induces a rearrangement of the latter which brings the two pyrene units into much closer proximity, thus originating a strong excimer emission (Fig. 17) [42]. Furthermore, as a consequence of the selective DP binding to the dizinc complex of L20 (28), a large

negative shift (about 0.1 V) in the potential of the ferrocene/ferrocenium couple is observed [42].

A sensing mechanism broadly similar to that of L20 can be envisaged for the 2,5-diphenyl-[1,3,4]-oxadiazole *bis*-TACN derivative L21 in the Zn^{2+}/Cd^{2+} optical discrimination [43].

L21 shows an absorption band at 272 nm in H_2O at pH = 2.00 which undergoes a slight blue-shift on increasing the pH (268 nm at pH = 12.0). The ligand shows an emission band at 356 nm (λ_{exc} = 272 nm) whose intensity decreases on increasing the pH, reaching the minimum at pH = 9.5. Starting from this pH value, an emission band at 475 nm appears due to excimer formation (Fig. 18a) [43]. The absorption spectra of L21 do not vary on changing the pH in the presence of 1 or 2 equivs. of Zn^{2+} or Cd^{2+}, indicating that the fluorogenic fragment is not involved in the coordination of the metal ions. However, in the presence of 1 equiv. of Cd^{2+}, the excimer band at 474 nm appears at a much lower pH value (7.5), reaching the maximum at pH = 7.7 (Fig. 18b). This behaviour is not observed in the presence of Zn^{2+} (both 1 and 2 equivs.) neither in the presence of 2 equivs. of Cd^{2+} [43].

L20
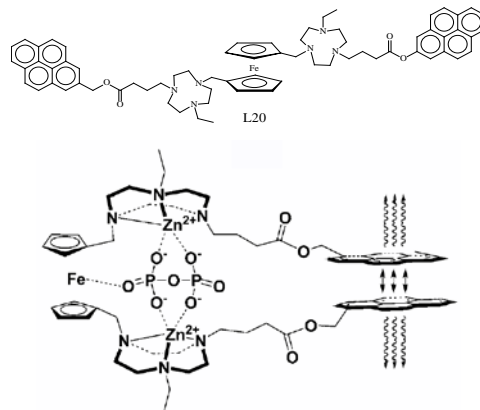
Figure 17. Mode of binding of (P2O7)4- to [Zn2(L20)]4+ (28) inducing a π-π staking of the pyrene aromatic units and a consequent fluorescence enhancement of pyrene excimer emission at 475 nm. Reprinted from Ref. [42] with permission from John Wiley and Sons. Copyright © 2010.

L21 shows an absorption band at 272 nm in H_2O at pH = 2.00 which undergoes a slight blue-shift on increasing the pH (268 nm at pH = 12.0). The ligand shows an emission band at 356 nm (λ_{exc} = 272 nm) whose intensity decreases on increasing the pH, reaching the minimum at pH = 9.5. Starting from this pH value, an emission band at 475 nm appears due to excimer formation (Fig. 18a) [43]. The absorption spectra of L21 do not vary on changing the pH in the presence of 1 or 2 equivs. of Zn^{2+} or Cd^{2+}, indicating that the fluorogenic fragment is not involved in the coordination of metal ions. However, in the presence of 1 equiv. of Cd^{2+}, the excimer band at 474 nm appears at a much lower pH value (7.5), reaching the maximum at pH = 7.7 (Fig. 18b). This behaviour is not observed in the

presence of Zn^{2+} (both 1 and 2 equivs.) neither in the presence of 2 equivs. of Cd^{2+} **[43]**.

This different behaviour, which is supported by potentiometric and NMR studies as well as DFT calculations, is ascribed to the different ionic radii of the two metal ions and to the consequences on the coordination modes of these metals to L21. In its mononuclear complex $[Cd(L21)]^{2+}$ (29), Cd^{2+} can be coordinated by both TACN binding side arms, affording a sandwich complex in which the PET process is inhibited by the metal coordination to all N-donor atoms and the twisted photoinduced charge transfer (TICT) is prevented by the stiffening of the whole structure (Fig. 18c), which favours the excimer formation between almost planar fluorogenic moieties. On the other hand, Zn^{2+} is coordinated to only one TACN unit in its mononuclear complex with L21, which leaves to the complex a high conformational freedom, as it is for the free ligand (Fig. 18d) **[43]**.
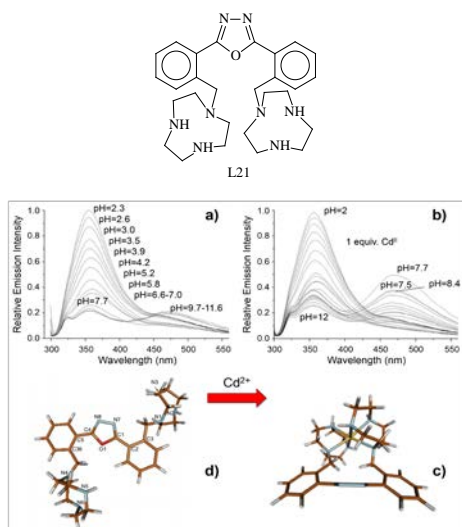

L21

Figure 18. Fluorescence emission spectra in H2O of a) L21, and b) L21/Cd2+ 1:1 molar ratio on changing the pH ([L21] = 2 10-5 M, λexc = 272 nm); DFT optimized geometries of c) [Cd(L21)]2+ (29), and d) L21. Adapted from Ref. [43] with permission from The Royal Society of Chemistry.

TACN derivatives have also been used in the development of fluorescent chemosensors for the enantiomeric recognition and sensing of chiral anions. As a further application of the idea that facing TACN units, separated by an appropriate spacer, can act as efficient and selective receptors/sensors relying on a geometrical size/cavity fitting and binding complementarity in the host-guest interaction, the receptor L22 has been synthesized for the recognition of chiral α-hydroxydicarboxylate anions in water **[44]**.

It consists of a (S)-BINOL (1,1'-bi-2-naphthol) unit bridging two TACN moieties. This ligand can add up to five protons at very

acidic pH values with the species $(H_2L22)^{2+}$ being predominant at pH = 7.0 **[44]**. The absorption band at 228 nm of the (S)-BINOL moiety shows a red-shift of 15 nm on increasing the pH from 7 to 12, accompanied by the formation of a new band at 370 nm, which is determined by the diprotonated BINOL group in the bis-zwitterionic form of L22.

As far as the fluorescence emission of L22 is concerned, the typical band at 365 nm of BINOL decreases on increasing the pH from 2 to 12 as a consequence of a PET process involving the lone pairs on the N-atoms; at alkaline pH values, the formation of a new emission band at 415 nm is observed, due to the deprotonation of the –OH groups of the BINOL moiety **[44]**. Potentiometric measurements show a marked binding selectivity of L22 for the (S,S)-tartaric acid in the considered pH range, with (R,R)/meso-tartaric, (S)-malic, (S)/(R)-lactic, fumaric and succinic acids being complexed in a very low percentage (at most 7%) or totally not complexed (Fig. 19a).
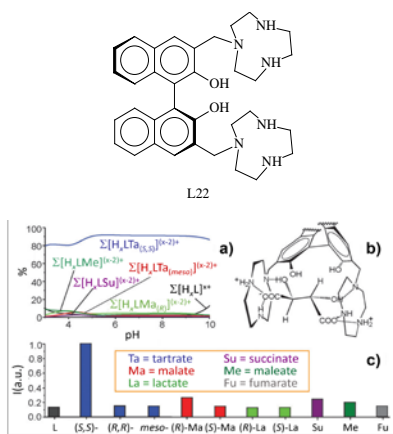

L22

Figure 19. a) Plots of the overall percentages of the L22 complexed species with (S,S)-tartaric ($H_2Ta_{(S,S)}$), (R)-malic ($H_2Ma_{(R)}$), maleic (H_2Me) and succinic (H_2Su) acids on changing the pH in H2O, in a competitive system containing L22 and the acids in equimolecular ratio (10^{-3} M), b) proposed interaction mode of (S,S)-tartrate with $(H_2L22)^{2+}$, c) normalized intensity emission at 410 nm (λ_{exc} = 279 nm) after the addition of each substrate (10 equivs.) to a water solution of L22 at pH = 7.00. Adapted from Ref. [44] with permission from The Royal Society of Chemistry.

While the very low binding affinity of L22 for the (S)/(R)-lactic anions can be ascribed to the presence of only one carboxylate group, which would enable the interaction with only one protonated TACN unit, for the other dicarboxylate anions featuring additional –OH functions, the configuration of the stereo-centres and the number of the hydroxyl functions are determinant for an effective encapsulation within the chiral pseudo-cavity delimited by the protonated TACN moieties of L22. ^{1}H-NMR measurements at pH = 7.00 support the interaction of each carboxylate group of the (S,S)-tartrate anion

in a *gauche* disposition with a TACN unit diprotonated on the secondary N-atoms. Such interactions would enable the simultaneous involvement of both –OH groups of the guest, each one with the tertiary N-atom from the proximal TACN unit (Fig. 19b). This interaction is prevented in the case of the (*R,R*)-tartrate, while only one –OH group could be involved in H-bonding with a tertiary N-atom in the case of *meso*-tartrate. The formation of the adduct [$H_2L22Ta_{(S,S)}$] at pH 7.0 in H_2O is also accompanied by a red-shit of the emission band from 370 to 420 nm (accounting for the deprotonation of the –OH group in the BINOL unit) and by a selective enhancement of the emission intensity (up to the addition of 5 equivs. of substrate), which results far higher than that observed in the same experimental conditions with the other considered carboxylate anions (Fig. 19c).

1.3 Poly-TACN Receptors and sensors.

The most interesting systems featuring a high number of TACN units at work for recognition and sensing of supramolecular functions is represented by nanoparticles (NPs) covered by TACN-containing monolayers. For example, CdSe/ZnS quantum dot (QD) nanoparticles have been covered with thiols terminating with TACN (L23) and other polyaza-macrocyles head groups *via* an amide link, as nanosized direct analogues of the classical PET supramolecular fluorophore-spacer-receptor fluorescent chemosensors for the Zn^{2+} detection in water [45].


QD NP L23
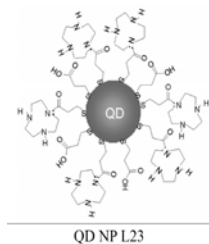
Adapted with permission from Ref. [45]. Copyright © 2008, American Chemical Society.

The monolayer formation on the surface of the QD nanoparticles causes a quenching of the fluorescence emission at 540 or 620 nm (λ_{exc} = 350 nm). Therefore, the core/shell NPs are in an OFF state in water at pH = 7.5, presumably because the photogenerated hole on the QD can be trapped on an accessible energy level on the polyaza ligand, giving rise to a charge separation that switches off the emission of the QDs. In the presence of increasing amounts of Zn^{2+}, the hole-transfer mechanism is interrupted by the N-donors coordination and the fluorescence emission of the core/shell nanoparticles is restored allowing the detection of both this metal ion in water and physiological mimicking samples with a detection limit lower than 2.4 μM and good selectivity in comparison with other important physiological metal ions and transition metals tested [45].

Recently, gold nanoparticles (d = 1.8±0.4 nm) covered with a monolayer of thiols terminating with a [Zn(TACN)]$^{2+}$ head group, Au NP·[Zn(TACN)], have emerged as very promising hybrid inorganic/organic materials for different supramolecular functions, including recognition and sensing processes taking place at the positively charged monolayer surface *via* multivalent interactions with oligoanions [46,47].

In these particular systems, the role of the gold nucleus is to organize and stabilize the monolayers at low concentrations and in a wide variety of conditions, including physiological conditions, rather than generating a detectable output signal (plasmon resonance, absorption, conductivity or redox behaviour changes) following the recognition or chemical events taking place at the functionalized monolayer surface [46,47].

The presence of Zn^{2+} ions on the surface of these monolayer protected gold nanoparticles not only offers numerous practical advantages for the interactions with small oligoanions, such as an increased binding affinity and higher surface saturation concentrations, but also allows to discriminate between structurally very closely related small anionic molecules at very low concentrations, therefore, the role of [Zn(TACN)]$^{2+}$ head groups is not just to provide a positively charged surface. In fact, it has been demonstrated that the binding affinity depends on the number of negative charges of the interacting oligoanion [48],on the chemical nature of the anionic group (phosphate *vs.* carboxylate) [49] and on the presence of hydrophobic moieties able to penetrate into the monolayer [50].

Au NP·[Zn(TACN)]
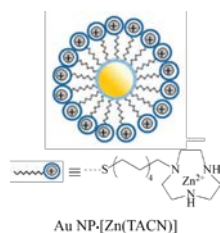
Adapted from Ref. [46] with permission from The Royal Society of Chemistry.

In fact, detailed studies have revealed that the interactions originate from a combination of electrostatic and hydrophobic interactions and coordination bonds, whose relative contribution depends on the structure of the molecules [50]. In terms of applications, just one type of Au NP·[Zn(TACN)] conjugated nanoparticles can be used for pattern-based sensing, similarly to a sensor array ("nose") based on different NPs [51]. To monitor the specific response patterns of Au NP·[Zn(TACN)] to various analytes with subtle chemical differences (NDP and NTP nucleotides; N = A, T, G, C nucleobases), an indicator-displacement assay (IDA) has been set up (Fig.s 20a and 20b) [52].
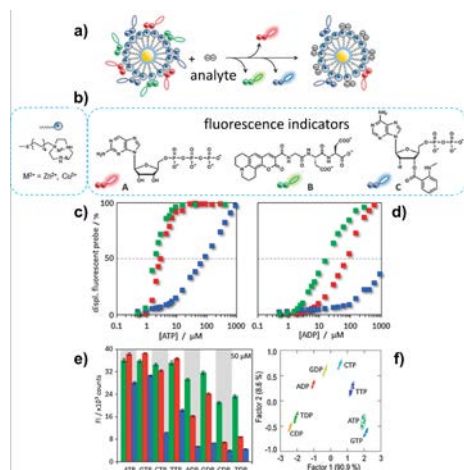
Figure 20. a) Schematic representation of the displacement of different fluorescent indicators from the positively charged surface of Au NP·[Zn(TACN)] upon addition of an analyte; b) molecular structure of the monolayers and of the fluorescent probes; c) relative displacement of the three fluorescent probes A (■), B (■) and C (■) from the surface of Au NP·[Zn(TACN)] as a function of the concentration of ATP and d) ADP; e) response pattern at 50 μM nucleotide concentration (each barrel represents the average of six independent measurements) and d) the corresponding PCA plot. Adapted from Ref. [52] with permission from The Royal Society of Chemistry.

In particular, three different fluorescent probes have been used at the same time, featuring different excitation/emission wavelengths and different relative binding affinities for the positively charged monolayer, but able to bind Au NP·[Zn(TACN)] under saturation conditions in aqueous buffer. A multi-indicator surface was generated by loading the three different probes contemporarily onto the surface of Au NP·[Zn(TACN)] at an individual concentration slightly lower than 1/3 of the respective surface saturation concentration. After 30 min. the thermodynamic equilibrium is reached, with all probes quantitatively bound to the surface of the NPs and their respective fluorescence emission effectively quenched [52].

As a proof of concept, consecutive amounts of ATP and ADP were initially added to a buffer (pH = 7.0) solution of dye-loaded Au NP·[Zn(TACN)] while measuring the fluorescence emission of the three probes using the respective excitation/emission wavelengths. As expected, a different displacement pattern of the three indicators was observed in agreement with a different binding affinity of ATP, ADP and the three probes for the positively charged monolayer in Au NP·[Zn(TACN)] (Fig.s 20c and 20d) [52]. The validity of the sensing system was confirmed by considering all nucleotide di- and triphosphates. At each

used concentration, every one of the eight analytes generates a different response pattern (Fig. 20e), demonstrating the capacity of the system to detect small structural differences and to work like a sensor array [52].

Principal component analyses (PCA) of the data sets confirmed the pattern-based sensing ability of Au NP·[Zn(TACN)] following different clustering of the data in connection with the different binding affinity of the nucleotides towards the positively charged surface of Au NP·[Zn(TACN)]. The performance of the sensing system can be further improved by using Cu^{2+} [52].

The possibility to discriminate oligoanions, such as ATP and ADP, on the base of their different binding affinity for the surface of Au NP·[Zn(TACN)], thus generating an optical signal following the displacement of a previously loaded optical probe, has nicely been applied to the detection of the protein kinase activity [53]. This enzymatic activity generally results in the transfer of a phosphate group to the substrate to afford the phosphorylated product and ADP. ATP and ADP compete to a different extent with the fluorescent probe for the monolayer surface. While ATP is able to display the quenched fluorescent probe from the surface of Au NP·[Zn(TACN)] nanoparticles turning ON its fluorescence emission, ADP, having a lower negative charge, is unable to perform the same operation. The fluorescence response is linearly related to the ATP/ADP ratio, thus allowing the detection of the kinase activity by adding aliquots of the enzyme solution to the assay solution followed by the measurement of the emission intensity of the free probe in solution [53]. On the other hand, under dissipative conditions, *i.e.* the hydrolytic enzyme that transforms ATP in ADP operates in the presence of Au NP·[Zn(TACN)] nanoparticles loaded with a fluorescent probe, a transient fluorescent signal can be generated using ATP as chemical fuel [54]. Furthermore, by changing the enzymatic system and the head group at the base of the positively charged monolayer, the system can gain a fuel-selectivity in the transient generation of the optical signal, thus mimicking natural complex systems able to respond in a distinct manner to different chemical imputs [55].

The tunable multivalent interactions that determine the binding affinity of small oligoanions for the surface of Au NP·[Zn(TACN)] nanosized systems, have been used to regulate the strength of the output signal of a self-assembled sensing system selective for Hg^{2+} [56]. A schematic representation of the mechanism at the base of this sensing assay is shown in Figure 21.

Hg^{2+} is added to a water solution at pH = 7.0 containing Au NP·[Zn(TACN)] (20 μM TACN head group), the fluorescent probe A at 90% of the saturation concentration (7.3 μM) and TDP (16 μM). The formation of the ternary complex TDP·Hg^{2+}·TDP causes the displacement of A from the surface of the nanoparticles with consequent turn ON of the fluorescent emission [56].

The concentration of TDP is as high as possible to favour the formation of the ternary complex and as low as possible to avoid the displacement of A by TDP itself. A plateau level of the fluorescence emission intensity is reached after the addition of about 7.0 μM Hg^{2+} corresponding to about 75% displacement of A. The fluorescence emission is hardly affected by the presence

of other metal cations, while the tolerance of anions depends on their negative charge with doubly and more highly charged anions being less or not tolerated at all, respectively, as they cause the displacement of A even at very low concentrations. Signal generation requires the displacement of probe A from the surface of Au NP·[Zn(TACN)] through competitive binding of the Hg^{2+} ternary complex formed with TDP. Therefore, on changing the number of phosphate groups attached to the recognition unit (thymine), it is possible to modulate the strength of the multivalent interactions with the positively charged monolayer and, therefore, to regulate the optical response of the dynamic system.
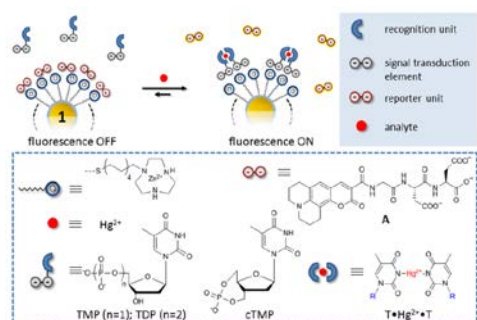

Figure 21. Sensing assay of Hg^{2+} in water based on Au NP·[Zn(TACN)]: the ternary complex TDP·Hg^{2+}·TDP formed upon addition of the analyte to the solution displays the quenched probe from the surface of the nanoparticles better than the un-complexed recognition unit, thus affording a fluorescence emission reporting signal. Reproduced with permission from Ref. [56]. Copyright © 2014, American Chemical Society.

This was demonstrated by using TMP and cTMP instead of TDP, observing a much lower optical signal induced by the same amount of added Hg^{2+} [56]. Interestingly, the addition of Hg^{2+} to a solution containing Au NP·[Zn(TACN)], A and mixtures of low-affinity ligands TMP/cTMP, resulted in a self-selection of the ternary complex TMP·Hg^{2+}·TMP on the surface of Au NP·[Zn(TACN)], driven by the different strength of the multivalent interactions of all possible ternary complexes with Au NP·[Zn(TACN)] [56].

This possibility to perform dynamic combinatorial chemistry on the multivalent surface of Au NP·[Zn(TACN)] nanosized systems has been further exploited for sensing purposes. The addition of Hg^{2+} or Ag$^+$ to a system composed of Au NP·[Zn(TACN)], the fluorescent probe A and a mixture of four different nucleotides (dGMP, dAMP, TMP and dCMP), leads to the self-selection of the ternary complexes TMP·Hg^{2+}·TMP or dGMP·Hg^{2+}·dGMP, respectively, which selectively causes the displacement of quenched A from the surface of the nanoparticles [57]. The driving force of the self-selection recognition and sensing process is the prevailing affinity of the multivalent monolayer surface for the metal-induced anionic complexes.

It has also been demonstrated that Au NP·[Zn(TACN)] nanosized systems can very efficiently catalyse transphosphorylation of 2-hydroxypropyl-4-nitrophenylphosphate (HPNP, Fig. 22), a model substrate for RNA hydrolysis (see the following Section), due to the cooperative action between vicinal oriented and organized [Zn(TACN)] head groups in the monolayer covering the gold nanoparticles [58]. The reaction, which follows a Michaelis-Menten saturation kinetics, produces p-nitrophenol, which is easily detectable.

This catalytic function of Au NP·[Zn(TACN)] can be nicely exploited to develop an alternative sensing assay for the discrimination of ATP and ADP [59]. Due to the fact that both ATP and ADP have higher binding affinities than HPNP for the gold nanoparticles, a structural analogous of HPNP is necessary, strong enough to display ADP but not ATP from the surface of Au NP·[Zn(TACN)]. The appropriate substrate has been identified as the 2-hydroxypropyl-(3-trifluoromethyl-4-nitro)phenyl phosphate (L24 in Fig. 23a) [59].
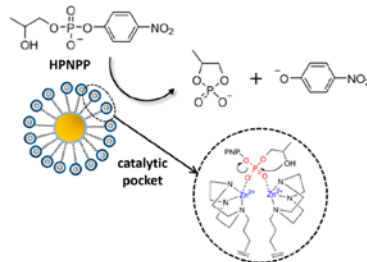

Figure 22. Transphosphorylation of 2-hydroxypropyl-p-nitrophenyl phosphate (HPNP) catalysed by vicinal pre-organized [Zn(TACN)] head groups of the monolayer on Au NP·[Zn(TACN)] nanosized systems. Reproduced with permission from Ref. [47]. Copyright © 2015, American Chemical Society.
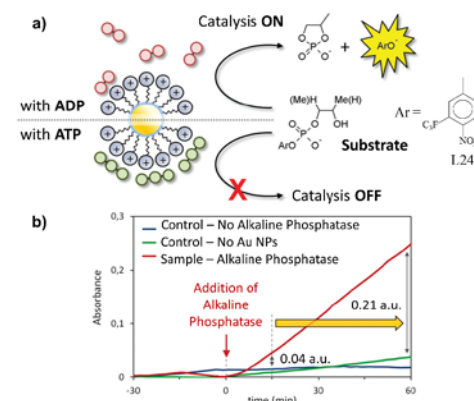

Figure 23. a) L24 competition with ADP for binding on the monolayer surface of Au NP·[Zn(TACN)] and consequent transphosphorylation catalysis by [Zn(TACN)] head

groups in the absence of ATP; b) transphosphorylation of L24 and catalytic signal amplification over ATP consumption by alkaline phosphatase. Adapted from Ref. [59] with permission from The Royal Society of Chemistry.

The higher binding affinity of L24 and the possibility for it to successfully compete with ADP for binding on the monolayer surface, enables a catalytically amplified optical signal only when ATP is absent (Fig. 23a) [59].

The overall system can be used to monitor the consumption of ATP by alkaline phosphatase. A significant increase of the absorbance at 392 nm (absorption wavelength of ArO⁻) is observed after the addition of the enzyme to a solution containing ATP, L24 and Au NP·[Zn(TACN)] under physiological conditions.

A catalytic amplified signal is observed, as compared to control experiments in the absence of either the enzyme or the nanosized artificial catalytic system for the L24 transphosphorylation (Fig. 23b) [59].

2. Metallo-enzyme mimicking (synzymes and nanozymes)

Small polyzamacrocycles, in particular tri- and tetraamino macrocycles, are often used as building blocks for the design of structural or functional models of metallo-biosites [60-63]. In fact, in many metallo-enzymes, first-row transition metals are often coordinated by three or four nitrogen donors, which offer an organized coordination environment to the metal [64,65]. From this point of view, small polyamino macrocycles, such as cyclen or TACN, feature a structurally organized set of donors capable to form stable complexes with transition metal cations. Furthermore, in metallo-enzymes, functional groups from the protein backbone often participate to the catalytic mechanism, reinforcing the overall interaction with the substrate *via* hydrogen bonds, electrostatic contacts or π-stacking and/or hydrophobic effects or being directly involved in the process of substrate modification. In this context, TACN contains three nitrogen donors within its rigid macrocyclic structure, reproducing in part the metal binding sites. This macrocycle can be easily functionalized at one or more nitrogen atoms, allowing for the insertion of pendant arms appropriately designed to interact with the substrate or to participate to the catalytic process. Finally, the N₃ donor set leads to the formation of stable complexes with transition metals, avoiding metal release in solution, and ensures good solubility to the complex in aqueous solution. However, the most attractive structural feature of these complexes is the presence of 'free' binding sites at the metal centres, which are occupied by water molecules in aqueous solution. The latter can be easily replaced by substrates, as often occurs in natural metallo-enzymes. Furthermore, the presence of just three nitrogen donors bound to the metal increases the acidity of the metal ions, leading to facile formation of metal-hydroxide functions, even at neutral pH value, which can play an active role in catalytic mechanisms, such as, in particular, the cleavage of the phosphate ester bond.

This property has prompted the use of metal complexes with transition metals as functional models for metallo-hydrolases, in particular phosphoesterases and RNAases [64,65], which often contain metal ions in their active centre. Zn²⁺ is the most common metal in these systems and in most cases a couple of metal ions work cooperatively in the active site.

In this context, a number of mono- and polynuclear first row transition metal complexes has been designed to test the cleavage ability toward the phosphodiester bond of DNA, RNA or their model compounds, in particular BNP and HPNP [6,8,63,66-71].

Considering the hydrolytic cleavage of the phosphate ester bond, as occurring in the case of BNP (BNP = *bis*(4-nitrophenyl)phosphate), which represents the most commonly used DNA model, the metal ion may be directly involved in the activation of substrates (modes a-c in Fig. 24). The metal can act as a Lewis acid catalyst *via* coordination of an oxygen atom of the ester to the metal (Fig. 24a), coordinating the nucleophile, such as a hydroxide anion (Fig. 24b) or activating the leaving group (Fig. 24c), thus favouring its departure from the substrate. However, the metal cation can also be indirectly involved in promoting the diester hydrolysis. A metal–bound hydroxide can behave as an intramolecular general base catalyst (Fig. 24d) or a metal-coordinated water molecule can act as an intramolecular general acid catalyst (Fig. 24e). In the case of BNP, the diester is generally hydrolysed to MNP [MNP = *mono*(4-nitrophenyl)phosphate] with the release of *p*-nitrophenate (NP), which can be easily detected monitoring the absorbance at *ca* 400 nm in the UV-vis region. The resulting monoester is much more resistant to cleavage and, in most cases, is not further hydrolysed.

In the case of HPNP [(2-hydroxypropyl)-*p*-nitrophenyl phosphate], the most used model for the RNA structure in mimicking studies, the metal complex catalyses a transesterification reaction in which a deprotonated hydroxyl group of HPNP performs a nucleophilic attack on phosphorous to afford a 2,3-cyclic phosphate and *p*-nitrophenate (Fig. 25a).
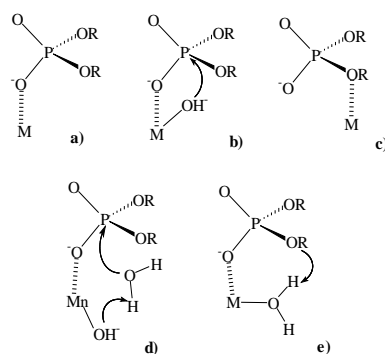

Figure 24. Possible roles of a metal ion in the hydrolytic cleavage of a phosphate diester, such as BNP (R = 4-nitrophenyl).

Beside the interaction of the metal with phosphate, as in the case of BNP, the metal can be involved in the cleavage thanks to the participation of the metal-bound hydroxide, which can assist the deprotonation of the HPNP hydroxyl within a general base mechanism (Fig. 25b). The proton transfer process and the nucleophilic attack of the deprotonated hydroxyl occur in the rate determining step of the reaction. Alternatively, the deprotonation of hydroxyl takes place in a pre-equilibrium step and the nucleophilic attack features the rate determining step in a specific base catalytic mechanism (Fig. 25c), in which the metal plays the main role of substrate activation *via* electrostatic/coordinative interactions with the deprotonated HPNP. In a recent theoretical study on HPNP transesterification catalysed by $[Zn(TACN)]^{2+}$ [72], has been pointed out that the energetic barrier for the HPNP cleavage is similar in the two mechanisms, accounting for the difficulty to distinguish the two pathways in complexes with TACN derivatives. As a matter of fact, the effective mechanism and, consequently, the role of the metal in the catalysed HPNP cleavage has been, and still is, subject of debate [68,72].
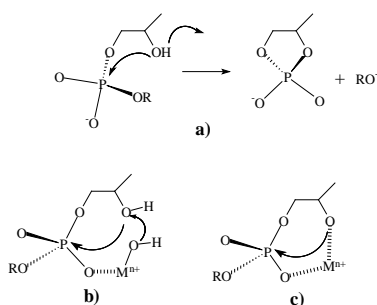

Figure 25. Cleavage of HPNP (a) and possible roles of a metal cation in the general base b) and specific base c) mechanisms

Among different metal cations, the most commonly used has been Zn^{2+} [67,70,71], due to its ubiquitous presence in hydrolytic metallo-enzymes. However, some authors have also analysed the cleaving ability of other metal complexes, such as Co^{3+} [66] or Cu^{2+} [8,73]. Both these metal ions form more stable complexes with TACN in water solution than Zn^{2+}, avoiding metal release in a larger pH range; moreover, the higher charge of Co^{3+} ensures a better binding ability for phosphate anions and a larger complex acidity, thus enhancing the hydrolytic ability of the complexes.

TACN has been often used as metal binding sites not only to afford mono-, bi- and polynuclear molecular complexes,but also to produce functional nanostuctured device, in both cases able to efficiently cleave DNA, RNA or their models. In this respect, the terms synzymes (synthetic enzymes) and nanozymes are nowadays often used [47,67,70]. Although this review is an overview of the TACN uses in supramolecular chemistry in the last 15 years, we will report also some previously published

cases of functional models for phosphatase/RNAase, which represent 'key' steps in the evolution of metallo-hydrolases.

2.1 Mononuclear complexes.

With the purpose to improve the hydrolytic ability of TACN complexes and to achieve a better comprehension of the mechanisms operating at the active site of metallo-enzymes, in particular phosphoesterases, a number of derivatized mononuclear complexes have been synthesized. The simplest derivatization of the TACN structure is represented by the N-functionalization with alkyl or aryl units. The pioneering work of Burstyn showed that the simple insertion of short alkyl units, such as isopropyl moieties, on the three nitrogen donors of TACN increases the hydrolytic efficiency of its Cu^{2+} complex toward the BNP and real DNA [73,74].

The Cu^{2+} complex with TACN (**30** in Fig. 26) catalytically cleaves BNP to MNP and NP, with a 2000-fold enhancement of the hydrolysis rate at 50 °C and pH 9.2. The Cu^{2+} complex is a monomer-dimer equilibrium (Fig. 26), with the monomer $[Cu(TACN)(OH)(H_2O)]^+$ species being the catalytically active species [73]. The hydrolysis first involves replacement of the water molecule with a BNP oxygen in the coordination sphere of Cu^{2+}, followed by the nucleophilic attack of the Cu^{2+} bound hydroxide to phosphorous and simultaneous release of NP (Fig. 27) [73]. The Cu^{2+} complex **31** with ligand 1,4,9-trisopropyltriazacyclononane (L25) catalyses BNP cleavage with the same catalytic mechanism [74]. As in the case of the Cu^{2+} complex with TACN, the initial rate of the hydrolytic process increases with pH (Fig. 28), likely due to the increasing formation in solution of the hydroxo complex active in the hydrolytic cleavage.
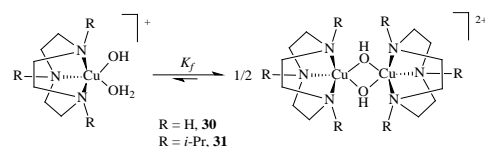

Figure 26. Schematic representation of the equilibrium between the $[Cu(TACN)(OH)(H_2O)]^+$ monomer and the $[Cu(TACN)(\mu-OH)]_2^{2+}$ dimer
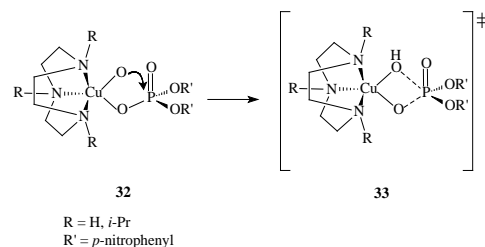

R = H, *i*-Pr
R' = *p*-nitrophenyl

Figure 27. Proposed mechanism for BNP hydrolysis catalyzed by the mononuclear complexes **30** and **31**.

More interestingly, **31** resulted to be significantly more active than the corresponding complex with TACN **30** (Fig. 26), the rate being 70-fold increased at pH 7.2 and 60-fold at pH 9.2 (at pH 7.2 the initial rate are $0.06 \cdot 10^{-8}$ and $4.28 \cdot 10^{-8}$ $M^{-1}s^{-1}$, respectively).

31 shows a lower tendency to form a bis-(μ-hydroxide) dimer than **30** (the K_f constant for the formation of the dimer, Figure 26, is $1.4 \cdot 10^2$ and $1.3 \cdot 10^2$ in the case of the Cu^{2+} complex with L25 and TACN, respectively), due to the steric hindrance of the i-propyl groups. However, the amount of the [CuL25(OH)(H2O)]+ active species in solution is only about two to three times as great for **31** as it is for **30**, only partially justifying the rate increase in the hydrolysis of BNP by **31** [75].

On the other hand, the activation enthalpy ($\Delta H^{\neq}$) for **31**-catalyzed BNP hydrolysis is by far lower than that reported for **30** [73] (51 kJ mol^{-1} at pH 9.2 and 90 kJ mol^{-1} at pH 9 for **31** and **30**, respectively), while the $\Delta S^{\neq}$ values are roughly the same. This suggested that both the catalyst-substrate complex (**32**, Fig. 27) and the following transition state (**33**) are destabilized in **31**- relative to **30**-catalyzed BNP hydrolysis, due to the steric repulsion between the i-propyl groups and the bulky substrate. Most likely, the catalyst-substrate complex **32** is destabilized to a greater extent than the transition state **33**, placing the catalyst-substrate complex, formed by fast ligand exchange, closer in energy to the transition state for **31** than for **30**, thereby increasing the rate of BNP hydrolysis.

Both **30** and **31** are also able to cleave the pBluescript II ks(-) DNA plasmid under anaerobic conditions at pH 7.8 [75]. In particular, **31** cleaves the supercoiled plasmid to its nicked form in 12 h and, in a longer time (24 h), to the linear form and results more efficient than complex **30**.

Interestingly enough, the hydrolytic activity increases with pH (**31** is twice more active at pH 7.8 than at pH 7.2) and with complex concentration, suggesting that the cleavage mechanism is similar to that observed in the case of BNP, at least in anaerobic conditions.
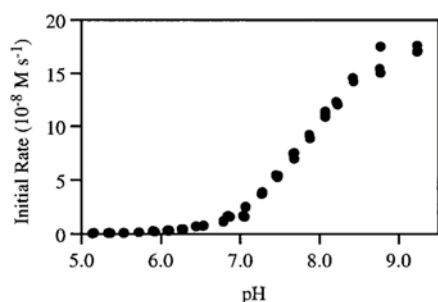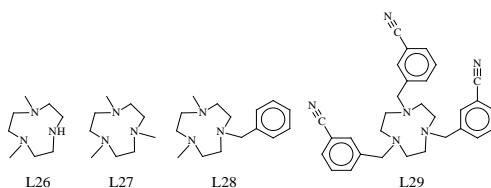
mM). Reprinted with permission from Ref. [74]. Copyright © 2002, American Chemical Society.

All their Cu^{2+} complexes were efficient hydrolytic agents for BNP, the pseudo-first order rate constants spanning from $1.24 \cdot 10^{-5}$ s^{-1} (L26) to $30.2 \cdot 10^{-5}$ s^{-1} (L29) at 50 °C and pH 7.4. The activity of the Cu^{2+} complexes increases in the order L26 < L27 ≈ L28 < L29, suggesting that the hydrolytic ability increases with the steric bulk of the ligands [78]. The Cu^{2+} complex with L27 shows a cleavage activity slightly higher than that observed for **31** [77], the pseudo-first order rate constant being $6.3 \cdot 10^{-5}$ s^{-1} and $4.3 \cdot 10^{-5}$ s^{-1}, respectively. This suggested a hydrolytic mechanism similar to that proposed by Burstyn. The increasing ability in BNP cleavage with the steric hindrance of the nitrogen substituents is also in agreement with the Burstyn hypothesis on the role played by substituent groups in determining the hydrolysis rate. On the light of these results, the hydrolysis of BNP by the L27 complex with Cu^{2+} was analysed more closely, determining the second order rate constants, and, overall, the thermodynamic parameters for BNP hydrolysis [77]. Their comparison with those reported for complexes with TACN and **31** [73] showed that the activation enthalpy $\Delta H^{\neq}$ is somewhat less favourable for **31** and [CuL27(H2O)(OH)]+ (**34**) with respect to [Cu(TACN)(H2O)(OH)]+, in agreement with an associative mechanism not favoured by bulkier ligands. The entropic contribution is negative for all three complexes, and increases in the order **31** (-110 J mol^{-1} K^{-1}) < **34** (-95 J mol^{-1} K^{-1}) < [Cu(TACN)(H2O)(OH)]+ (-79 J mol^{-1} K^{-1}). As a matter of fact, the higher cleavage efficiency of the former two complexes is essentially due to the more favourable entropic contribution. Spiccia and co-workers suggested that the transition state is likely more compact than the initial state, in which both OH$^-$ and BNP are coordinated to Cu^{2+}, and is stabilized relative to the initial state when alkyl substituents are introduced, thus reducing the overall activation energy for BNP cleavage, in agreement with Burstyn's conclusions. Interestingly enough, **34** was found to be also able to hydrolyse the primary product of BNP cleavage, MNP, to inorganic phosphate and NP at pH 7.4 and 50 °C (k_{OBS} = $1.93 \cdot 10^{-6}$ s^{-1}), a not common feature for Cu^{2+} complexes [7-14]

Figure 28. pH dependence of [CuL25]$^{2+}$ (**31**) mediated BNP hydrolysis rate (323 K, [NaNO3] 0,1 M, [complex] = [BNP] = 0.60 M, MES (pH 5.1-6.4), HEPES (pH 6.5-7.1), HEPPSO (pH 6.8-8.2) or CHES (pH 8.4-9.2) buffers (50

Side arms have been used not only to lower the energetic barrier of the nucleophilic attack by the metal-bound hydroxide, but also to increase the affinity for the substrate, in particular DNA. In this context, intercalating groups, such as acridine or its derivatives, can be used to increase the binding ability of TACN complexes towards nucleic acids.

Burstyn and co-workers linked an acridine orange unit, a known dye able to intercalate within the DNA nucleobases, to a TACN moiety *via* a hexamethyl chain (L30) [79].

Ligand L30 was able to cleave the pBluescript II ks(-) DNA plasmid to its nicked and linear form in the presence of 1 eq. of Co^{2+}, Mn^{2+}, Cu^{2+} and Zn^{2+} (Fig. 29a), Cu^{2+} being ca. twice more efficient than the other metal cations. The Cu^{2+} complex with L30 (**35**) was somewhat more efficient in aerobic conditions (ca. 20% in 5.0 μM concentration, Fig. 29b), as already observed for the $[Cu(TACN)]^{2+}$ complex, indicating that an O_2-dependent cleavage mechanism is also active. More interestingly, the Cu^{2+} complexes with TACN and L30 exhibit very different dose-response behaviours (Fig. 30) [80]. In fact, **35** exhibited consistent concentration dependent increases in the extent of DNA cleavage under anaerobic conditions, while the complex with TACN is maximally efficient at 25 μM and at higher concentrations it becomes less effective at cleaving DNA, probably due to the formation of inactive hydroxo-bridged dimers [73,80]. **35** increases in effectiveness toward DNA cleavage as the concentration is increased and at 100 μM is approximately 2.4 times more effective than the TACN complex, probably thanks to the effect of the intercalator on the metal complex-DNA interaction. The neighbour exclusion effect, which rules out that two neighbouring sites of an occupied intercalation site in DNA can be occupied [81], makes it unlikely that two **35** complexes will be in close contact to form the inactive hydroxo-bridged dimers. The fact that **35** is less effective at lower concentrations than the TACN one suggests that there may be cooperativity between the monomeric complexes in the cleavage process. Individual cationic metal complexes may collaborate to promote DNA hydrolysis without forming inactive dimers, a process which is hampered by neighbour exclusion effect in the presence of an intercalating agent. Overall, this result suggests that simply tethering a DNA-cleaving metal complex to a DNA-binding functionality does not necessarily result in an increased rate of DNA cleavage.
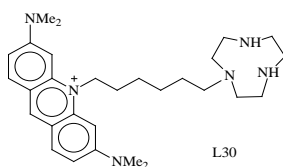
One of the most exploited functionalization of macrocyclic rings for the development of biomimetic complexes consists in the insertion of a side arm containing a guanidinium ion. This group, present in the amino acid arginine, is often found in the binding site of enzymes to coordinate oxoanions, in particular carboxylates or phosphates. In fact, the guanidinium group shows a planar and rigid structure, with a geometrical complementarity to these oxoanions, which allows the formation of a two-point hydrogen bonding chelate motif (Fig. 31) [82,83].

The guanidinium unit present in the arginine side chain is involved in the substrate activation and transition-state stabilization, while the serine residue provides a nucleophilic hydroxyl group, leading to the formation of the phosphorylated enzyme during the catalytic cycle [84].

The metal cation and the guanidinium groups act as Lewis acids and electrostatic catalysts; however, the guanidinium groups may act also as Brønsted acids. In fact, the release of the leaving group may require a proton transfer from a guanidinium unit. The possible mechanisms involving the cooperation of a metal ion and a guanidinium moiety in the cleavage of phosphodiesters are sketched in Figure 32a-b, while the transesterification reaction occurring in the cleavage of RNA or its model compounds are shown in Figure 32c.

In this context, Graham and Spiccia reported the Cu^{2+} complexes of ligands L31 (**36**) and L32 (**37**), featuring pairs of ethyl- and propylguanidine pendant arms [85]. The X-ray crystal structure of **36** in its deprotonated and uncharged form (Fig. 33) showed that the guanidine secondary nitrogen adjacent to the TACN unit is strongly coordinated to the metal centre, reducing its ability to coordinate and activate the phosphate esters. As a result, this complex possesses a negligible ability in both BNP and HPNP hydrolysis.
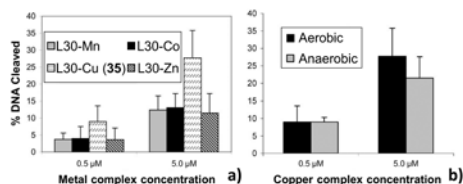

Figure 29. (a) Aerobic DNA cleavage activity of L30 in the presence of the different metal ions, expressed as percentage of supercoiled plasmid DNA converted to nicked and linear forms at pH 7.8 and 50 °C after 12 h and (b) comparison of the extent of DNA cleavage by **35** under aerobic and anaerobic conditions (the y axis reports the percentage of cleaved supercoiled plasmid DNA) at pH 7.8 and 50 °C after 12 h. Adapted from Ref. [79] with permission from The Royal Society of Chemistry.
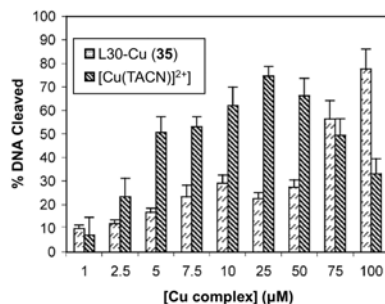

Figure 30. Comparison of anaerobic DNA cleavage by the $[Cu(TACN)]^{2+}$ complex and the intercalator-linked **35**, expressed as percentage of cleaved supercoiled DNA at pH 7.8, 50 °C after 24 h). Adapted from Ref. [79] with permission from The Royal Society of Chemistry.

L30

Conversely, in the case of **37**, the pseudo-first order rate constant for BNP hydrolysis at pH 7 and 50 °C (k_{OBS} = 7.24·10⁻⁵ s⁻¹) is 40-fold higher than found for the [Cu(TACN)]²⁺ complex (k_{OBS} = 1.7·10⁻⁶ s⁻¹). HPNP cleavage is *ca* 10-fold faster in the presence of **37** at pH 7 and 25 °C (k_{OBS} = 3.2·10⁻⁵ s⁻¹) than by [Cu(TACN)]²⁺ (k_{OBS} = 3.58· 10⁻⁶ s⁻¹) [85].

The greater activity of the complex could be the result of the activation of the phosphate ester or the stabilization of transition states through electrostatic/hydrogen-bonding interactions with the guanidine pendants, or a restriction in the formation of inactive dihydroxo-bridged Cu²⁺ dimers by N-functionalization of the TACN macrocycle. However, in comparison with L25-L29, the introduction of guanidinium pendants in L32 does not greatly enhance the rate of BNP hydrolysis by their Cu²⁺ complexes, suggesting that the pendant guanidinium groups have only marginal influence. Interestingly enough, in the cleavage of supercoiled pBR322 plasmid DNA at pH 7 and 37 °C both Cu²⁺ complexes **36** and **37** are active. While **36** shows a similar activity to that found for the TACN analogue, **37** is *ca* twice more active, indicating that the Cu²⁺ ion and the guanidinium side arms could play a cooperative role in the hydrolytic cleavage. Finally, experiments carried out in aerobic and anaerobic conditions showed that the mechanism is prevalently hydrolytic, the oxidative pathway playing a minor role (30% in aerobic conditions).

This study was also extended to TACN derivatives containing a single guanidinium group linked to the macrocycle *via* an alkyl (L33-L35) [86] or xylyl bridge (L36-L38) [87].
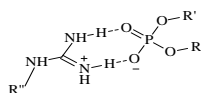

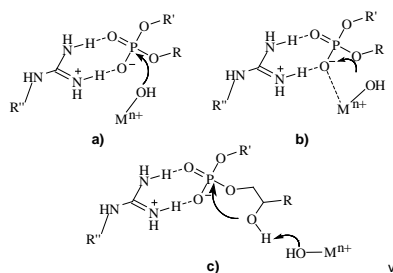Figure 31. Interaction mode of guanidinium with phophates.

Figure 32. Cooperative roles of metal and guanidinium ions in DNA (a,b) and RNA (c) cleavage involving phosphate activation by interaction with guanidinium (a), activation by interaction with both guanidinium and metal ion (b) and activation with guanidinium and simultaneous deprotonation of a hydroxyl group by a M-OH function.

Interestingly, the X-ray crystal structure of the Cu²⁺ complex with L33 showed that the ligand forms a monohydroxo-bridged binuclear copper(II) complex (Fig. 34) in which each metal centre is coordinated by a non-protonated guanidine unit, affording a stable five-membered chelate ring. In contrast, L34 and L35 form mononuclear complexes in which the guanidinium pendants remain protonated and do not coordinate. The latter complexes are more reactive toward the phosphodiesters BNP and HPNP than the analogues with L33 and L36-L38, featuring xylyl-linked guanidine groups (for instance in BNP cleavage at 50 °C and pH 7, k_{OBS} = 10.2·10⁻⁶ s⁻¹ and 7.0 10⁻⁶ s⁻¹ for the Cu²⁺ complexes with L34 and L35, respectively, *vs* k_{OBS} = 2.39·10⁻⁶ s⁻¹ for [CuL38]²⁺, the most active among the complexes with L33 and L36-L38). This suggests that more flexible alkyl pendants of L34 and L35 allow the guanidinium groups to better interact with the Cu²⁺-bound phosphate ester, favouring the cleavage. A different behaviour was found in the case of DNA cleavage. The complexes with L33-L35 are able to cleave the phosphodiester bond of the pBR 322 DNA plasmid at pH 7 and 50 °C faster than both [Cu(TACN)]²⁺ and the complexes with *bis*(alkylguanidine) ligands (**36** and **37**) (for instance k_{OBS} = 5.51·10⁻⁵ s⁻¹ for [CuL35]²⁺, the less active mono-alkylguanidinium-TACN complex, *vs* k_{OBS} = 2.53·10⁻⁵ s⁻¹ for **36**, the most active di-alkylguanidinium-TACN complex), indicating that the former can better access the sugar–phosphate backbone and that the guanidinium groups likely act cooperatively with the Cu²⁺ centre to accelerate the cleavage.

Differently from BNP and HPNP, the complexes with the aryl guanidinium-TACN ligands L36-L38 have similar reactivity in DNA cleavage with respect to the alkylguanidine-linked analogues [87]. The complex of the *o*-xylyl derivative L36 cleaves DNA 22-fold faster than the Cu²⁺ complex with TACN. In the former complex, in fact, the guanidinium group is well-positioned to promote charge-assisted H-bonding interactions with neighbouring phosphodiester groups (Fig. 34).[8]
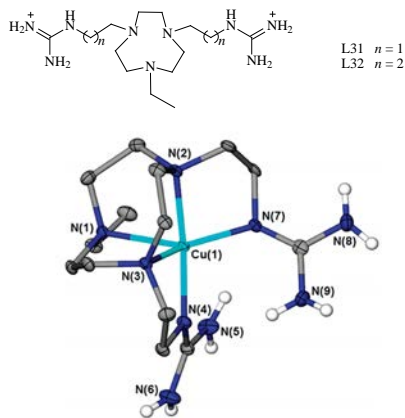

L31   *n* = 1
L32   *n* = 2

Figure 33. X-ray crystal structure of **36** (the ligand is in its neutral form). Reprinted with permission from Ref. [85]. Copyright © 2011, American Chemical Society.

This complex also represents a rare case where the sequential cleavage of supercoiled DNA (form I) to relaxed form II, to linear form III, and finally to DNA oligomers was followed and rate constants determined for each transformation.

Savio *et al.* independently tested the cleaving ability of L37 complexes with Cu^{2+} and Zn^{2+} toward the RNA model HPNP in DMSO:H_2O 80:20 solution at 50 °C and pH 9 and 9.8, respectively, and 50 °C [88]. The reaction rate was remarkably enhanced in the presence of the Cu^{2+} and Zn^{2+} complexes (k_{OBS} = 5.1·10^{-4} s^{-1} and 1.0·10^{-3} s^{-1} for the Cu^{2+} and Zn^{2+} complexes, respectively) with respect to the corresponding complexes with TACN (k_{OBS} = 1.3·10^{-5} s^{-1} and 1.3·10^{-4} s^{-1} for the Cu^{2+} and Zn^{2+} complexes, respectively).

In the case of Cu^{2+}, at pH 9 the metal-bound water molecule is 50% deprotonated, while guanidine is in its protonated and charged form. The authors proposed that the observed rate acceleration is due to a large extent of cooperation between the guanidinium group, which can give rise to charge assisted hydrogen bonding interactions with the phosphate group, and the Cu-OH group, which can assist the deprotonation of the hydroxyl group of HPNP (Fig. 35).

The lower rate enhancement observed in the presence of Zn^{2+} at pH 9.8 (at this pH the zinc-bound water molecule is also 50% deprotonated) is probably due to a more modest cooperation between the Zn-OH and guanidinium groups in the cleavage process.

The TACN unit has been also functionalized with a cationic tetrapeptide side arm to improve the binding and cleavage ability of its Zn^{2+} and Cu^{2+} complexes toward DNA, exploiting the possible insertion of the polypeptide chain within the DNA grooves.

bonding interactions between protonated guanidine and phosphate groups. Reprinted with permission from Ref. [87] Copyright © 2011, American Chemical Society.

The TACN derivative containing an appended LKKL (L = Leucine, K = Lysine) sequence (L39) acts as a tetradentate ligand for both Zn^{2+} and Cu^{2+}, the pyridine linker being coordinated to the metal centre. Both complexes bind and cleave the pUC18 DNA plasmid to its nicked and linear forms at pH 6 and 37 °C [89]. The Cu^{2+} complex with L39 (**38**) is the most efficient and cleaves the plasmid 4-fold faster than the analogous Cu^{2+} complex with the PyTACN parent compound, which contains a pyridine unit linked to the TACN moiety *via* a methylene bridge. In both cases the cleavage mechanism is likely to occur *via* an oxidative pathway, thanks to the Cu^{2+}-mediated generation of radical oxygen species, in particular the superoxide anion. The enhanced cleavage ability of the **38** complex with respect to [Cu(PyTACN)]$^{2+}$ is explained by the presence of the tetrapeptide chain, positively charged due to lysine protonation, which intercalates within the minor groove. Although no sequence-specific binding was observed, the intercalation effectively induces an improved binding affinity, *via* weak forces, to the DNA-minor groove, resulting in groove selectivity on the nuclease activity.

The increased efficiency in phosphate ester cleavage of TACN derivatives containing cationic pendant arms, such as alkyl guanidinium groups, has inspired the investigation of their mechanistic role. Zhao *et al.* have recently analysed the mechanism of BNP hydrolysis by the Cu^{2+} complexes with ligands L33 and L35, considering as possible cleaving agents both the mono- and hydroxo-bridged dinuclear species [90].

L33 *n* = 1
L34 *n* = 2
L35 *n* = 3

L36 *o*-xylyl
L37 *m*-xylyl
L38 *p*-xylyl
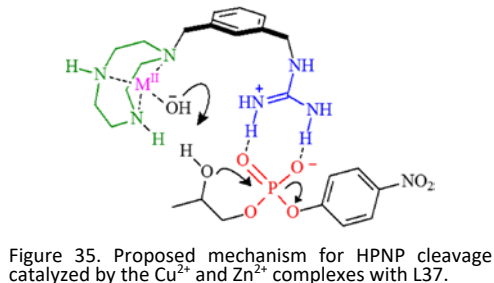
Figure 35. Proposed mechanism for HPNP cleavage catalyzed by the Cu^{2+} and Zn^{2+} complexes with L37.
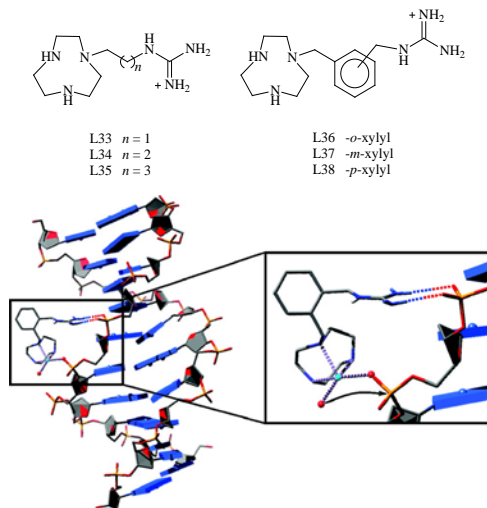
38

Figure 34. Proposed mode of interaction between the complex with L36 and DNA and the subsequent attack of a Cu^{2+}-bound hydroxide on a phosphodiester group. Dashed bonds represents charge-assisted hydrogen
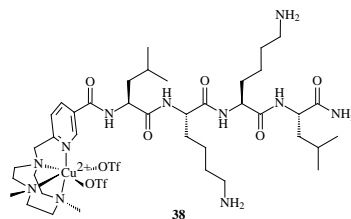
DFT calculations found that in the case of L33, which contains a short ethylene linker between guanidine and TACN, the tertiary amine of the guanidine pendant is not protonated and binds to

the Cu^{2+} centre (Fig. 36). In this case, the most active species are dinuclear complexes and hydrolysis occurs *via* a concerted mechanism in which a Cu^{2+} ion acts as anchoring point for BNP, while a hydroxide anion, bound to the second Cu^{2+} centre, acts as nucleophile (Fig. 36a). An amine group of guanidine facilitates the departure of the leaving group. Conversely, in the case of L35, in which a longer butylene bridge links the guanidine to TACN, the most active species is a protonated mononuclear [Cu(L35H)OH][2+] complex. The guanidinium group is not involved in metal binding and the hydrolytic process occurs *via* a nucleophilic attack of the Cu-OH function at phosphorous accompanied by leaving group detachment favoured by its interaction with the protonated guanidine (Fig. 36b). The latter mechanism is more energetically favoured than that found for the L33 dinuclear complex, in agreement with the experimentally observed greater hydrolytic ability in the case of Cu^{2+} complex with L35.

Beside simple alkyl/aryl groups, TACN has been also linked to a guanidinium group *via* more structured molecular scaffolds, such as a *cone*-calix[4]arene platform [91,92]. This is the case of the regioisomers L40 and L41, which differ in the position (1,2 in L40 and 1,3 in L41) of the calix[4]arene upper rim functionalization Their Cu^{2+} and Zn^{2+} were tested as catalysts in the cleavage of the phosphate ester bond of HPNP, dinucleotides (GpA, GpU, CpA, UpU) and BNP.

On the basis of potentiometric titrations, the authors determined the species present in the solvent mixture used (DMSO:H$_2$O 80:20), allowing them to analyse the complexes efficiency at a pH value (between 8.8 and 9.9, depending on the complex) where the metal ion is completely bound to the TACN unit, the 50% of the TACN-bound M-OH$_2$ groups are dissociated to give active M-OH species and the guanidine is protonated. In these conditions, the Zn^{2+} and Cu^{2+} complexes with protonated L40 and L41 enhance the cleavage rate of HPNP at 25 °C. While the reaction rate is scarcely affected by the functionalization position of the calix[4]arene, the Cu^{2+} complexes result markedly more effective than the Zn^{2+} complexes.
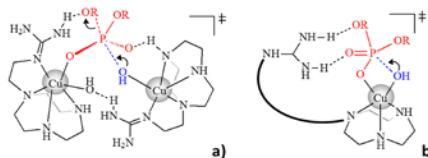

Figure 36. Energetically favoured hydrolytic mechanisms for the Cu^{2+} complexes of L33 (a) and L35 (b). Charges are omitted.

In comparison with the corresponding complexes with TACN, the rate is 1300 and 900 times increased by the Cu^{2+} complexes of L40 (**39**) and L41 (**40**), respectively, while a modest 3.6 and 5.5-fold enhancement is observed in the case of the corresponding Zn^{2+} complexes. This result suggests, at least in the case of Cu^{2+}, that the transesterification of HPNP occurs *via* a cooperative mechanism involving the interaction of guanidinium with phosphate and Cu-OH-assisted

deprotonation of the hydroxyl group, which can act as nucleophile in the transient state of the reaction (Fig. 37a) [91]. A similar remarkable rate enhancement was also observed in the case of dinucleotides GpA, GpU, UpU and ApA, in which the phosphate ester bond is likely to be cleaved with a mechanism analogue to that proposed for HPNP. In this case, however, the catalytic efficiency also depends on dinucleotides. For instance, **39** is the most efficient catalyst in CpA transesterification, while **40** is the best catalyst in the case of GpA [91,92]. A different scenario is found in the case of the DNA model BNP,[92] which is hydrolysed by the Cu^{2+} and Zn^{2+} complexes of the same ligand with similar good efficiencies, as a result of a high degree of synergism between the TACN-bound metal and the protonated guanidine (Fig. 37b) in both Cu^{2+} and Zn^{2+} complexes. In this case, however, the complexes with the 1,2-regioisomer are better catalysts than the corresponding complexes with the 1,3-one. For instance, **39** induces a 1400-fold enhancement of the hydrolytic rate with respect to [Cu(TACN)][2+], cleaving BNP one order of magnitudo faster than **40**, accounting for a higher cooperative role between metal-bound hydroxide and guanidinium ion in BNP hydrolysis in the case of the complexes of the L40 regioisomer.
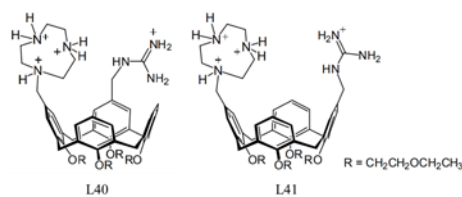
Reprinted with permission from Ref. [92]. Copyright © 2016, American Chemical Society.
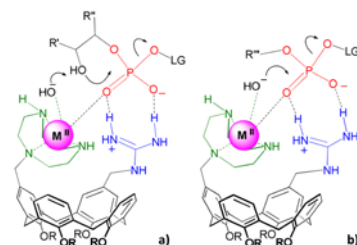
Figure 37. Proposed mechanism for HPNP cleavage (a) and BNP hydrolysis (b) by the Cu^{2+} and Zn^{2+} complexes with L40 Reprinted with permission from Ref. [92]. Copyright © 2016, American Chemical Society.

Alcoholic groups have also been appended to the TACN backbone with the purpose to exploit the formation of alcoholate nucleophilic functions upon metal binding by the alcoholic group. However, a pioneering work of Morrow and Richard showed that the ethanolic side arm of ligand L42 does not deprotonate upon Zn^{2+} coordination [93-95]. The complex is able to cleave HPNP to give cyclic phosphate and *p*-

nitrophenate, but the nucleophilic attack is given by a Zn-OH function generated at alkaline pH by the deprotonation of a Zn^{2+}-bound water molecule.

In addition to the ethanol pendant, ligand L43 also contains a guanidinium group appended to the TACN frame. The cleaving ability of L43 was tested toward pUC 19 DNA plasmid [96]. L43 efficiently cleaves the supercoiled DNA plasmid to its nicked and linear forms (k_{OBS} = 0.131 h^{-1}) following a Michaelis-Menten kinetics and displaying by far higher activity in DNA cleavage than simple TACN at pH 7.2 and 37 °C. Interestingly enough, the Zn^{2+} complex with L43 (**41**)possesses a remarkable cleaving ability only at slightly acidic pH, **41** being *ca* 10-fold more active (k_{OBS} = 0.151 h^{-1}) than the metal-free ligand L43 (k_{OBS} = 0.015 h^{-1}) at pH 6. The cleaving ability is strongly reduced at pH 7.2. The authors suggest that DNA cleavage promoted by L43 occurs thanks to the protonation of guanidine that allows for electrostatic interactions with the DNA phosphate backbone, while the ethanol pendant can act as nucleophile (Fig. 38). The same mechanism is also proposed in the case of **41** at pH 6. The unusual reduced activity of complex **41** at neutral pH was related to the deprotonation of guanidinium and the possible coordination of guanidine to Zn^{2+}, inhibiting its interaction with the DNA phosphate groups.

2.2 Di- and polynuclear complexes.

In Nature, many phosphoesterases are activated by two or more metal ions at close distance, in most cases Zn^{2+} ions. This is the case, for instance, of alkaline phosphatases, phospholipase C, the Klenow fragment of DNA polymerase I and P1 nuclease [65,84]. In light of this consideration, several systems containing two TACN units have been synthesized, in order to assembly two metal cations at the appropriate distance to simultaneously interact with a phosphate moiety.
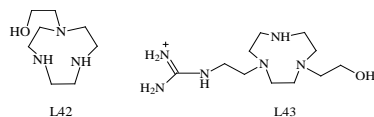
In fact, bridging coordination of phosphate to two metal cations decrease the electron density at phosphorous, making it more susceptible to a nucleophilic attack, as actually occurs in most dinuclear phosphatases[65,84].

On the basis of these considerations, in the nineties Chin and co-workers developed a number of binuclear Co^{3+}, Cu^{2+} and La^{3+} systems able to bind and cleave phosphate esters [66]. Among these, the dicobalt assembly $[Co_2(\mu\text{-OH})_2(TACN)_2(H_2O)_2]^{4+}$ (Fig. 39a) is able to bind phosphate esters, such as dimethyl phosphate and methyl *p*-nitrophenylphosphate in aqueous solution. In the latter case, the coordination is followed by the cleavage of the P-O bond and release of *p*-nitrophenate, as sketched in Figure 39b [66]. Experiments in ^{18}O labelled water showed that the hydrolytic cleavage occurs via nucleophilic attack of a bridging oxide generated by hydroxide deprotonation [97]. The complex enhances the hydrolysis rate of the substrate of 12 orders of magnitude, as a result of both

double Lewis acid activation, due to coordination of phosphate to two electrophilic metal centres, and the formation of a strongly nucleophilic oxide anion. However, the hydrolysis rate was also found to depend on the basicity of the leaving group, decreasing with the pK_a value. Therefore, leaving group activation also cooperates in rate acceleration probably thanks to the interaction of the leaving group oxygen with the metal [98,99].
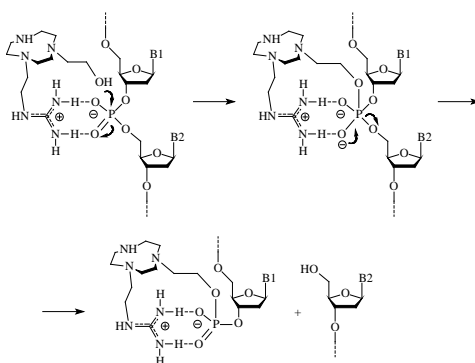

Figure 38. Proposed mechanism for DNA cleavage by L43. A similar mechanism, involving possible Zn^{2+}-assisted deprotonation of the ethanolic pendant followed by the nucleophilic attack of the R-O-generated function is also suggested its Zn^{2+} complex **41**.
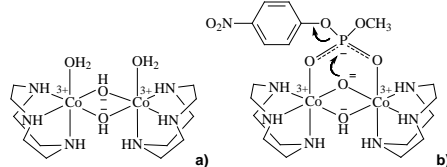

Figure 39. Sketch of the $[Co_2(\mu\text{-OH})_2(TACN)_2(H_2O)_2]^{4+}$ (a) and proposed mechanism for catalysed hydrolysis of methyl *p*-nitrophenyl phosphate (b).

This analysis has been also extended to less charged and acidic metal ions, such as Cu^{2+} and Zn^{2+}. The dinuclear Cu^{2+} complex with ligand L44 [100], containing two TACN macrocycles linked by a 1,8-dimethylnaphthalene unit, was able to hydrolyse ApA to adenosine, 2'-AMP and 3'-AMP (k_{OBS} = 4.2·10^{-7} s^{-1} at pH 7.3 and 50 °C) as well as 2',3'-*c*AMP to 2'-AMP and 3'-AMP (k_{OBS} = 2.2·10^{-4} s^{-1} at pH 6 and 25 °C) several hundreds times more faster than the mononuclear Cu^{2+} complex with TACN. The active species in the hydrolysis of both substrates was found to be the monohydroxo complex, as sketched in Figure 40. In both cases, the simultaneous participation of both metals in phosphate binding implies a double Lewis acid nucleophile activation in the overall cleavage mechanism (Fig.s 40a,b). While in the case of ApA, the formation of both 2'-AMP and 3'-AMP suggests that the 2'-hydroxyl group of the dinucleotide acts as intramolecular

nucleophilic catalyst (Fig. 40a), in *c*AMP the nucleophilic attack is given by the metal-bound hydroxide group (Fig. 40b).

This study has been extended by Morrow and co-workers to the triphosphate m7GpppG and GpppG by using the Cu^{2+} complexes with the bis-TACN derivatives L45-L48 [101,102]. While m7GpppG is fluorescent and can be used to study the binding of triphosphate to the Cu^{2+} complexes, exploiting the dependence of its fluorescence emission on Cu^{2+} complex concentration, GpppG is an optimal model system of 5'-cap structure of RNA and can be used to analyse the hydrolytic ability of the complexes. It was shown that the dinuclear complexes can form adducts with these model systems with both complex to triphosphate 1:1 and 2:1 stoichiometry. The analysis of the hydrolysis of GpppG at pH 7.3 and 37 °C showed that the dinuclear complexes with ligands L45 and L46 containing the xylyl spacers resulted the most efficient, being able to hydrolyse GpppG to GMP and GDP *ca* 100 times faster than the [Cu(TACN)]$^{2+}$ complex. The dinuclear complexes hydrolysed GpppG more efficiently through the formation of 2:1 complex-GpppG adducts [102]. Noteworthy, L45 is known for the formation of a [Cu$_2$L45(μ-OH)$_2$]$^{2+}$ complex [103], containing bridging hydroxide anions, normally considered scarcely nucleophilic agents, due to the low pK_a value for their formation upon metal-bound H$_2$O deprotonation. The authors proposed that binding of Cu^{2+} to a multidentate triphosphate chain may change the metal coordination environment, thus also changing the pK_a of the Cu-OH units.
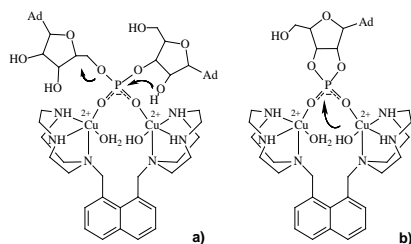

Figure 40. Proposed mechanism for the hydrolysis of ApA (a) and *c*AMP (b) by the dinuclear Cu^{2+} complex with L44.

Most likely, the activation of the triphosphate chain by four Cu^{2+} ions is followed by the delivery of a Cu-OH group to the triphosphate chain to promote the hydrolysis in the overall catalytic mechanism.

Spiccia *et al.* analysed the hydrolytic ability toward the phosphate ester bond of BNP of the dinuclear Cu^{2+} complexes with ligand L45 as well as the structurally isomeric ligand L49 containing an *o*-xylyl bridge replacing the *m*-xylyl unit of L45 [104]. Interestingly enough, only the complex with L49 induced a significant increase (*ca* 20-fold) of the BNP hydrolysis rate at 50 °C and pH 7.4 with respect to [Cu(TACN)]$^{2+}$ (k_{OBS} = 52·10^{-7} s^{-1} and 2.5·10^{-7} s^{-1}, respectively), while the complex with L45 produced a mere 4-fold increase (k_{OBS} = 8.6·10^{-7} s^{-1}), in agreement with the presence in solution at neutral pH of a scarcely nucleophilic [Cu$_2$L45(μ-OH)$_2$]$^{2+}$ complex. In the case of

the L49 complex, the shortness of the *o*-xylyl link between the two TACN units would prevent the formation of the [Cu$_2$(μ-OH)$_2$]$^{2+}$ core, making the L49 binuclear complex active in the hydrolytic process through the formation of more nucleophilic Cu-OH species.

Beside DNA/RNA models, binuclear complexes with Cu^{2+} have also been used for binding and cleavage of DNA .This is the case of the dicopper complex with L50, in which each Cu^{2+} ion is bound by a single TACN unit, while both phenol hydroxyl groups deprotonate upon bridging coordination to the two metals, affording a [Cu$_2$L50(-H)$_2$]$^{2+}$ complex [105].

The complex significantly interacts with calf-thymus DNA, with a binding constant of 1.0·10^5 M^{-1}. Binding to DNA induces hypochromism in the UV absorption band of phenol at 220 nm and also partially displaces intercalated ethydium bromide. This suggested a moderate intercalative binding mode of the complex, *via* the rigid methylphenol moieties. The complex fast cleaves the form I of the pBR322 DNA plasmid to forms II and III in aerobic conditions.
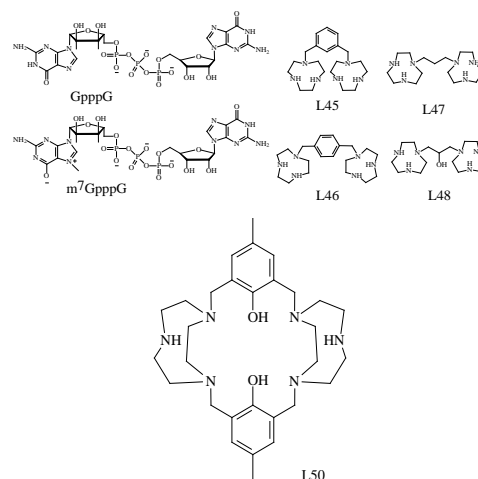
The cleavage is not inhibited by DMSO and SOD, optimal scavengers for the hydroxyl radical and superoxide, respectively, while L-histidine, which rapidly reacts with singlet oxygen, partially decreases strand scission. On these bases, the authors suggest an oxidative pathway specifically involving the formation of singlet oxygen.

More recently, Montagner and Erxleben reported a dinuclear Cu^{2+} complex with ligand L51 (**42**), containing a single *p*-methylphenol linker between two TACN units [106]. Similarly to the copper complex of L50, each Cu^{2+} ion is bound to a TACN unit, while the deprotonated phenolate group and a hydroxide anion bridge the two metals (Fig. 41a). Differently from [Cu$_2$L50(-H)$_2$]$^{2+}$, **42** cleaves the DNA plasmid pUC19 *via* a hydrolytic mechanism not involving oxygen radical species. The analysis of the hydrolysis of the *bis*(2,4-dinitrophenyl)phosphate, BDNPP, to give (2,4-

dinitrophenyl)phosphate and 2,4-dinitrophenate showed that the cleavage mechanism occurs *via* a nucleophilic mechanism involving the coordination of phosphate to a Cu^{2+} ion followed by the nucleophilic attack of the bridging hydroxide to phosphorous (Fig. 41b).

The results described above with Cu^{2+} and Co^{3+} complexes outline that the simultaneous interaction and activation of the phosphate groups with both metal cations play a crucial role in determining the hydrolysis ability of dinuclear complexes.

Among dinuclear complexes, much attention has been devoted to the cleavage processes promoted by Zn^{2+} complexes, due to the presence of this metal in most hydrolytic enzymes.

An appropriate way to investigate the role of the distance between two metal ions can be the analysis of the ability in phosphate ester bond cleavage by Zn^{2+} complexes with ligands containing two metal binding units kept at almost fixed distances by rigid aromatic spacers. This is the case of ligands L15 and L16 (*vide supra*): while in L15 the macrocyclic moieties are held at close distance by the short quinoxaline linker, L16 contains two [9]aneN$_3$ units *ca* 9 Å far apart [107]. Both ligands form dinuclear Zn^{2+} complexes in which each metal is bound by a single macrocyclic unit, although, in the case of the L16 complexes, one phenanthroline nitrogen atom is also involved in metal coordination. For both ligands, the formation of dinuclear complexes is accompanied by simultaneous deprotonation of metal-bound water molecules to give up to trihydroxylated dinuclear species.

L51
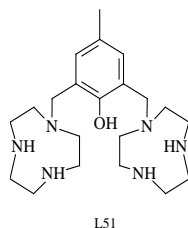
In the case of the dinuclear complex with L16, the simultaneous deprotonation of two coordinated water molecules occurs at slightly alkaline pH values to give the $[Zn_2L16(OH)_2]^{2+}$ and $[Zn_2L16(OH)_3]^+$ species and the formation of the monohydroxo complex $[Zn_2L16(OH)]^{3+}$ is not observed. Both the $[Zn_2L16(OH)_2]^{2+}$ and $[Zn_2L16(OH)_3]^+$ complexes are able to cleave BNP, affording MNP and phosphate. The dinuclear complexes with L15 show a different behaviour. In fact, the $[Zn_2L15(OH)]^{3+}$ and $[Zn_2L15(OH)_2]^{2+}$ are totally unable to hydrolyse BNP. This is likely due to the quinoxaline bridge, that keeps at short distance the two zinc(II)-[9]aneN$_3$ units, favouring the assembly of scarcely nucleophilic $Zn_2(\mu\text{-}OH)$ or $Zn_2(\mu\text{-}OH)_2$ units, embedded and shielded by the cavity delimited by the two macrocyclic moieties and the aromatic linkage. Conversely, the tri-hydroxo $[Zn_2L15(OH)_3]^+$ complex displays an impressive hydrolysis rate constant in BNP cleavage of $4.3 \cdot 10^{-5}$ M^{-1} s^{-1} at 35 °C. The tri-hydroxo complex $[Zn_2L15(OH)_3]^+$ is almost two orders of magnitude more active than the corresponding L16 one [107].

The pK_a value (9.0 log units) for the formation of $[Zn_2L15(OH)_3]^+$ is too high to be ascribed to a bridging hydroxide anion and can be related to the formation of a single-metal bound OH$^-$ function. Therefore, this species is expected to possess a more nucleophilic character than $[Zn_2L15(\mu\text{-}OH)]^{3+}$ and $[Zn_2L15(\mu\text{-}OH)_2]^{2+}$. The high activity in BNP cleavage of $[Zn_2L15(OH)_3]^+$, however, cannot simply be due to the enhanced nucleophilicity of a Zn—OH function, since the pK_{a3} value for $[Zn_2L15(OH)_3]^+$ is equal or similar to those reported for the dinuclear complex $[Zn_2L16(OH)_3]^+$.
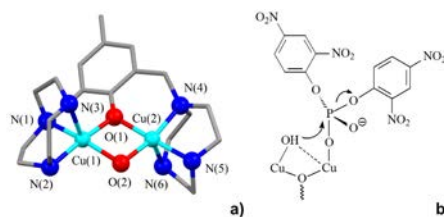

Figure 41. Crystal structure of **42** with atom numbering scheme (a) and proposed mechanism for BDNPP hydrolysis (b).

Semiempirical PM3 calculations carried out on $[Zn_2L15(OH)]^{3+}$, $[Zn_2L15(OH)_2]^{2+}$ and $[Zn_2L15(OH)_3]$ showed that the former two complexes feature each Zn^{2+} coordinated to the nitrogen atoms of a [9]aneN$_3$ moiety with one or two, respectively, OH$^-$ groups bridging the two metal ions, while the $[Zn_2L15(OH)_3]^+$ species still contains a bridging hydroxide anion (Fig. 42) but, at the same time, two OH$^-$ groups, are bound to a single Zn^{2+} ion [107]. The rather rigid molecular architecture of L15, which contains two [9]aneN$_3$ binding units at only slightly variable distance from each other, allows the two Zn^{2+} ions to be placed at an optimal distance to achieve a strong interaction and activation of the substrate, through a bridging interaction of BNP with both the two electrophilic metal centres (Fig. 43).

At the same time, the binding of the third hydroxide leads to the detachment of one bridging OH$^-$ from one of the metals, giving rise to a more open conformation of the complex, which leaves catalytic sites accessible on the two metal ions, while the two singly bound hydroxide groups are available to act as nucleophiles in the overall cleavage mechanism (Fig. 43) [107].

The ability of the dizinc complex with L14 (*vide supra*) to bind and cleave DNA has been tested by Liu and coworkers [108]. L14 displays a molecular architecture similar to L15 and L16, with a 2,6-dimethylpyridine spacer linking two TACN units. The complex displays a binding constant for calf thymus DNA in aqueous solution at pH 6.8 30-fold higher than the $[Zn(TACN)]^{2+}$ complex. At the same time, the dinuclear complex with L14 cleaves the supercoiled DNA plasmid PUC 19 to give the II and III forms much faster than the $[Zn(TACN)]^{2+}$ (the pseudo first order rate constants are 0.139 h^{-1} and 0.0425 h^{-1}, respectively, at 37 °C and pH 6.8). This suggested a cooperative role of the two metals in the cleavage process, probably through the simultaneous interaction of both metals with a phosphate group. Interestingly enough, the higher values of the hydrolysis

rate are found at slightly acidic pH values (pH 6-6.8). The rate constants decrease as the pH increases from 6.8 to 9. The authors suggest that at slightly acidic pH values the monohydroxo complex $[Zn_2L14(OH)]^{3+}$, containing a single nucleophilic Zn-OH function, would be present in solution. By increasing the pH, the formation in solution of the less charged $[Zn_2L14(OH)_2]^{2+}$ and $[Zn_2L14(OH)_3]^+$ species, as previously found by Lippolis and Bencini [107], would decrease the interaction of the Zn^{2+} ions with phosphate, leading to a consequent decrease of the hydrolysis rate.
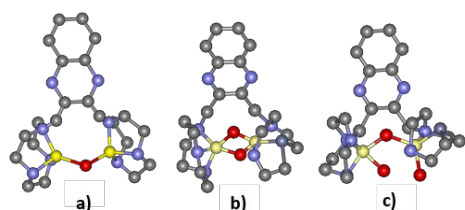

Figure 42. Calculated structure (PM3 level) of the $[Zn_2L15(OH)]^{3+}$ (a), $[Zn_2L15(OH)_2]^{2+}$ (b) and $[Zn_2L15(OH)_3]^+$ (c) complexes.
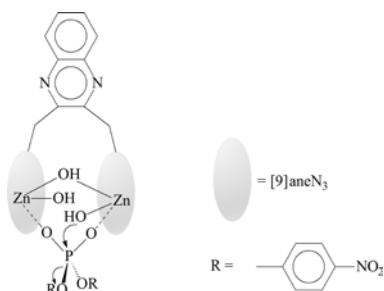

Figure 43. Proposed mechanism for BNP cleavage promoted by the $[Zn_2L15(OH)_3]^{4+}$ complex. Charges are omitted for clarity.

Taking inspiration from Nature, where the metal binding sites are inserted in proteic structures, Scrimin *et al.* inserted two TACN-functionalized R-amino acids in a helix-forming peptide [109].

Despite its short sequence, the resulting heptapeptide L52 was found to assume a 3_{10}-helical conformation in aqueous solution at pH 8, which is lost only at acidic pH values (pH 3.5). L52 forms a stable dinuclear Zn^{2+} complex in aqueous solution, which shows clear evidence of cooperativity between the two metal ions in the transesterification reaction of HPNP. The dinuclear complex is more active than the mononuclear complex with TACN, the rate constant for transesterification ($k_{OBS} = 21.0 \cdot 10^{-6}$ s^{-1} at pH 7) being *ca* 3-fold higher than that found for the Zn^{2+} complex with TACN ($k_{te} = 7.0 \cdot 10^{-6}$ s^{-1}). On the contrary, the dinuclear complex with L53, which still contains two TACN units but lacks any specific conformation, is less active than $[Zn(TACN)]^{2+}$. The proposed mechanism for the transesterification, shown in Figure 44, points out a clear cooperativity between the two metals in the overall catalytic process. Basically, the defined secondary structure of L52 organizes the two Zn-TACN units at an optimal distance (6.3 Å, calculated from molecular models) to allow the simultaneous binding of phosphate to one metal ion and the activation of the hydroxyl groups, which deprotonate upon interaction with the second Zn^{2+} ion, to give an intramolecular nucleophilic attack at phosphorous.

L52

L53
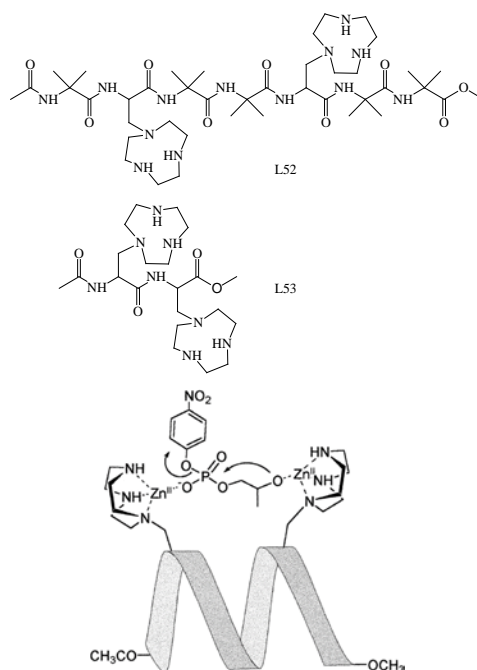
Figure 44. Proposed mechanism for HPNP transesterification promoted by the dizinc complex with L52. Reprinted with permission from Ref. 109 Copyright © 1999, American Chemical Society.

The dizinc(II) complex with L52 resulted also able to cleave plasmidic DNA, *via* the formation of hydrolytically active TACN-bound Zn-OH hydroxo complexes [110].

Among dinuclear Zn^{2+} complexes, the complex with ligand L48, designed by Morrow and coworkers, has been probably the most investigated in search of cleaving agents for the phophodiester bond [93,111-115]. The ligand features two TACN units linked by a hydroxypropyl spacer and can form a stable dinuclear Zn^{2+} complex, in which each metal is coordinated by a macrocyclic triamine and the bridging deprotonated hydroxyl group (Fig. 45) [93]. As a result, the two metals are separated by 3.66 Å, an optimal distance to cooperate in phosphate binding.

Furthermore, it was shown that a Zn^{2+} water molecule deprotonates at slightly alkaline pH values (pK_a = 8.0) affording a $[Zn_2(L48(-H))OH]^{2+}$ complex (**43**) [93]. The dizinc(II) complex is able to catalyse the cleavage of the phosphate ester bond in HPNP transesterification. Michaelis-Menten analysis afforded a k_{cat} value of $4.1 \cdot 10^{-3}$ s^{-1} in aqueous solution at pH 7.6 and 25 °C [93].

The complex results to be a far better catalyst than the mononuclear complex with L42 at pH 7.6, which features a higher pK_a value (9.1) and a lower k_{cat} ($1.2 \cdot 10^{-4}$ s^{-1}) [93]. Interestingly enough, the authors also compared the ability of **43** in cleaving HPNP and the oligoribonucleotide A_6, containing six adenosine moieties, with that of corresponding complexes with the binucleating ligands L16, L42 and 1,5-bis(1,4,7-triazacyclonon-1-yl)pentane, containing a pentane flexible bridge between two TACN units [112].
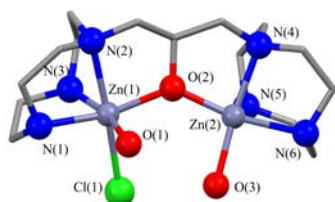

Figure 45. Crystal structure of the $[Zn_2(L48(-H))Cl(H_2O)_2]^{2+}$ complex.

While the dizinc complex with L48 increases 120-fold the rate acceleration in HPNP transesterification with respect to the $[Zn(TACN)]^{2+}$ complex, the cleavage by the other Zn^{2+} dinuclear complexes is only 3-5-fold accelerated at pH 7.6 and 25 °C. Similarly, the complex is by far the most active in the cleavage of the oligonucleotide at pH 7.5 and 37 °C [112].

These results suggested that the two Zn^{2+} cations act cooperatively in the cleavage process. The two metal ions cooperative rate enhancement at neutral pH could be due to several factors, including enhancement in substrate binding by cooperation of the two metals, transition state stabilization due to increased electrostatic interaction between the dianionic substrate with the cationic complex and, finally, lowering of the metal-bound water pK_a, with consequent increase of the percentage of the monohydroxo species **43** present in solution. The latter, in fact, could act as a base catalyst favouring the deprotonation of HPNP *via* a proton transfer process from its hydroxyl group to the catalyst (Fig. 46) [93,112,113].

However, the mechanism initially proposed and depicted in Figure 46 has been subject of debate. The kinetic mechanism of HPNP has been successively revised and elucidated by Hengge and Morrow on the light of the analysis of kinetic isotopic effects (KIE), measured by using isotopically marked HPNP esters (Fig. 47) [114]. In this study, the authors showed that the deprotonation of the nucleophilic hydroxyl group occurs in a pre-equilibrium step, ruling out a general-base mechanism, in which deprotonation is concerted with nucleophilic attack.

Conversely, a specific-base mechanism occurs in the successive rate-determining step, which involves concerted nucleophilic attack of deprotonated hydroxyl group at phosphorous and leaving group departure. This study does not completely clarify, however, the interaction mode of deprotonated HPNP with the catalyst.

From this point of view, kinetic measurements carried out on the uridine-containing RNA model (uridine 3'-(4-nitrophenyl)phosphate) in D_2O solution showed the absence of any primary solvent deuterium isotopic effect, indicating, once again, that in the transesterification process deprotonation of the ester occurs prior to rate-determining cleavage, and rules out a possible proton transfer process from UpPNP to the catalysts in the rate-determining transition state.
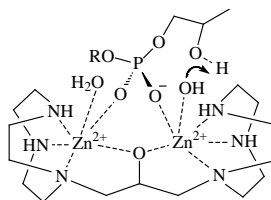
Figure 46. Proposed mechanism for HPNP transesterification catalysed by **43**.
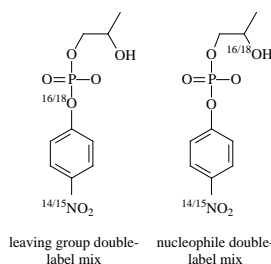
Figure 47. Sketch of the isotopically marked HPNP substrates used to elucidate the cleavage mechanism catalyzed by **43**

On these bases it was also proposed that most of the observed rate acceleration is due stabilization of the transition state *via* electrostatic interactions between the cationic dizinc complex and UpPNP [115]. Intramolecular tethering of two metal ions at the macrocyclic ligands across the bridging alkoxide ion would have the effect of generating a highly positively charged core of unusual catalytic activity, able to stabilize the transition state *via* solely electrostatic interactions.

This could also apply to HPNP cleavage. However, HPNP is less bulky than UpPNP and can bind closely to the cationic core to achieve stabilization of the transition state. Interaction of UpPNP with the catalyst could be less effective, perhaps due to steric interactions between the catalyst and non-reacting portions of this substrate [111].

The mechanism of HPNP and, in particular, the interaction mode of the phosphate group with Zn^{2+}, was further elucidated on the light of DFT calculations by Phillips and Zhao, that confirmed the specific-base concerted mechanism found by Hengge and Morrow, and overall, pointed out that the phosphate group tightly interacts with the dizinc core *via* a bridging coordination [116]. Interaction of the hydroxyl group of HPNP with a Zn^{2+} ion is also envisaged (Fig. 48).
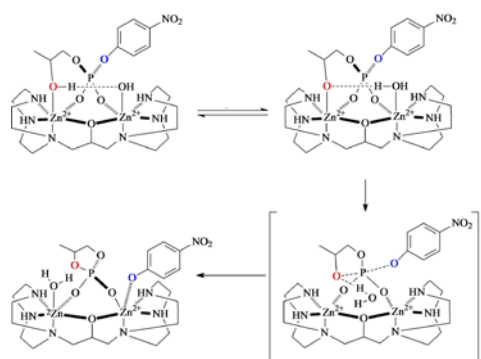

Figure 48. Concerted mechanism for HPNP cleavage catalyzed by 43 involving first a pre-equilibrium in which the hydroxyl group deprotonates, followed by the rate-determining step featuring concerted nucleophilic attack of the deprotonated hydroxyl group to phosphorous and detaching of the leaving group.

Complexes with ligands capable to bind more than two metal ions have also been developed to obtain more efficient receptors for phosphate anions. This is the case of ligand L54, which contains three TACN units in a tripodal arrangement [117]. The ligand is able to bind three Cu^{2+} and Mn^{3+} ions, whose complexes with HPO_4^{2-} and, in the case of the Cu^{2+} complex, $HAsO_4^{2-}$, were isolated and structurally characterized. The crystal structure of the HPO_4^{2-} complex shows the phosphate anion bridging the three Cu^{2+} centres (Fig. 49). Preliminary studies showed that this complex is able to catalyse the hydrolysis of 4-nitrophenylphosphate with a greater efficiency than its mononuclear TACN analogue.

Polynuclear complexes can also be obtained by inserting TACN units in oligopeptide chains through an appropriate spacer. Scarso and Scrimin appended to the tripodal ligand tren (tren = tris(2-aminoethyl)amine) three equal heptapeptides featuring a 3_{10} helical conformation. In each polypeptide chain the L55 amino acid was inserted in order to append a TACN unit as a lateral side arm [118]. The resulting ligand L56 can bind up to four Cu^{2+} or Zn^{2+} metal cations. The acetylated derivative of L55, L57, was also synthesized for comparison purposes in the kinetic study.

Binding of the metals to the tren-based ligand induces a change from an open to a closed conformation in which the three short peptides are aligned in a parallel manner with the

azacyclononane units pointing inward within the pseudocavity they define (Fig. 50).

The tetranuclear Zn^{2+} complex with L56 was found able to catalytically hydrolyse HPNP. Michaelis-Menten analysis of the rate constants determined in the presence of increasing amount of the substrate gave $k_{cat} = 3.9 \cdot 10^{-4}$ s^{-1} at pH 7 and 40 °C [118]. The cleavage rate increases with Zn^{2+} concentration, e. g., with the number of Zn^{2+} ions bound to L56, suggesting that the metal ions play a cooperative in substrate cleavage. The transesterification rate was found up to 50-fold higher than that observed for the Zn^{2+} complex with the acetylated amino acid L57. The increased cleavage efficiency is likely to be due to the presence of a binding pseudocavity and a catalytic site for the substrate. The metal centres not only are involved in the binding but also in the catalytic process.
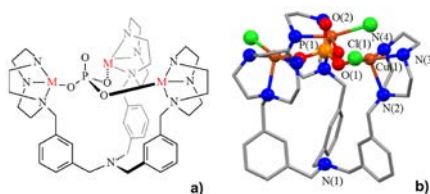
Figure 49. Drawing of ligand L54 (a) and crystal structure of the $[CuCl_3(\mu_3-HPO_4)L54]^+$ cation (b).
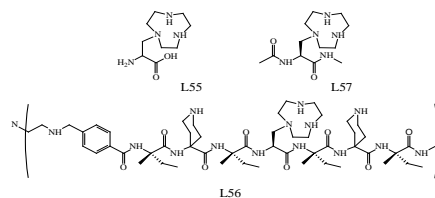
The cleavage can occur either *via* direct coordination of the HPNP hydroxyl to a Zn^{2+} ion, resulting in a decrease of its pK_a, thus allowing the formation of its conjugate base or *via* a general base catalytic mechanism, involving a Zn-OH function as base for deprotonation of the alcoholic function, that then would become available for intramolecular transesterification. Interestingly enough, the addition of Zn^{2+} to a solution of L56 and the formation of the tetranuclear complex causes a decrease of the cleavage ability of the ligand toward a linear 29-mer RNA substrate at pH 7.0 and 37 °C. Polyamines are known for their ability to cleave RNA, exploiting the presence of intramolecular acid-base cooperation of neutral amines and ammonium cations present in solution at pH 7.

The decreased cleavage activity was interpreted in terms of the closed conformation formed in the presence of Zn^{2+} ions, which would prevent the interaction of the TACN macrocycle with the

RNA phosphate groups. Therefore, while in the case of HPNP Zn^{2+} acts as a positive allosteric effector by enhancing the catalytic efficiency of the system, in the case of the polyanionic RNA substrate, Zn^{2+} switches off the cleavage activity, behaving as a negative allosteric regulator [118]. To confirm the positive allosteric role of the Zn^{2+} cations in HPNP cleavage, Scrimin and coworkers also synthesized simpler tren-based systems containing a single peptide bond that links the TACN unit to tren (L58-L60) [119]. A 1,4-disubstituted benzene was also inserted as spacer to avoid the collapse of the arms, which would result in inactive complexes. The only difference between L59 and L60 is the acetylation in the latter on the secondary amines of tren, which prevents metal binding in this site. Since tren possesses a better binding ability towards Zn^{2+} than TACN, the first metal is expected to bind to the tren unit of L58 and L59 and coordination to the TACN units is accomplished only in the presence of four Zn^{2+}.
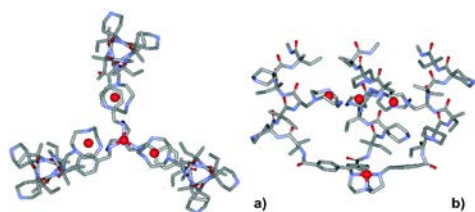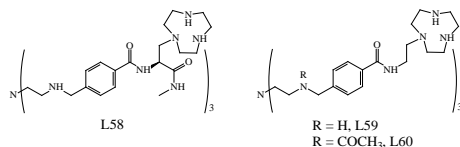

Figure 50. Molecular model of the tetranuclear Zn^{2+} complex with L56: top (a) and side (b) views. Copyright © 2002, The National Academy of Sciences.

As a matter of fact, in the case of L58 and L59, the cleavage rate of HPNP increases in the presence of increasing amounts of Zn^{2+} in solution, with a more marked enhancement when four equivalents of Zn^{2+} are added. This is not the case of L60, which shows a much lower activity in HPNP cleavage in the presence of the metal and no increase when four eq. of Zn^{2+} are added. These results showed that in the cleavage of HPNP by the Zn^{2+} complexes with L58 and L59 the first metal ion has a structural (allosteric) function, generating a tripodal pseudocavity where the substrate can be hosted, while the remaining three Zn^{2+} ions play a functional (catalytic) role, cooperating in the acceleration of the transesterification process (Fig. 51).

Beside tren-based oligopeptides, polypeptide chains containing two or four TACN units (L61-L63 in Fig. 52a) were also synthesized for HPNP hydrolysis [120]. Once again, four (L61) or two (L62 and L63) TACN units were appended to the polypeptide chain by inserting the TACN-containing L55 amino acid. Furthermore, the L55 amino acids (ATAMP in Fig. 52, ATAMP = *(S)*-2-Amino-3-[1-(1,4,7-

Triazacyclononane)]Propanoic Acid) were located in the appropriate positions to allow the TACN units to face each other within the same helix or between the two helices. The three polypeptides where appropriately designed to fold in a hairpin helix-loop-helix motif, which was actually found in solution for all three systems (see Fig. 52b for the L61 case).
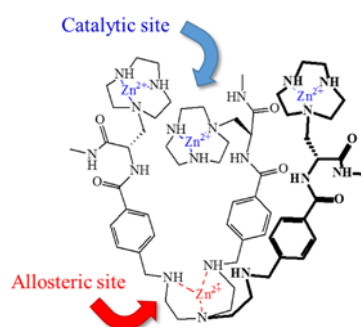
Figure 51. Suggested role of metal ions in the HPNP cleavage by the complexes with L58 and L59.

Ac-N-A-A-D-Nle-E-A-A-I-K-**ATANP**(11)-L-A-E-**ATANP**(15)-Nle-A-A-K-
-G-P-V-D-
H_2N-G-A-R-A-F-A-E-F-**ATANP**(34)-K-A-L-**ATANP**(30)-E-A-Nle-Q-A-A-
L61

Ac-N-A-A-D-Nle-E-A-A-I-K-A(11)-L-A-E-R(15)-Nle-A-A-K-
-G-P-V-D-
H_2N-G-A-R-A-F-A-E-F-**ATANP**(34)-K-A-L-**ATANP**(30)-E-A-Nle-Q-A-A-
L62

Ac-N-A-A-D-Nle-E-A-A-I-K-A(11)-L-A-E-**ATANP**(15)-Nle-A-A-K-
-G-P-V-D-
H_2N-G-A-R-A-F-A-E-F-R(34)-K-A-L-**ATANP**(30)-E-A-Nle-Q-A-A-
L63   a)
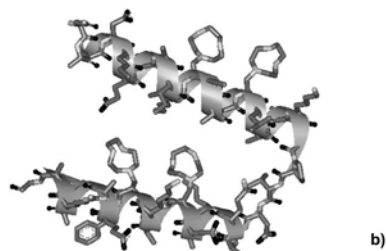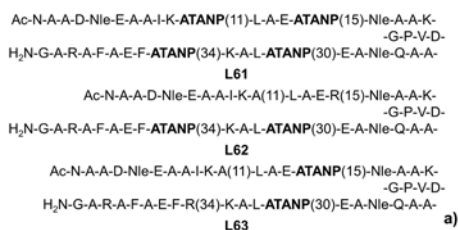
Figure 52. Amino acid sequences of polypeptides L61-L63 (ATANP = L55) (a) and helix-loop-helix conformation likely adopted by L61. Adapted from Ref. [120] with permission from John Wiley and Sons. Copyright © 2004.

All three complexes were able to accelerate HPNP cleavage in aqueous solution at 37 °C [120]. The transesterification reaction was found dependent on the number of Zn^{2+} ions coordinated by the polypeptides and the tetranuclear Zn^{2+} complex with L61 resulted the most active, with second order rate constant k =

0.16 $M^{-1} s^{-1}$ and 380-fold acceleration of substrate cleavage in saturation conditions. The authors suggest a cooperative role between (at least two) metal ions with a mechanism which is likely to require activation of the nucleophilic hydroxyl group of HPNP and its facilitated attack to phosphate *via* its interaction with at least a single metal cation [120].

2.3 Nanostructured systems.

A common strategy to achieve cooperativity between metal cations in substrate binding and activation is their assembly in multivalent structures able to develop multiple single interactions with a target substrate. To the purpose of generating multivalent tools for DNA/RNA and their mimics cleavage, TACN units have been recently linked to dendrimers, gold nanoparticles and polymers, which will be discussed hereafter.

Reaction of gold nanoparticles (NPs) protected with a monolayer of 1-sulfanyloctane with a TACN derivative (L57) containing an alkyl chain functionalized with the thiol group at its end, by using the site exchange procedure [121] yielded the functionalized NPs AuNP1-TACN [122].

Cu^{2+} binding by TACN gives rise to an absorption band at 648 nm, which can be spectrophotometrically monitored and used to determine the concentration of the macrocyclic units in solutions containing the functionalized NPs.

AuNP1-TACN
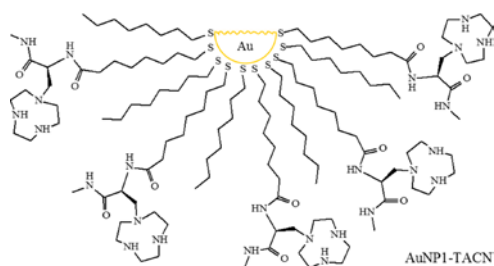
Binding of Zn^{2+} leads to a polyfunctional system able to cleave HPNP in aqueous solution at pH 7.4 and 40 °C. The plot of the observed rate constants as a function of the eq. of Zn^{2+} added to the solution of NPs (Fig. 53a) shows that the maximum activity is found when the system is fully loaded with Zn^{2+}, e. g. in the presence of 1 eq. of the metal (normalized for the number of TACN units present in the catalyst).

The rate acceleration measured upon the addition of increasing amounts of Zn^{2+} up to saturation shows a sigmoidal behaviour, with a clear enhancement of the cleavage hydrolysis after the addition of the first 30% of Zn^{2+} ions. This result suggests a cooperativity between metal ions, likely involving a couple of TACN-bound metal ions in the transesterification process (Fig. 54) [70,109].

Michaelis-Menten analysis of the rate constants gave k_{cat} and K_M values of $4.2\cdot10^{-3} s^{-1}$ and 0.93 mM, respectively. The activity of the full loaded NPs, normalized for the number of metal centres present in the catalyst, resulted 600-times higher for the

mononuclear Zn^{2+} complex with L57, which corresponds to the TACN binding unit linked to the NPs. The pH dependence of cleavage rate was also evaluated (Fig. 53b) allowing for the determination of the pK_a of the Zn^{2+}-bound water molecules on the NPs. Its values, 7.4, was 0.4 log units lower than that found for the Zn^{2+} complex with TACN [109].
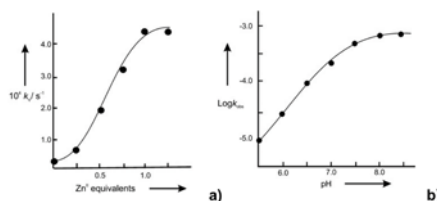

Figure 53. Dependence of the rate constant for the cleavage of HPNP by AuNP1-TACN on the amount of Zn^{2+} ions (40 °C, pH 7.5, [AuNP1-TACN] = 0.1 mM) (a) and of the rate of cleavage of HPNP by Zn^{2+}- AuNP1-TACN as a function of pH (40 °C, [Zn^{2+}- AuNP1-TACN] = 0.1 mM). Adapted from Ref. [122] with permission from John Wiley and Sons. Copyright © 2004.
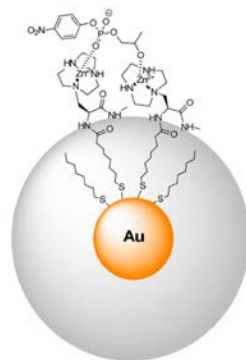
Figure 54. Proposed mechanism for HPNP cleavage by TACN functionalized Au NPs. Reprinted from Ref. [70] (CC BY 4.0 license).

This would increase the concentration of Zn-OH function available for the catalytic process, which is likely to involve facilitated deprotonation of the hydroxyl group of the nucleophile. These results clearly outline cooperativity between at least two Zn^{2+}-bound TACN units. The NPs were found also able to greatly enhance the cleavage of dinucleotides, such as ApA (second-order rate constants $3.0\cdot10^{-4} s^{-1} M^{-1}$), CpC ($3.6\cdot10^{-4} s^{-1} M^{-1}$) and UpU ($1.2\cdot10^{-2} s^{-1} M^{-1}$), with the greater rate enhancement observed for UpU.

Following this approach, Au NPs functionalized with TACN derivatives differing on the length of the linker between the macrocyclic unit and the NP, have also been prepared (AuNP2-TACN – AuNP5-TACN) [58,123].

AuNP3-TACN and AuNP4-TACN possess linkers with the same length, but differ for the presence in AuNP4-TACN of two

oxygen atoms replacing two methylene groups of AuNP3-TACN. The cleavage rate of HPNP in the presence of Zn^{2+} occurs *via* Michaelis-Menten kinetics and is strongly affected by the spacer, as shown in Figure 55 [123]. In fact, the activity of the NPs coated with longer alkyl-spaced TACN units, AuNP3-TACN and AuNP5-TACN, in the presence of Zn^{2+} is substantially higher than that of AuNP2-TACN. Finally, despite the equal length of the spacers in AuNP3-TACN and AuNP4-TACN, the latter is remarkably less active at any Zn^{2+} concentration.

Analysis of the cleavage at different Zn^{2+}/AuNP-TACN ratio showed a sigmoidal rate increase with Zn^{2+} concentration and provided evidences for the involvement of two Zn^{2+}-TACN complexes in the catalytic process. Therefore, these systems allow the self-assembly of the bimetallic catalytic sites for substrate interaction (Fig. 56). At the same time, the reactivity is modulated by polarity. The insertion of longer alkyl chains leads to the obtainment of a microenvironment with a polarity lower than that of bulk water. In such conditions the ability of the metal ions to stabilize, most likely by electrostatic/coordinative interactions, the dianionic transition state formed during HPNP cleavage is increased, and consequently, the reaction become faster. The lower activity found for AuNP4-TACN, in which the polarity of the chain is increased by the presence of ether groups, confirms this hypothesis [123].
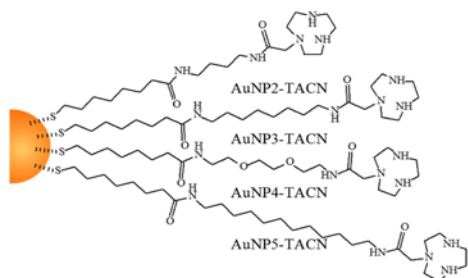
Gold NPs coated with self-assembled monolayer of enantiomerically pure thiols containing TACN macrocycles have been also synthesized and used for the binding and cleavage of chiral substrates. Prins *et al.* assembled, starting from simple dioctylamine-passivated Au NPs, the (+)-AuNP6-TACN and (-)-AuNP6-TACN (Fig. 57) systems by using as reactant the same thiol unit used for AuNP1-TACN [124].

In this case, however, the chirality of the head group was derived from the use of L or D serine in the synthesis of the TACN-functionalized thiol. To test the cleaving activity of these NPs the authors used as substrate the trifluoromethyl derivative of HPNP, indicated herein with CF_3HPNP, containing a 4-nitrophenyl group substituted by a CF_3 group at position 3 (Fig. 48). This substrate is more reactive than HPNP and features greater use flexibility when probing different reaction conditions.

Both the Zn^{2+} complexes (+)-AuNP6-[Zn(TACN)] and (-)-AuNP6-[Zn(TACN)] cleave (+)-CF_3HPNP at pH 7 and 40 °C with pseudo-

first-order rate constants of $1.1 \cdot 10^{-4}$ s^{-1} and $2.0 \cdot 10^{-4}$ s^{-1}, respectively.
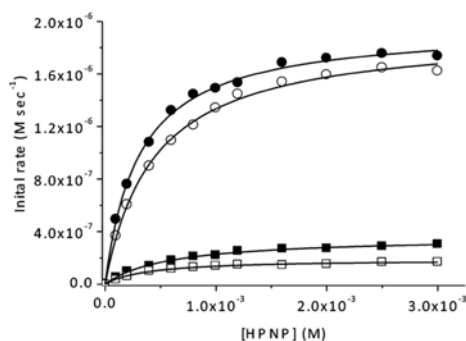

Figure 55. Rate of HPNP cleavage promoted by AuNP-TACN and Zn^{2+} as a function of the concentration of HPNP (●, AuNP5-TACN; ○, AuNP3-TACN; ■, AuNP2-TACN; □, AuNP4-TACN) ([AuNP-TACN, in TACN units] = [Zn^{2+}] = $2.0 \, 10^{-5}$ M, pH = 7.5, 40 °C). Reprinted with permission from Ref. [123] Copyright © 2014, American Chemical Society.
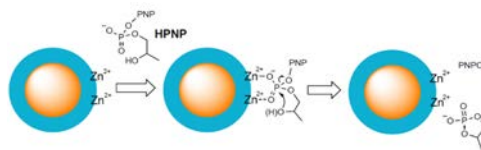

Figure 56. Proposed mechanism for HPNP cleveage in the presence of the Au NP-TACN catalyst. Reprinted with permission from Ref. [123] Copyright © 2014, American Chemical Society.

An opposite situation is found in the case of (-)-CF_3HPNP, where the better catalyst is (-)-AuNP6-[Zn(TACN)] [$k_{OBS} = 2.1 \cdot 10^{-4}$ s^{-1} *vs* $1.1 \cdot 10^{-4}$ s^{-1} for (+)-AuNP6-[Zn(TACN)]]. Both systems follow a Michaelis-Menten kinetics with a k_{cat} 38% higher in the case of the cleavage of (+)-CF_3HPNP by (+)-AuNP6-[Zn(TACN)] ($3.5 \cdot 10^{-3}$ s^{-1} *vs* $2.5 \cdot 10^{-3}$ s^{-1} for (-)-AuNP6-[Zn(TACN)] at pH 6.5 and 40 °C). Conversely, the K_M values are very similar, suggesting that the observed chiral selectivity does not originate from enantioselective binding, but is likely to be related to the stabilization of the transition state in the case of the most active (+)-AuNP6-[Zn(TACN)].

(-)-AuNP6-[Zn(TACN)] also cleaves NpN ribodinucleotides (N = A, C, G or U) at pH 8 and 40 °C [124]. The rate acceleration was higher in the case of UpU, with a second-order rate constant of $2.5 \cdot 10^{-2}$ s^{-1} M^{-1}. (+)-AuNP6-[Zn(TACN)] showed the same cleaving ability toward UpU. Interestingly, a different situation was found in the case of the Cu^{2+} complex. In fact (-)-AuNP6-[Cu(TACN)] is a better catalyst than (+)-AuNP6-[Zn(TACN)] in UpU cleavage, the second-order rate constants being $17.4 \cdot 10^{-4}$ s^{-1} M^{-1} and $4.3 \cdot 10^{-4}$ s^{-1} M^{-1} a pH 8, respectively. These results point out that NPs coated with chiral binding units can be able

to enantioselective cleavage, likely due to the assembly on the surface of NPs of chiral catalytically active pockets.
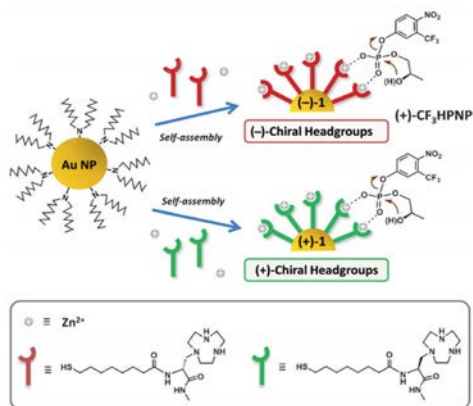

Figure 57. Schematic representation of the self-assembly of chiral thiols on the surface of dioctylamine-passivated gold nanoparticles to give (+)-AuNP6-[Zn(TACN)] and (-)-AuNP6-[Zn(TACN)], as catalyst of CF₃HPNP. Reprinted from Ref. 124 with permission from John Wiley and Sons. Copyright © 2016.

Beside Au NPs, dendrimers have been also used as multivalent systems to achieve cooperative cleavage by multiple TACN-bound metal ions. Reaction of a DAB [poly(propylene imine)] dendrimer, [a dendrimer containing a diaminobutane core and poly(propylene imine)-derived branches], with a BOC-diprotected TACN derivative containing an activated pentafluorophenylacetate ester side arm, leads to the formation of dendrimers with different degrees of functionalization after acetylation of the remaining free amine groups (indicated with D1a-D1f in Figure 58) [125]. The percentage of TACN introduced as terminal group of the dendrimer was controlled by varying the molar ratio between the two reactants.

Analysis of HPNP cleavage by D1a-D1f in the presence of increasing Zn^{2+} amounts pointed out that the pseudo first-order rate constants show a sigmoidal increase with metal concentration up to a 1:1 metal to TACN molar ratio.
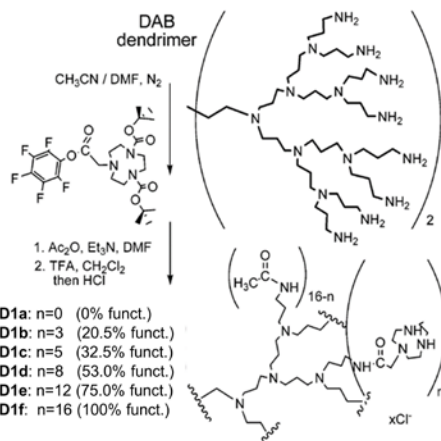
Figure 58. Adapted with permission from Ref. [125], Copyright © 2007, American Chemical Society.

Lo Schema contiene imperfezioni nei drawing originali (ad esempio una catena etilenica del TACN nel drawing in basso). . Vanno poi tolti i reagenti usati nei vari step della sintesi, lasciando solo il drawing del derivato del TACN. Va infine tolto xCl⁻ in fondo a sinistra

At the same time, as shown in Figure 59, the rate constants increase with the functionalization degree of dendrimers. Furthermore, analysis of the dependence of the rate constants on the molar fraction of TACN complex of the dendrimers pointed out that two TACN-bound metal ions are involved in the cleavage process, as sketched in Figure 60. Michaelis-Menten analysis of the hydrolysis rates gave $k_{cat} = 1.55 \cdot 10^{-2}$, a value 3.7-fold higher than that found with AuNP4-[Zn(TACN)] NPs [123]. TACN-functionalized dendrimers were also synthesized by dimerization of two equal polypeptide dendrons (D2-(TACN)₂ – D5-(TACN)₁₆) as sketched in Figure 61 [126].
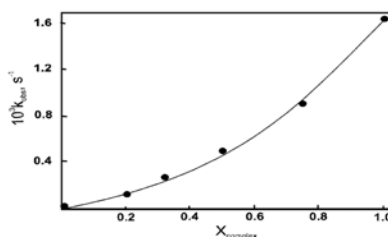
Figure 59. Observed rate constants for HPNP cleavage by dendrimers D1a–f as a function of the equivalents of Zn^{2+} added (Zn^{2+} concentration is normalized to the percentage of TACN units present on the dendrimers) at pH = 7.5 and 40 °C. Reprinted with permission from Ref. [125], Copyright © 2007, American Chemical Society.

The kinetics study of HPNP cleavage and the comparison between the transesterification ability of the different multivalent systems, performed at constant concentration of TACN, showed that the Zn^{2+} complexes formed by dendrons D2-$(TACN)_2$ – D5-$(TACN)_{16}$ and dendrimers D6-$(TACN)_4$ – D9-$(TACN)_{32}$ catalyse HPNP cleavage with enzyme-like saturation behaviour. Both k_{cat} and second order rate constants k_{cat}/K_M values increase with the dimension of dendrimers. Clustering of multiple [Zn(TACN)] units on the surface of dendrimers, indeed, generates powerful catalysts and actually dendrimer D9-$(TACN)_{32}$, in 600 nM concentration, accelerates the cleavage rate 80.000 times with respect to the uncatalysed reaction. The largely positive dendritic effect was attributed to the number of catalytic sites occupied by the substrate molecules in saturation conditions and to the efficiency of the systems to generate catalytic sites in which multiple active [Zn(TACN)] moieties can cooperatively work in substrate cleavage.

Dendrons were also anchored on solid supports and functionalized with TACN at their ends, with the purpose to achieve new materials, which could be potentially used to develop new automated protocols or exploited for solid phase synthesis. This is the case of dendrimers D10 and D11, formed by beads of resyn Tentagel MP4 or MP8, mixed polystirene-poliethyleneglycol functionalized with lysine-based dendrons, which are derivatized with TACN at their ends. The Zn^{2+} complexes with the resulting materials efficiently cleaves HPNP at pH 7 and 40 °C, following a Michaelis-Menten kinetics.
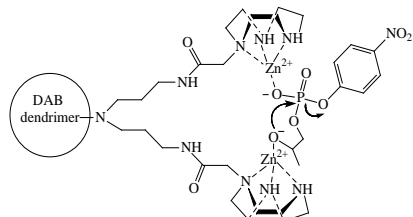
Figure 60. Suggested mechanism for HPNP cleavage catalyzed the Zn^{2+} complexes with TACN-functionalized dendrimers D1b-D1f containing
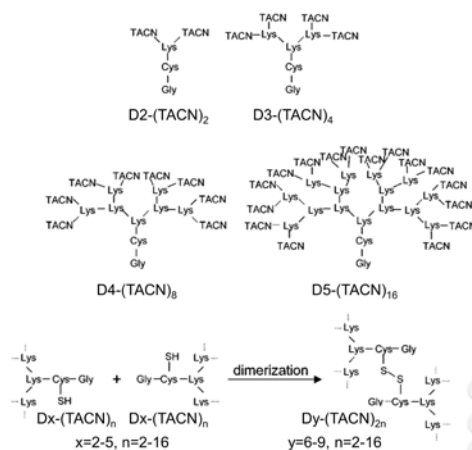
Figure 61. Adapted with permission from Ref. [126], Copyright © 2008, American Chemical Society.

The corresponding parameters k_{cat} and K_M are similar to that of the corresponding dendrons in solution, indicating that the catalytic properties are mantained when the active sites are inserted within appropriate materials [127].

Although Zn^{2+} complexes have been the most investigated, due to their almost ubiquitous presence in metallo-enzymes deputed to cleave the phosphate ester bond, attempts to use different metals have been also performed [128-131]. A recent example is given by the silica NPs SiNP1-TACN – SiNP4-TACN (Fig. 62), which contain TACN units supported to the silica NP *via* butyl or octyl linkers [131]. Ethyl or propanol blockers have been also anchored on the NP. The Cu^{2+} complexes with these NPs where tested as hydrolytic agents for BNP and Paraoxon (diethyl-4-nitrophenyl phosphate) in water at pH 7.8. SiNP3-[CuTACN] and SiNP4-[CuTACN] resulted the most efficient as hydrolytic agents for BNP and Paration, indicating that the Si NPs containing catalytic sites more exposed to the solvent give the higher rate enhancements.
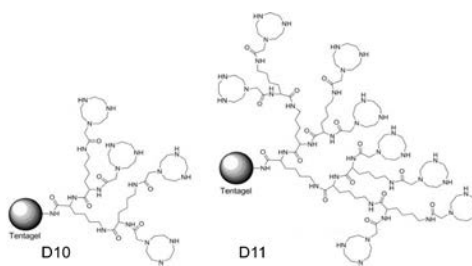
Adapted from Ref. 127 with permission from Elsevier. Copyright © 2009.
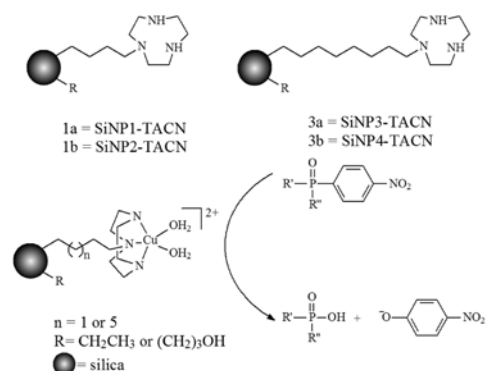
Figure 62. Schematic representation of NPs SiNP1-TACN – SiNP4-TACN (a) and sketch of the phosphate ester bond cleavage by their Cu(II) complexes.

However, these systems appear at least one order of magnitude less active than the [Cu(TACN)]²⁺ complex at pH 7.2 and 25°C, probably due to a more difficult access to the catalytic site and to inhibition by hydrolysis products that are slow to leave the NP surface.

3. Structure and Functions/Properties.

As it has already emerged from the examples described in the previous paragraphs, the design of TACN derivatives is virtually endless and, depending on the type of substituents and the metal ions coordinated, the systems obtained can be used for different applications. A selection of TACN derivatives in which the structure of the ligand or the complex is strictly related to its function is reported in this paragraph.

3.1 Luminescence.

The development of luminescent lanthanide ions complexes for bio-imaging applications has attracted considerable attention in the last decades and various reviews have been devoted to the topic [132-137]. Lanthanides exhibit unique features which are crucial for bio-imaging, such as sharp emission bands in the visible or near infra-red (NIR) regions (depending on the element), large pseudo-Stokes shifts, long decay times (> 1 ms) which allow for time-resolved measurements and a high signal-to-noise ratio [138]. TACN conformational rigidity offers the possibility to form tri-capped trigonal prismatic complexes with large lanthanide ions and numerous examples have appeared in the literature so far. In particular Parker, Maury and co-workers have reported several examples of Eu³⁺ complexes featuring TACN tris-substituted carboxylate or phosphinate derivatives to impose local C_3 symmetry to the metal [139,140]. In particular, the Eu³⁺ complex of L64 (**44**) [140] showed, interesting features such as significant higher fluorescent intensity (relative emission intensity passes from 10% in water to 75% in DMF) and lifetime (from 0.72 ms in water to 1.17 ms in DMF) by increasing solvent polarity. **44** was used to stain human liver

adenocarcinoma cells (HepG2) thanks to its high brightness and it revealed the mytochondria distribution better than the common stain MitoTracker Green (Fig. 63).

Thanks to its high molecular weight (M>500), the complex is not able to cross the inner mitochondrial membrane and shows a low mitochondrial toxicity (IC50 > 100 μM after 24 h in the MTT assay). Moreover, compared to MitoTracker Green, complex **44** is able to penetrate deeper into the cell because it does not perturb mitochondrial DNA and organelles function.

Other examples of phosphinate and carboxylate derivatives of TACN whose Eu complexes are able to stain mitochondria were reported by the same group [141].

Parker and co-workers developed a series of phosphinate derivatives containing negatively charged carboxylic or sulfonic moieties able to suppress cellular uptake or adsorption to living cells, allowing for labelling membrane receptors [139]. Indeed, as the phospholipids in the cell membrane are negatively charged, the interaction with the complexes should be disfavoured, as a result of repulsive Coulombic interactions at physiological pH. In particular, with the Eu³⁺ complex of the benzylguanine bioconjugated L65, nonspecific labelling of living HEK cells is suppressed, permitting the development of a bioassay for the G-protein-coupled receptor (GPCR) on living cells expressing the cholecystokinin-2 (CCK2) receptor. The detection of GPCR-CCK2 was evaluated in time-resolved Förster resonance energy transfer (TR-FRET) both in plate-based format and using TR-FRET microscopy. Another family of similar anionic Eu-complexes was developed to selectively stain lysosomes and measure real-time lysosomal pH in living cells [142].

The same group also reported several examples of luminescent chiral lanthanide complexes based on TACN showing the possibility to prepare enantiopure emissive complexes able to act as responsive chiral probes for application in circularly polarised luminescence (CPL) spectroscopy and microscopy [143-146]. In particular, the Eu³⁺ complexes of L66 (**45**) and L67 (**46**) in their enantiopure Δ or Λ forms were used to differentiate and detect objects using a time-gated camera, following near-UV flash excitation [147].
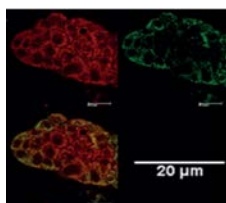

L64

L65

R = CH₂CONH(CH₂)₃SO₃⁻
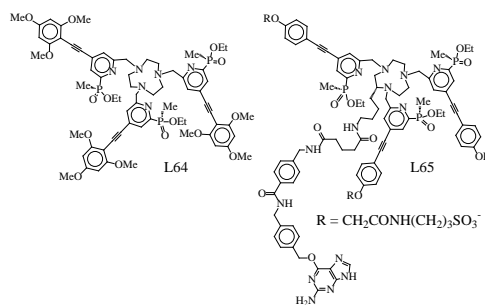
Figure 63. Complex **44** in HepG2 cells in red, showing higher definition and resolution compared to images with MitoTracker Green, and a co-localized image. Reprinted from Ref. 140 with permission from John Wiley and Sons. Copyright © 2014.

As shown in Fig. 64, chiroptical selection (i.e. separation of left and right handed circularly polarised light emitted by the two enantiomers) could be achieved using a modified time-resolved Zeiss Axiovert 200M epifluorescence microscope set-up. In particular, Figures 64a and 64b show that authors were able to demonstrate that when selecting for right circularly polarised light, the top piece of paper deposited with Λ-[**46**] is brighter than the bottom one (Fig. 64a). When using left circular polarized light (Fig. 64b) the *vice versa* is observed.

An interesting and rare example of Gd^{3+} complex exhibiting phosphorescence at room temperature was recently reported by Nakai and co-workers [148]. Crystals of the Gd^{3+} complex of L68 (**47**), as shown in Fig. 65, present a phosphorescent blue emission which can be shifted to green when doped with 1-naphtol, while in solution and in the microcrystalline form no emission is observed. Authors suggest that this is probably due to the lack of π-π interactions between the phenolato moieties in the solid state, which prevents self-quenching of the excited states and the effective inhibition of O$_2$ in crystal packing.

The analogous luminescent Tb^{3+} complex showed interesting oxygen sensitive properties: its quantum yield passed from 0.91 under N$_2$ to 0.054 under air [23].

The first example of Sm(III) complex as an emitter for 2-photon microscopy was reported by Maury *et al.* [149]. The Sm^{3+} complex of L69 (**48**) was found to be efficient for 2P imaging applications both in the NIR-to-visible regions and in the more challenging NIR-to-NIR microscopy configuration, as shown in Fig. 66.

45 R = R' = OMe
46 R = Me, R' = H
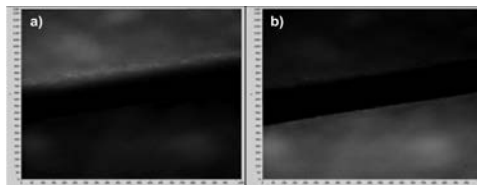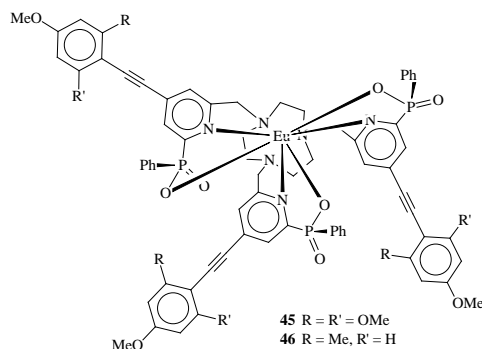
Figure 64. Microscopy images following sample excitation using a 365 nm UV-LED (tacq.= 7.2 ms per frame, 395 nm dichroic mirror, λem LP-420 nm) of Λ- and Δ-europium(III) complexes **45** and 46 recorded on a custom-built microscope incorporating a chiroptical selector unit. a) Time-resolved image of (top) Λ-[**46**] and (bottom) Δ-[**46**] using the RIGHT (horizontal polarisation) circularly polarised light chiroptical channel. b) Time-resolved image of (top) Λ-[**46**] and (bottom) Δ-[**46**], using the LEFT (vertical polarisation) circularly polarised light channel. Reproduced from Ref. [147] with permission from The Royal Society of Chemistry.

Recently, the same group described the possibility of using Tb^{3+} complexes as viscosity probes in cells [150]. Although the aryl-aryl rotation of the antennae causes weaker quantum yields and shorter luminescent lifetime than the analogous non-functionalised carboxypyridine complex, however, by blocking internal rotations of the biaryl antennae in a crowded environment, the energy back transfer to the ligand is reduced, leading to sensitivity toward viscosity of the complex.

The presence of PEG groups in the Tb^{3+} complex of L70 (**49**) improved its solubility and enabled to explore viscosity inside the cells. An increase in the quantum yield and fluorescent lifetime was detected in the nucleus region confirming higher microviscosity in that region than in the other compartments of the cell.
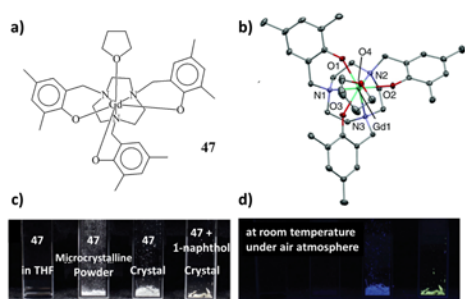
Figure 65. a) Complex **47**, b) its ORTEP representation, and photographs of **47** in THF solution, as microcrystalline powder, as crystals and in the presence of 1-naphtol under visible c) and UV light d). Adapted from Ref. [148] with permission from The Royal Society of Chemistry.

Figure 66. a) Sm^{3+} complex **48** and microscopy images of T24 cells fixed with paraformaldehyde under laser irradiation at l = 745 nm by using 48 b) in the visible channel and c) in the NIR channel. Adapted from Ref. [149] with permission from John Wiley and Sons. Copyright © 2015.

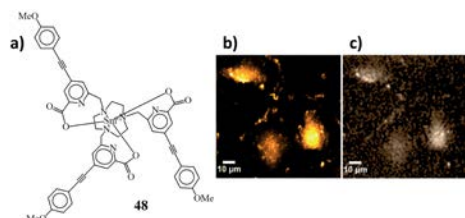### 3.2 Radiolabelling.

Derivatives of TACN can be efficiently used to chelate radiometal ions for applications in medical diagnosis as well as cancer therapy. Indeed, in order to use radioactive isotopes for *in vivo* applications, the stability constants of the radiometal-ligand complexes should be extremely high, so that after the injection into a patient any radiometal loss is avoided, thus preventing transchelation and hydrolysis processes[151-153]. Moreover, the complexes should be targeted with a biologically active molecule to address them towards a specific organ. Isotopes such as ^{68}Ga, ^{64}Cu, [86]Y, [89]Zr, and [44]Sc, have been efficiently used for positron emission tomography (PET) imaging, providing non-invasive images of a variety of molecular processes and targets [[152]. Notni and co-workers have developed ^{68}Ga radiopharamceuticals derived from Tri-Azacyclononane-Phosphinic acids (TRAP) [154]. The authors functionalised a TRAP derivative, L71, with cyclo(RGDfK), a cyclic peptide that possesses high integrin affinity. $\alpha_v\beta_3$ integrin is a heterodimeric transmembrane adhesion receptor studied for angiogenic, oncological and cardiological evaluations.
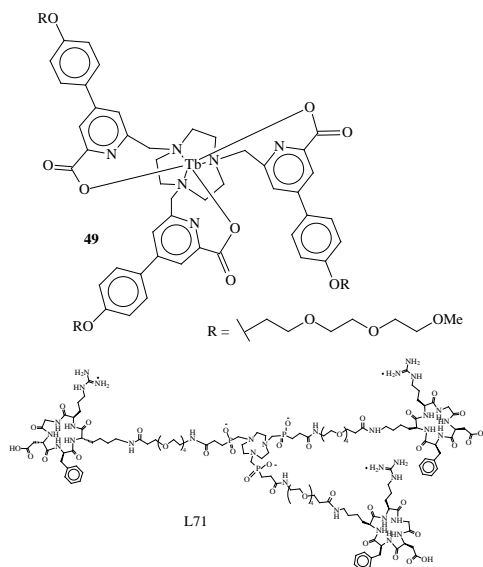
The activity of ^{68}Ga-L71 complex was compared with that of the clinically tested ^{18}F-Galacto-RGD on athymic nude mice bearing M21 ($\alpha_v\beta_3$-positive) and M21L (very low $\alpha_v\beta_3$-expressing) human melanoma xenografts on right and left shoulders, showing a 7.3-fold higher $\alpha_v\beta_3$-integrin affinity and 3.9-fold higher tumour uptake of the ^{68}Ga-L66 complex (Fig. 67).

The same authors also demonstrated that ^{64}Cu can be used as an alternative radiolabel to ^{68}Ga with the same ligand for PET imaging at early time points (1-2 h after injection) [155].

TRAP derivatives were also used to achieve a dendrimeric system for the development of multimodal imaging probes[156]. The study demonstrated that the dendrimer containing four TRAP units was able to uptake a ^{68}Ga concentration ten times higher than its monomer analogous, due to a cooperative interaction of the linked chelator systems. The dendrimer was targeted with KuE-pentynoic acid, an inhibitor for the prostate-specific membrane antigen (PSMA). The system showed a remarkable affinity for PSMA and the ^{68}Ga complex was successfully used for PET imaging of human prostate carcinoma.

Dendrimers of polyglycerol sulphate (dPGS) functionalised with 1,4-bis(2-pyridinylmethyl)-TACN (dmpTACN) and radiolabelled with ^{64}Cu were recently described (L72 and L73) [157].

In vivo PET studies on healthy Wistar rats showed accumulation in spleen, liver and kidney with a presence of the radiolabelled complexes even after 30 days in RES organs.
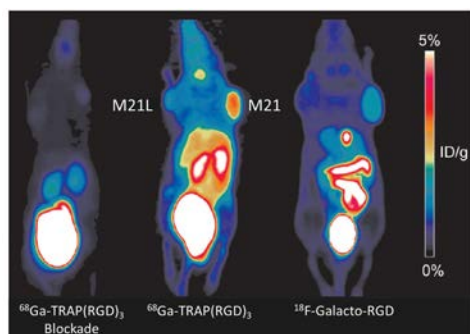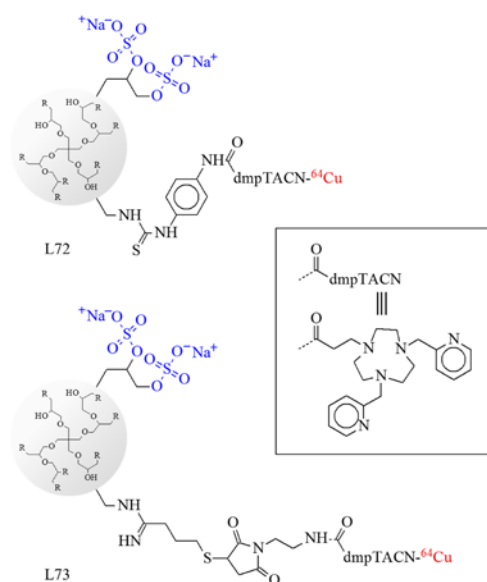
Figure 67. MicroPET scans (MIP, 75 min p. i.) of nude mouse bearing tumour xenografts on both shoulders (left: M21L, right: M21). Adapted from Ref. [154] with permission from John Wiley and Sons. Copyright © 2011.

Various multifunctional nanoplatforms have been developed for imaging purposes using different systems. Micelles of various block copolymers were conjugated with antibodies or targeting peptides, TACN-N,N',N''-triacetic acid (NOTA) for ^{64}Cu-labeling and PET imaging and with the anticancer drug doxorubicin [158-160]. ^{64}Cu- and ^{66}Ga-NOTA was also conjugated to nanographene oxide sheets targeted with monoclonal antibodies for *in vivo* tumor imaging [161,162]. However, the same authors have recently demonstrated that ^{64}Cu can be intrinsically labelled onto nanographene oxide sheets via covalent interactions between the metal and the π

electrons of graphene, suggesting that the presence of a chelator for radiometals in this type of nanoplatforms can be avoided [163]. Mesoporous silica nanoparticles (NPs) were functionalised on their surface with thiol groups, then PEGylated, conjugated with TRC105 antibody specific for endoglyn (a marker for tumour angiogenesis, which is almost exclusively expressed on proliferating endothelial cells) and labelled with ^{64}Cu using NOTA. *In vivo* PET imaging, biodistribution and blocking studies were performed in 4T1 murine breast tumour-bearing mice to evaluate and confirm their tumour specific targeting capability, which was validated by various *in vitro* and *ex vivo* experiments. Authors also demonstrated the enhanced tumour-targeted delivery efficiency of doxorubicin in 4T1 tumour-bearing mice after intravenous injection of DOX-loaded NOTA-mSiO$_2$-PEGTRC105 nanoparticles [164].

An interesting example of MCM-41 radiolabelled with ^{99m}Tc was recently reported [165]. ^{99m}Tc is used in over 80% of global diagnostic procedures in nuclear medicine. The Tc(VII) core TcO$_3$$^+$ forms a stable complex with TACN which can easily undergo [3+2] cycloaddition reactions with alkenes. In particular, the reaction of 5-(bicycloheptenyl)triethoxysilane can be used to graft norbornene onto the surface of mesoporous silica with a stereoselective [3+2] cycloaddition reaction.
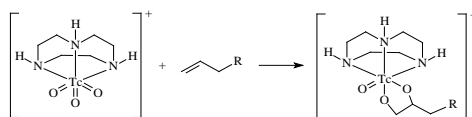
The use of superparamagnetic iron oxide NPs (SPIONs) allows for the development of multimodal diagnostic tools for PET and MRI. Examples of SPIONs labelled with ^{64}Cu-NOTA [166] and ^{64}Cu-dmpTACN have been reported [167, 168] and tested both *in vitro* and *in vivo*.

A derivative of NOTA used for radioimmunotherapy (RIT) is the so-called NETA ({4-[2-(bis-carboxymethyl-amino)-ethyl]-7-carboxymethyl-[1,4,7]triazonan-1-yl}-acetic acid). NETA is an octadentate ligand containing the NOTA skeleton and a flexible acyclic tridentate pendant arm and it is a promising chelator for of α- and β-emitters, including ^{90}Y, ^{177}Lu, ^{212}Bi, ^{213}Bi and ^{212}Pb. A derivative of NETA called 3p-*C*-NETA (L74) was synthesised using an unprecedented synthetic method based on the region-specific ring opening of the aziridinium ion [169].

The radiolabelling of L74 with ^{90}Y and ^{177}Lu was found to be very efficient and the complexes were stable in serum for at least 14 days. A derivative of L74 conjugated to an antibody was also synthesised for RIT applications and the biodistribution of ^{90}Y and ^{177}Lu complexes was evaluated *in vivo* on nude mice bearing ZR-75-1 human breast cancer [170].

3.3 Miscellanea.

The development of molecular thermometers and refrigerants have recently received high interest. Bendix, Evangelisti and co-

workers have described the unusual complex [{FeF$_3$-(Me$_3$TACN)}$_2$Gd$_3$F$_2$(NO$_3$)$_7$(H$_2$O)(CH$_3$CN)]·4 CH$_3$CN (**50**) shown in Fig. 68 [171].

The magnetic data show a temperature dependence of the magnetic susceptibility, with χT values going from 33.3 to 28.5 cm^3 mol^{-1} K^{-1} on cooling, suggesting the presence of intra-complex ferromagnetic interactions.

Magnetocaloric effects were also evaluated by obtaining the isothermal magnetic enthropy changes −ΔS$_m$ at different ΔB (from 0 to 7 T) (Fig. 69).
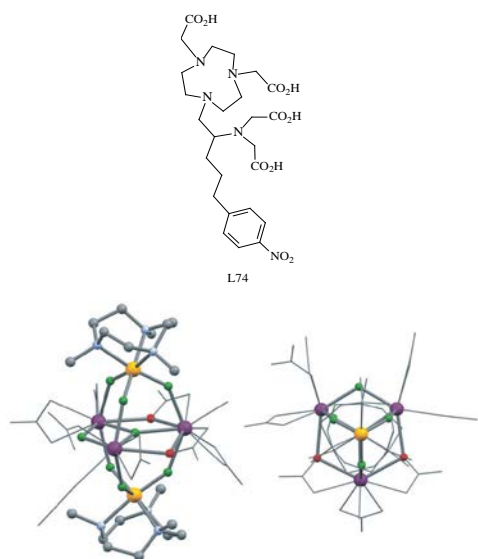
L74

Figure 68. Crystal structure of complex **50** shown in perspective (left) and along the Fe···Fe direction (right). Gd purple, Fe yellow, F green, O red, N blue, C gray. For clarity, the auxiliary Gd ligand sphere is shown as a wireframe. Reprinted from Ref. [171] with permission from John Wiley and Sons. Copyright © 2014.

The first transition metal examples of ^{1}H-NMR shift agents (paraSHIFTS) for thermometry applications were reported by Morrow and Tsitovich [172]. Magnetic Resonance Spectroscopy (MRS) can be successfully used for temperature mapping deep in tissues during hyperthermia therapy for cancer treatment. Paramagnetic lanthanide complexes have been developed for this purpose. However, due to their anionic nature, their ^{1}H-NMR resonances are sensitive to pH changes or the presence of the metal ions, such as Ca^{2+} cations. Fe^{2+} and Co^{2+} complexes of 6-methyl-2-picolyl appended TACN are high-spin and the metal is six-coordinated both in the solid state and in water. The exceptional rigidity of the complexes and their highly dispersed proton resonances allow for paraSHIFTS applications as the proton resonances of the methyl groups in the macrocyclic substituents are narrow and present no line-broadening up to 60 °C.

When using 3-fluoro-2-picolyl derivatives of TACN, spin crossover and high-spin Fe^{2+} complexes could be used for ^{19}F magnetic resonance thermometers [173].
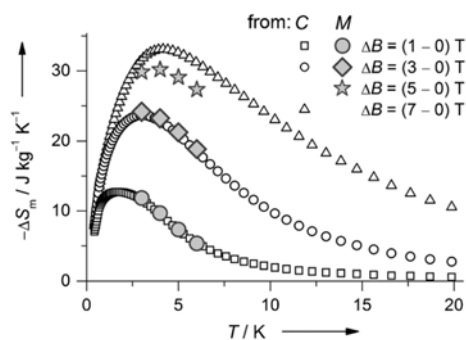
Figure 69. Magnetic entropy changes −ΔSm corresponding to the labelled magnetic field changes, ΔB, for complex **50**, as obtained from specific heat C and magnetization M data. Adapted from Ref. [171] with permission from John Wiley and Sons. Copyright © 2014.

Carlos, Zheng and co-workers reported the first example of a ratiometric luminescent thermometer based on an Eu/Tb complex using a phosphonate derivative of TACN [174], the complex **51** [Eu$_{0.102}$Tb$_{0.898}$(notpH$_4$)(NO$_3$)(H$_2$O)]$_2$·8H$_2$O (where notpH$_4$ (Claudia, va bene questo cambio?) is TACN-1,4,7-triyl-tris(methylenephosphonic acid, L75). Upon excitation at 393 nm, the emission of **51** was found to be temperature-dependent at low temperature, as show in Fig. 70.

A Fe^{3+} complex (**52**) of a TACN derivative bearing three methyl imidazole pendant arms (L76) has been proposed for the development of aqueous redox-flow batteries (Fig. 71) [175].

The complex exists in different forms in a large range of pH and exhibits pH-sensitive redox couples that span $E_{1/2}$(Fe^{3+}/Fe^{2+}) = 317 to -270 mV *vs*. NHE at pH 3.3 and pH 12.8, respectively, with the differences due to the acid-base equilibria of the imidazole substituents rings. The system demonstrates high charge/discharge capacities at both acidic and alkaline conditions throughout 100 cycles.
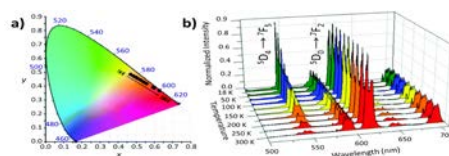
Figure 70. a) Commission International d'Eclairage (CIE) chromaticity diagram showing the temperature-dependent (x, y) colour coordinates of complex **51** changing from yellow (0.48, 0.48), at 18 K, to red (0.64, 0.37), at 300 K. b) Emission spectra of complex **51** recorded between 18 and 300 K. The excitation wavelength is 393 nm. Adapted from Ref. [174] with permission from The Royal Society of Chemistry.

Slep and co-workers have recently described the first SC-XRD characterization of a {RuNO}[7] (according to the Enemark–Feltham formalism) [176] complex ([Ru(Me₃TACN)(bpy)(NO)]²⁺) (**53**, Fig. 72a), whose solutions proved sensitive to a 365 nm irradiation source leading to NO release [177] This is particularly interesting for photodynamic therapy as it is well established that NO could cause cellular apotheosis. However, for practical applications it would be desirable that the NO photorelease from a metal complex occurs when the complex is irradiated in the visible range of the spectrum.

The same authors were able to obtain this result with a {FeNO}[7] complex [Fe((CH₂Py₂)₂MeTACN)(NO)]²⁺ (**54**, Fig. 72b), which is thermally and air-stable in solution and when irradiated with a 450 nm light source is able to release the coordinated NO [178].
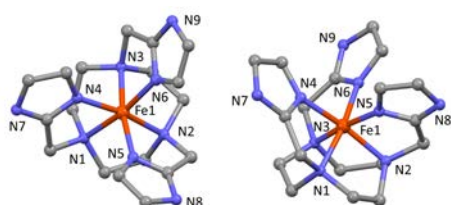
Figure 71. Ball and stick views of complex **52**. Hydrogen atoms and counterions have been omitted for clarity. Fe orange, N blue, C gray. Reprinted from Ref. [175] with permission from John Wiley and Sons. Copyright © 2017.
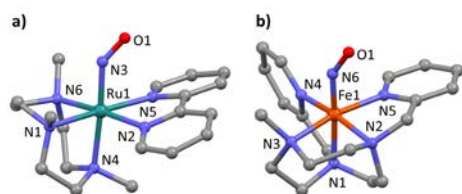
Figure 72. Ball and stick views of complexes **53** (a) and **54** (b). Hydrogens and counterions have been omitted for clarity. Fe orange, Ru petroleum green, O red, N blue, C gray. Figure 72a is adapted with permission from Ref. 177, Copyright © 2016, American Chemical Society. Figure 72b is reproduced from Ref. [178] with permission from The Royal Society of Chemistry.

A series of TACN-based oligomers with aromatic phenyl groups in the backbone were tested as non-viral gene delivery vectors [179]. Oligomers L77 and L78 showed high DNA binding ability and *in vitro* transfection experiments showed a higher transfection efficiency than commercially available cationic polymers such as polyethyleneimine (PEI), normally used for gene delivery.

Prins' group has described various examples of nanosystems containing TACN derivatives able to exert different functions.

Nucleotides-stabilized vesicles were very recently reported to self-assembling a [Zn(TACN)]²⁺ complex bearing a C₁₆ alkyl chain with GMP [180]. DLS, TEM and fluorescent measurements demonstrated that the aggregation of the [C16-Zn(TACN)]²⁺ system is dependent from the concentration of GMP present in solution. Moreover, upon addition of Ag⁺ ions in solution the authors were able to control the self-aggregation of the vesicles into large clusters caused by selective interactions between Ag⁺ and GMP (Fig. 73a). Silver ions produced *in situ* by the oxidation of an Ag surface caused the formation of the clusters only in close proximity (0.5-1 mm) of the Ag surface, opening the route to the possibility to spatially control the formation of the aggregates.

Gold NPs (d = 1.8±0.4 nm) covered with a monolayer of C9-thiols terminating with [Zn-TACN]²⁺ were used to form nanoproteins from the self-aggregation of different peptides on the highly positively charged surfaces of the nanoparticles (Fig. 73b) [181].
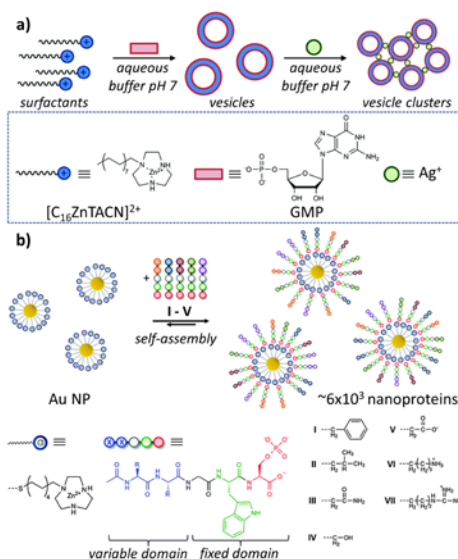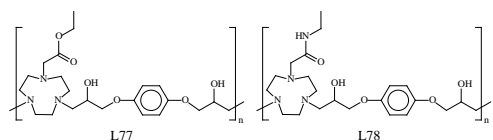
Figure 73. Cartoons representing: a) nucleotides-stabilised vesicles; b) nanoproteins. Reproduced from Refs. [180] and [181], respectively, with permission from The Royal Society of Chemistry.

The chosen peptides were characterized by a constant domain containing a phosphorylated Ser residue for binding to the NPs, a fluorescent Trp residue to monitor the binding event and a Gly residue as a flexible spacer. The variable domain contained different aminoacids (polar, apolar and anionic). Depending on the nature of the variable domain, different affinities for the NPs surface were observed and, when a mixture of peptides was added to the NPs, up to 17 peptides were assembled on the surface giving rise to a nano-object with a high degree of complexity. Moreover, the surface composition could be simply tuned by changing the nature and ratio of the added peptide fragments.

Finally, two TACN derivatives, 1,4,7-tris(4-carboxybenzyl)-1,4,7-triazacyclononane and 1,4,7-tris(3-(4-benzoate)prop-2-yn-1-yl)-1,4,7-triazacyclononane, namely L79 and L80, were used to generate two three-dimensional cadmium metal organic frameworks (MOFs), with general formula $Cd_2(\textbf{L79})(H_2O)_3](NO_3)_{0.7}(HCOO)_{0.2}Br_{0.1}$ (**55**) and $Cd(H\textbf{L80})(H_2O)_2$ (**56**) whose crystal structures are shown in Figure 74.[182]

L79 and L80
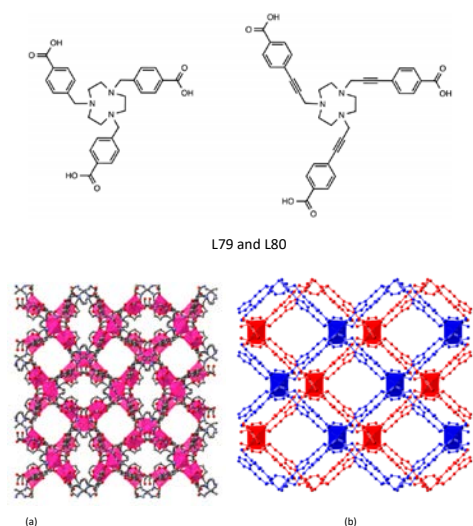
Figure 74. View of the open channels along the c axis showing the coordination polyhedra of Cd nodes for complex **55** (a) and view along the c axis showing the interpenetrated framework and the coordination polyhedral of the Cd nodes for complex **56**. (hydrogen atoms are omitted for clarity). Reproduced from Ref. 182 with permission from The Royal Soxiety of Chemistry.

The asymetric unit of 50 contains two crystallographically independent Cd2+ ions, both adopting a hexacoordinated geometry involving both the carboxylate and the nitrogen atoms of the macrocyclic unit. In contrast, 51 displays a 2-fold interpenetrated structure where the node is a mononuclear complex in which the Cd atom exhibits a seven coordination geometry. Both materials show a high permanent porosity and good CO_2 adsorption properties with a high selectivity over N_2 and CH_4.

Conclusions

The conclusions section should come in this section at the end of the article, before the acknowledgements.

Conflicts of interest

In accordance with our policy on Conflicts of interest please ensure that a conflicts of interest statement is included in your manuscript here. Please note that this statement is required for all submitted manuscripts. If no conflicts exist, please state that "There are no conflicts to declare".

Acknowledgements

The acknowledgements come at the end of an article after the conclusions and before the notes and references.

Notes and references

‡ Footnotes relating to the main text should appear here. These might include comments relevant to but not central to the matter under discussion, limited experimental and spectral data, and crystallographic data.
§
§§

1   J.L. Atwood, J.W. Steed (Eds.), Encyclopedia of Supramolecular Chemistry, Marcel Dekker Inc., NY U.S.A., 2004, ISBN: 0-8247-5056-X.
2   Macrocyclic and Supramolecular Chemistry - How Izatt-Christensen Award Winners Shaped the Field, R.M. Izatt (Ed.), John Wiley & Sons, UK, 2019. ISBN: 1119053846.
3   Q. He, G.I. Vargas-Zúñiga, S.H. Kim, S.K. Kim, J.L. Sessler, *Chem. Rev.*, 2019 in press.
4   S.M. Pinto, V. Tomé, M.J.F. Calvete, M.M.C.A. Castro, E. Tóth, C.F.G.C. Geraldes, *Coord. Chem. Rev.*, 2019, **390**, 1-31.
5   A.C. Harnden, D. Parker, N.J. Rogers, *Coord. Chem. Rev.*, 2019, **383**, 30-42.
6   F. Mancin, P. Scrimin, P. Tecilla, *Chem. Commun.*, 2012, **48**, 5545-5559.
7   T. Joshi, M. Kubeil, A. Nsubuga, G. Singh, G. Gasser, H. Stephan, ChemPlusChem, 2018, **83**, 1-12.

8   T. Joshi, B. Graham, L. Spiccia, *Acc. Chem. Res.*, 2015, **48**, 2366-2379.

9   L.F. Lindoy, K.-M. Park, S.S. Lee, *Chem. Soc. Rev.*, 2013, **42**, 1713-1727.

10 Macrocyclic Chemistry: Current Trends and Future Perspectives, K. Gloe (Ed.), Springer Netherlands, Dordrecht, 2005. ISBN: 1-4020-3364-8.

11 P. Chaudhuri, K. Wieghardt in Prog. Inorg. Chem., S.J. Lippard (Ed.), John Wiley & Sons, 2007, pp 329-436.

12 A.J. Blake, I.A. Fallis, S. Parsons, S.A. Ross, M. Schröder, *J. Chem. Soc., Dalton Trans.*, 1996, 525-532.

13 A.J. Blake, J.P. Danks, W.-S. Li, V. Lippolis, M. Schröder, *J. Chem. Soc., Dalton Trans.*, 2000, 3034-3040.

14 L. Tei, A.J. Blake, V. Lippolis, C. Wilson, M. Schröder, *Dalton Trans.*, 2003, 204-210.

15 M. Mameli, M.C. Aragoni, M. Arca, M. Atzori, A. Bencini, C. Bazzicalupi, A.J. Blake, C. Caltagirone, F.A. Devillanova, A. Garau, M.B. Hursthouse, F. Isaia, V. Lippolis, B. Valtancoli, *Inorg. Chem.*, 2009, **48**, 9236-9249.

16 Y. Mikata, Y. Nodomi, A. Kizu, H. Konno, *Dalton Trans.*, 2014, **43**, 1684-1690.

17 M. Aguado Tetilla, M.C. Aragoni, M. Arca, C. Caltagirone, C. Bazzicalupi, A. Bencini, A. Garau, F. Isaia, A. Laguna, V. Lippolis, V. Meli, *Chem. Commun.*, 2011, **47**, 3805-3807.

18 A. Bencini, V. Lippolis, B. Valtancoli, *Inorg. Chim. Acta*, 2014, **417**, 38-58.

19 A. Bencini, F. Caddeo, C. Caltagirone, A. Garau, M.B. Hursthouse, F. Isaia, S. Lampis, V. Lippolis, F. Lopez, V. Meli, M. Monduzzi, M.C. Mostallino, S. Murgia, S. Puccioni, J. Schmidt, P.P. Secci, Y. Talmon, *Org. Biom. Chem.*, 2013, **11**, 7751-7759.

20 P. Benndorf, S. Schmitt, R. Köppe, P. Oña-Burgoas, A. Scheurer, K. Meyer, P.W. Roesky, *Angew. Chem. Int. Ed. Engl.*, 2012, **51**, 5006-5010.

21 a) I. Castro-Rodriguez, H. Nakai, L. N. Zakharov, A. L. Rheingold, K. Meyer, *Science*, 2004, **305**, 1757-1759; b) I. Castro-Rodriguez, K. Meyer, *J. Am. Chem. Soc.*, 2005, **127**, 11242-11243.

22 J.P. Cross, P.G. Sammes, *J. Lumin.*, 2004, **110**, 101-111.

23 H. Nakai, T. Goto, K. Kitagawa, K. Nonaka, T. Matsumoto, S. Ogo, *Chem. Commun.*, 2014, **50**, 15737-15739.

24 H. Nakai, K. Kitigawa, H. Nakamori, T. Tokunaga, T. Matsumoto, K. Nozaki, S. Ogo, *Angew. Chem. Int. Ed. Engl.*, 2013, **52**, 8722-8725.

25 H. Nakai, J. Seo, K. Kitagawa, T. Goto, T. Matsumoto, S. Ogo, *Dalton Trans.*, 2016, **45**, 9492-9496.

26 H. Nakai, M. Kuyama, J. Seo, T. Goto, T. Matsumoto, S. Ogo, *Dalton Trans.*, 2017, **46**, 9126-9130.

27 S.J. Butler, B.K. McMahon, R. Pal, D. Parker, J.W. Walton, *Chem. Eur. J.*, 2013, **19**, 9511-9517.

28 B.K. McMahon, D. Parker, *RSC Adv.*, 2014, **4**, 37649-37654.

29 E.R. Neil, M.A. Fox, R. Pal, D. Parker, *Dalton Trans.*, 2016, **45**, 8355-8366.

30 M. Roger, M. Regueiro-Figueroa, C.B. Azzeddine, V. Patinec, C.S. Bonnet, C. Platas-Iglesias, R. Tripier, *Eur. J. Inorg. Chem.*, 2014, 1072-1081.

31 Z. Li, Z.-R. Geng, C. Zhang, X.-B. Wang, Z.-L. Wang, *Biosensors and Bioelectronic*, 2015, **72**, 1-9.

32 X. Zeng, C. Bornholdt, D. Over, O. Reinaud, *Org. Lett.*, 2011, **20**, 5660-5663.

33 D. Over, X. Zeng, C. Bernholdt, J. Marrot, O. Reinaud, *Inorg. Chem.*, 2013, **52**, 14089-14095.

34 A. Brown, T. Bunchuay, C.G. Crane, N.G. White, A.L. Thompson, P.D. Beer, *Chem. Eur. J.*, 2018, **24**, 10434-10442.

35 T. Mori, K. Okamoto, H. Endo, J.P. Hill, S. Shinoda, M. Matsukura, H. Tsukube, Y. Suzuki, Y. Kanekiyo, K. Ariga, *J. Am. Chem. Soc.*, 2010, **132**, 12868-12870.

36 T. Mori, K. Okamoto, H. Endo, K. Sakakibara, J.P. Hill, S. Shinoda, M. Matsukura, H. Tsukube, Y. Suzuki, Y. Kanekiyo, K. Ariga, *Nanoscale Res. Letter.*, 2011, **6**, 304.

37 C. Bazzicalupi, A. Bencini, E. Faggi, A. Garau, C. Giorgi, V. Lippolis, A. Perra, B. Valtancoli, *Dalton Trans.*, 2006, 1409-1418.

38 C. Bazzicalupi, A. Bencini, C. Giorgi, B. Valtancoli, V. Lippolis, A. Perra, *Inorg. Chem.*, 2011, **50**, 7202-7216.

39 E. Arturoni, C. Bazzicalupi, A. Bencini, C. Caltagirone, A. Danesi, A. Garau, C. Giorgi, V. Lippolis, B. Valtancoli, *Inorg. Chem.*, 2008, **47**, 6551-6563.

40 C. Bazzicalupi, A. Bencini, S. Puccioni, B. Valtancoli, P. Gratteri, A. Garau, V. Lippolis, *Chem. Commun.*, 2012, **48**, 139-141.

41 F. Bertoli, A. Bencini, A. Garau, C. Giorgi, V. Lippolis, A. Lunghi, F. Totti, B. Valtancoli, *Chem. Eur. J.*, 2016, **22**, 14890-14901.

42 Z. Zeng, A.A.J. Torriero, A.M. Bond, L. Spiccia, *Chem. Eur. J.*, 2010, **16**, 9154-9163.

43 M. Formica, G. Ambrosi, V. Fusi, L. Giorgi, M. Arca, A. Garau, A. Pintus, V. Lippolis, *New J. Chem.*, 2018, **42**, 7869-7883.

44 A. Bencini, C. Coluccini, A. Garau, C. Giorgi, V. Lippolis, L. Messori, D. Pasini, S. Puccioni, *Chem. Commun.*, 2012, **48**, 10428-10430.

45 M.J. Ruedas-Rama, E.A.H. Hall, *Anal. Chem.*, 2008, **80**, 8260-8268.

46 C. Pezzato, S. Maiti, J.L.-Y. Chen, A. Cazzolaro, C. Gobbo, L.J. Prins, *Chem. Commun.*, 2015, **51**, 9922-9931.

47 L. Prins, *Acc. Chem. Res.*, 2015, **48**, 1920-1928.

48 R. Bonomi, A. Cazzolaro, A. Sansone, P. Scrimin, L.J. Prins, *Angew. Chem. Int. Ed. Engl.*, 2011, **50**, 2307-2312.

49 G. Pieters, A. Cazzolaro, R. Bonomi, L.J. Prins, *Chem. Commun.*, 2012, **48**, 1916–1918.

50 G. Pieters, C. Pezzato, L. J. Prins, *Langmuir*, 2013, **29**, 7180-7185.

51 U. H. F. Bunz and V. M. Rotello, *Angew. Chem., Int. Ed.*, 2010, **49**, 3268-3279.

52 C. Pezzato, B. Lee, K. Severin, L.J. Prins, *Chem. Commun.*, 2013, **49**, 469-471.

53 C. Pezzato, D. Zaramella, M. Martinelli, G. Pieters, M.A. Pagano, L.J. Prins, *Org. Biomol. Chem.*, 2015, **13**, 1198-1203.

54 C. Pezzato, L.J. Prins, *Nature Commun.*, 2015, **6**, 7790.

55 F. della Sala, S. Maiti, A. Bonanni, P. Scrimin, L.J. Prins, *Angew, Chem. Int. Ed. Engl.*, 2018, **57**, 1611-1615.

56 S. Maiti, C. Pezzato, S.G. Martin, L.J. Prins, *J. Am. Chem. Soc.*, 2014, **136**, 11288-11291.

57 S. Maiti, L.J. Prins, *Chem. Commun.*, 2015, **51**, 5714-5716.

58 G. Zaupa, C. Mora, R. Bonomi, L.J. Prins, P. Scrimin, *Chem. Eur. J.*, 2011, **17**, 4879-4889.

59 C. Pezzato, J.L-Y. Chen, P. Galzerano, M. Salvi, L.J. Prins, *Org. Biom. Chem.*, 2016, **14**, 6811-6820.

60 P. Cragg, *Supramolecular chemistry: from biological inspiration to biomedical applications,* Springer Science+Business Media, Dordrecht, 2007, ISBN 978-90-481-2582-1.

61 E. Kimura, E. Kikuta, *J. Biol. Inorg. Chem.* 2000, **5**, 139-155.

62 S. Aoki, E. Kimura *J Biotechnol.* 2002, **90**, 129-155.

63 E. Kuah, S. Toh, J. Lee, Q. Ma, Z. Gao, *Chem. Eur. J.* 2016, **22**, 8494-8430.

64 I. Bertini, H. Gray, E.I. Stiefel, J.S. Valentine, Eds. *Biological Inorganic Chemistry* University Science Books, Mill Valley, CA, 2007, ISBN 978-1891389436.

65 W.N. Lipscomb, N. Sträter, *Chem. Rev.*, 1996, **96**, 2375-2434.

66 J. Chin, *Curr. Op. Chem. Biol.* 1997, **1**, 514-521.

67 F. Mancin, P. Scrimin, P. Tecilla, U. Tonellato, *Coord. Chem. Rev.,* 2009, **253**, 2150-2165.

68 S. Mikkola, T. Lönnberg, H. Lönnberg, *Beilstein J. Org. Chem.*, 2018, **14**, 803-837.

69 E.L. Legg, J.N. Burstyn, *Coord. Chem. Rev.,* 1998, **173**, 133-165.

70 F. Mancin, L.J. Prins, P. Pengo, L. Pasquato, P. Tecilla, P. Scrimin, *Molecules,* 2016, **21** 1014.

71 J.R. Morrow, O. Iranzo, *Curr. Op. Chem. Biol.,* 2004*, 8*, 192–200.

72 X. Zhang, Y. Zhu, H. Gao, C. Zhao, *Inorg. Chem.,* 2014, **53**, 11903-11912.

73 E.L. Hegg, S. Mortimore, C.-L. Cheung, J.E. Huyett, J.N. Burstyn, *Inorg. Chem.,* 1999, **38**, 2961-2968.

74 K.M. Deck, T.A. Tseng, J.N Burstyn, *Inorg Chem.,* 2002, 669-677.

75 K.A. Deal, J.N. Burstyn, *Inorg. Chem.,* 1996, **35**, 2792-2798.

76 F.H. Fry, P. Jensen, C.M. Kepert, L. Spiccia, *Inorg. Chem.*, 2003 **42**, 5637-5644.

77 F.H. Fry, A.J. Fischmann, M.J. Belousoff, L. Spiccia, J. Bruegger, *Inorg. Chem.*, 2005, **44**, 941-950.

78 M.J. Belousoff, M.B. Duriska, B. Graham, S.R. Batten, B. Moubaraki, K.S. Murray, L. Spiccia, *Inorg. Chem.*, 2006, **45**, 3746-3755.

79 T.-S.A. Tseng, J.N. Burstyn, *Chem. Commun.,* 2008, 6209-6211.

80 E.L. Hegg, J.N. Burstyn, *Inorg. Chem.*, 1996, **35**, 7474–7481.

81 E.D. Horowitz, S. Lilavivat, B.W. Holladay, M.W. Germann, N.V. Hud, *J. Am. Chem. Soc.,* 2009, **131**, 5831–5838.

82 P. Blondeau, M. Segura, R. Pérez-Fernández, J. de Mendoza, *Chem. Soc. Rev.* 2007, **36**, 198–210.

83 R. Savio, *Chem. Eur. J.,* 2015, **21**, 10960-10971.

84 D.E. Wilcox, *Chem. Rev.,* 1996, **96**, 2435–2458.

85 L. Tjioe, T. Joshi, J.L. Brugger, B. Graham, L. Spiccia*, Inorg. Chem.,* 2011, **50**, 621–635.

86 L. Tjioe, T. Joshi, C.M. Forsyth, B. Moubaraki, K.S. Murray, J. Brugger, B. Graham, L. Spiccia, *Inorg. Chem.*, 2012, **51**, 939-953.

87 L. Tjioe, A. Meininger, T. Joshi, L. Spiccia, B. Graham, *Inorg. Chem.*, 2011, **50**, 4327-4339.

88 R. Salvio, R. Cacciapaglia, L. Mandolini, *J. Org. Chem.,* 2011, **76**, 5438-5443.

89 M. Soler, E. Figueras, J. Serrano-Plana, M. Gonzalez-Bartulos, A. Massaguer, A. Company, M.A. Martínez, J. Malina, V. Brabec, L. Feliu, M. Planas, X. Ribas, M. Costas, *Inorg. Chem.* 2015, **54**, 10542–10558.

90 X. Zhang, X. Liu, D. L. Philips, C. Zhao, *Dalton Trans*, 2016, **45**, 1593-1603.

91 R. Savio, S. Volpi, R. Cacciapaglia, A. Casnati, L. Mandolini, F. Sansone *J. Org. Chem.,* 2015, **80**, 5887-5893.

92 R. Savio, S. Volpi, R. Cacciapaglia, F. Sansone, L. Mandolini, A. Casnati *J. Org. Chem.,* 2016, **81**, 4728-4735.

93 O. Iranzo, A. Y. Kovalevsky, J.R. Morrow, J.P. Richard, *J. Am. Chem. Soc.* 2003, **125**, 1988-1993.

94 C.S. Rossiter, R.A. Mathews, J.R. Morrow, *Inorg. Chem.,* 2005, **25**, 9397-9404.

95 C.S. Rossiter, R.A. Mathews, J.R. Morrow, J.P. Richard, *Dalton Trans.,* 2007, 3804-3811.

96 X. Sheng, X.-M. Lu, J.-J. Zhang, Y.-T. Chen, G.-Y. Lu, Y. Shao, F. Liu, Q. Xu *J. Org. Chem.,* 2007, **72**, 1799-1802.

97 D. Wanhon, A.-M. Lebuis, J. Chin, *Angew Chem Int Ed Engl.,* 1995, **34**, 2412-2414.

98 N.H. Williams, W. Cheung, J. Chin, *J. Am. Chem. Soc.*, 1998, **120**, 8079-8087.

99 N.H. Williams, A.-M. Lebuis, J. Chin, *J. Am. Chem. Soc.,* 1999, **121**, 3341-3348.

100 M. J. Young, J. Chin, *J. Am. Chem. Soc.,* 1995, **117**, 10577-10578.

101 K.P. McCue, D.A. Voss, Jr., C. Marks, J.R. Morrow, *J. Chem. Soc., Dalton Trans.,* 1998, 2961-2963.

102 K.P. McCue, J.R. Morrow, *Inorg. Chem.,* 1999, **38***, 6136-6142.

103 L.J. Farrugia, P.A. Lovatt, R.D. Peacok, *J. Chem. Soc., Dalton Trans.*, 1997, 911-912.

104 F.H. Fry, L. Spiccia, P. Jensen, B. Moubaraki, K.S. Murray, E.R.T. Tiekink, *Inorg Chem.,* 2003*, 42*, 5594-5693.

105 J. Qian, W. Gu, H. Liu, F. Gao, L. Feng, S. Yan, D. Liao, P. Cheng. *Dalton Trans.*, 2007, 1060-1067.

106 D. Montagner, V. Gandin, C. Marzano, A. Erxleben, *J. Inorg. Biochem.,* 2015, **145**, 101-107.

107 M. Arca, A. Bencini, E. Berni, C. Caltagirone, F.A. Devillanova, F, Isaia, A. Garau, C. Giorgi, V. Lippolis, A. Perra, L. Tei, B. Valtancoli, *Inorg. Chem.,* 2003, **42**, 6929-6939.

108 X. Sheng, X. Guo, X.-M. Lu, Y. Shao, F. Liu, Q. Xu, *Bioconjugate Chem.*, 2009, **19**, 490-498.

109 P. Rossi, F. Felluga, P. Tecilla, F. Formaggio, M. Crisma, C. Tomiolo, P. Scrimin *J. Am. Chem. Soc.,* 1999, **121**, 6948-6949.

110 C. Sissi, P. Rossi, P. Felluga, F. Formaggio, M. Palumbo, P. Tecilla, C. Toniolo, P. Scrimin, *J. Am. Chem. Soc.,* 2001, **123***, 3169–3170.

111 J.P. Richard, J.R. Morrow, *Chem. Commun.,* 2003, 22832-2833.

112 O. Iranzo, T. Elmer, J.P. Richard, J.R. Morrow, *Inorg. Chem.,* 2003, **42**, 7737-7746.

113 O. Iranzo, J.P. Richard, J.R. Morrow, *Inorg. Chem.,* 2004, **43**, 1743-1750.

114 T. Humphry, S. Iuer, O. Iranzo, J.R. Morrow, J.P. Richard, P. Paneth, A.C. Hengge, *J. Am. Chem. Soc.,* 2008, **130**, 17858-17866.

115 M.-Y. Yang, O. Iranzo, J.P. Richard, J.R. Morrow, *J. Am. Chem. Soc.,* 2005, **125**, 1064-1065.

116 H. Gao, Z. Ke, N.J. DeYonker, J. Wang, H. Xu, Z.-W. Mao, D.L. Lee, C. Zhao, J. Am. Chem. Soc., 2011, **133**, 2904-2915.

117 R. Cao, P. Muller, S. J. Lippard, *J. Am. Chem. Soc.,* 2010, **132**, 17366-17369.

118 A. Scarso, U. Scheffer, M. Göbel, Q.B. Broxterman, B. Kaptein, F. Formaggio, C. Toniolo, P. Scrimin, *PNAS*, 2002, **99**, 5144-5149.

119 A. Scarso, G. Zaupa, F.D. Houillon. L.J. Prins, P. Scrimin, *J. Org. Chem.,* 2007, **72**, 376-385.

120 P. Rossi, P. Tecilla, L. Nalzer, P. Scrimin, *Chem. Eur. J.,* 2004, **10**, 4163-4170.

121 M.J. Hostetler, S.J. Green, J.J. Stokes, R.W. Murray, *J. Am. Chem. Soc.,* 1996, **118**, 4212– 4213.

122 F. Manea, F.B. Houillon, L. Pasquato, P. Scrimin, *Angew. Chem., Int. Ed.,* 2004, **43**, 6165– 6169.

123 M. Diez-Castellnou, F. Mancin, P. Scrimin, *J. Am. Chem. Soc.,* 2014, **136**, 1158-1161.

124 J.L.-Y. Chen, C. Pezzato, P. Scrimin, L.P. Prins, *Chem. Eur. J.,* 2016, **22**, 7028-7032.

125 M. Martin, F. Manea, R. Fiammengo, L.J. Prins, L. Pasquato, P. Scrimin, *J. Am. Chem. Soc.,* 2007, **129**, 6982-6983.

126 G. Zaupa, L. J. Prins, P. Scrimin, *J. Am. Chem. Soc.,* 2008, **130**, 5699-5709.

127 G. Zaupa, L.J. Prins, P. Scrimin, *Bioorg. Med. Chem. Lett.,* 2009, **19**, 3816-3820.

128 C.M. Hartshorn, J.R. Deschamps, A. Singh, E.L. Chang, *React. Funct. Polym.,* 2003, **55**, 219-229.

129 G.M. Bonora, S. Drioli, F. Felluga, F. Mancin, P. Rossi, P. Scrimin, P. Tecilla, *Tetrahedron Lett.,* 2003, **44** , 535-538.

130 B.R. Bodsgard, J.N. Burstyn, *Chem. Commun.,* 2001, 647-648.

131 B.R. Bodsgard, R.W. Clark, A.W. Ehrbar, J.N. Burstyn, *Dalton Trans.*, 2009, 2365-2373.

132 A.J. Amoroso, I.A. Fallis, S.J.A. Pope, *Coord. Chem. Rev.,* 2017, **340**, 198-219.

133 A.J. Amoroso, S.J.A. Pope, *Chem. Soc. Rev.,* 2015, **44**, 4723-4742.

134 S.J. Butler, M. Delbianco, L. Lamarque, B.K. McMahon, E.R. Neil, R. Pal, D. Parker, J.W. Walton, J.M. Zwier, *Dalton Trans.,* 2015, **44**, 4791-4803.

135   E.J. New, D. Parker, D.G. Smith, J.W. Walton, *Cur. Opinion in Chem. Biol.*, 2010, **14**, 238-246.

136   S. Shuvaev, M. Starck, D. Parker, *Chem. Eur. J.*, 2017, **23**, 9974-9989.

137   E. Terreno, D.D. Castelli, A. Viale, S. Aime, *Chem. Rev.*, 2010, **110**, 3019-3042.

138   J.M. Zwier, H. Bazin, L. Lamarque, G. Mathis, *Inorg. Chem.*, 2014, **53**, 1854-1866.

139   M. Delbianco, V. Sadovnikova, E. Bourrier, G. Mathis, L. Lamarque, J.M. Zwier, D. Parker, *Ang. Chem. Intern. Ed.*, 2014, **53**, 10718-10722.

140   M. Soulié, F. Latzko, E. Bourrier, V. Placide, S.J. Butler, R. Pal, J.W. Walton, P.L. Baldeck , B. Le Guennic, C. Andraud, J.M. Zwier, L. Lamarque, D. Parker, O. Maury, *Chem. Eur. J.*, 2014, **20**, 8636-8646.

141   J.W. Walton, A. Bourdolle, S.J. Butler, M. Soulie, M. Delbianco, B.K. McMahon, R. Pal, H. Puschmann, J.M. Zwier, L. Lamarque, O. Maury, C. Andraud, D. Parker, *Chem. Commun.*, 2013, **49**, 1600-1602.

142   M. Starck, R. Pal, D. Parker, *Chem. Eur. J.*, 2016, **22**, 570-580.

143   N.H. Evans, R. Carr, M. Delbianco, R. Pal, D.S. Yufit, D. Parker, *Dalton Trans.*, 2013, **42**, 15610-15616.

144   J.W. Walton, R. Carr, N.H. Evans, A.M. Funk, A.M. Kenwright, D. Parker, D.S. Yufit, M. Botta, S. De Pinto, K.L. Wong, *Inorg. Chem.*, 2012, **51**, 8042-8056.

145   E.R. Neil, A.M. Funk, D.S. Yufit, D. Parker, *Dalton Trans.*, 2014, **43**, 5490-5504.

146   E.R. Neil, M.A. Fox, R. Pal, L.O. Pålsson, B.A. O'Sullivan, D. Parker, *Dalton Trans.*, 2015, **44**, 14937-14951.

147   A.T. Frawley, R. Pal, D. Parker, *Chem. Commun.*, 2016, **52**, 13349-13352.

148   H. Nakai, K. Kitagawa, J. Seo, T. Matsumoto, S. Ogo, *Dalton Trans.*, 2016, **45**, 11620-11623.

149   A.T. Bui, A. Grichine, S. Brasselet, A. Duperray, C. Andraud, O. Maury, *Chem. Eur. J.*, 2015, **21**, 17757-17761.

150   A.T. Bui, A. Grichine, A. Duperray, P. Lidon, F. Riobé, C. Andraud, O. Maury, *J. Am. Chem. Soc.*, 2017, **139**, 7693-7696.

151   T.I. Kostelnik, C. Orvig, *Chem. Rev.*, 2019, **119**, 902-956.

152   E.W. Price, C. Orvig, *Chem. Soc. Rev.*, 2014, **43**, 260-290.

153   C.F. Ramogida, C. Orvig, *Chem. Commun.*, 2013, **49**, 4720-4739.

154   J. Notni, J. Šimeček, P. Hermann and H.J. Wester, *Chem. Eur. J.*, 2011, **17**, 14718-14722.

155   J. Šimeček, H.J. Wester, J. Notni, *Dalton Trans.*, 2012, **41**, 13803-13806.

156   D. Reich, A. Wurzer, M. Wirtz, V. Stiegler, P. Spatz, J. Pollmann, H.J. Wester, J. Notni, *Chem. Commun.*, 2017, **53**, 2586-2589.

157   K. Pant, D. Gröger, R. Bergmann, J. Pietzsch, J. Steinbach, B. Graham, L. Spiccia, F. Berthon, B. Czarny, L. Devel, V. Dive, H. Stephan, R. Haag, *Biocon. Chem.*, 2015, **26**, 906-918.

158   J. Guo, H. Hong, G. Chen, S. Shi, T.R. Nayak, C.P. Theuer, T.E. Barnhart, W. Cai, S. Gong, *ACS Ap. Mat. Interf.*, 2014, **6**, 21769-21779.

159   J. Guo, H. Hong, G. Chen, S. Shi, Q. Zheng, Y. Zhang, C.P. Theuer, T.E. Barnhart, W. Cai, S. Gong, *Biomat.*, 2013, **34**, 8323-8332.

160   Y. Xiao, H. Hong, A. Javadi, J.W. Engle, W. Xu, Y. Yang, Y. Zhang, T.E. Barnhart, W. Cai, S. Gong, *Biomat.*, 2012, **33**, 3071-3082.

161   H. Hong, K. Yang, Y. Zhang, J.W. Engle, L. Feng, Y. Yang, T.R. Nayak, S. Goel, J. Bean, C.P. Theuer, T.E. Barnhart, Z. Liu, W. Cai, *ACS Nano*, 2012, **6**, 2361-2370.

162   H. Hong, Y. Zhang, J.W. Engle, T.R. Nayak, C.P. Theuer, R.J. Nickles, T.E. Barnhart, W. Cai, *Biomat.*, 2012, **33**, 4147-4156.

163   S. Shi, C. Xu, K. Yang, S. \Goel, H.F. Valdovinos, H. Luo, E.B. Ehlerding, C.G. England, L. Cheng, F. Chen, R.J. Nickles, Z. Liu, W. Cai, *Ang. Chem. Int. Ed.*, 2017, **56**, 2889-2892.

164   F. Chen, H. Hong, Y. Zhang, H.F. Valdovinos, S. Shi, G.S. Kwon, C.P. Theuer, T.E. Barnhart, W. Cai, *ACS Nano*, 2013, **7**, 9027-9039.

165   M.A. Wuillemin, W.T. Stuber, T. Fox, M.J. Reber, D. Brühwiler, R. Alberto, H. Braband, *Dalton Trans.*, 2014, **43**, 4260-4263.

166   X. Yang, H. Hong, J.J. Grailer, I.J. Rowland, A. Javadi, S.A. Hurley, Y. Xiao, Y. Yang, Y. Zhang, R.J. Nickles, W. Cai, D.A. Steeber, S. Gong, *Biomat.*, 2011, **32**, 4151-4160.

167   J.A. Barreto, M. Matterna, B. Graham, H. Stephan, L. Spiccia, *New J. Chem.*, 2011, **35**, 2705-2712.

168   K. Pombo-García, K. Zarschler, J.A. Barreto, J. Hesse, L. Spiccia, B. Graham, H. Stephan, *RSC Adv.*, 2013, **3**, 22443-22454.

169   H.S. Chong, H.A. Song, C.S. Kang, T. Le, X. Sun, M. Dadwal, H. Lee, X. Lan, Y. Chen, A. Dai, *Chem. Commun.*, 2011, **47**, 5584-5586.

170   C.S. Kang, X. Sun, F. Jia, H.A. Song, Y. Chen, M. Lewis and H.S. Chong, *Biocon. Chem.*, 2012, **23**, 1775-1782.

171   K.S. Pedersen, G. Lorusso, J.J. Morales, T. Weyhermüller, S. Piligkos, S.K. Singh, D. Larsen, M. Schau-Magnussen, G. Rajaraman, M. Evangelisti, J. Bendix, *Ang. Chem. Int. Ed.*, 2014, **53**, 2394-2397.

172   P.B. Tsitovich, J.M. Cox, J.B. Benedict, J.R. Morrow, *Inorg. Chem.*, 2016, **55**, 700-716.

173   A.E. Thorarinsdottir, A.I. Gaudette, T.D. Harris, *Chem. Sci.*, 2017, **8**, 2448-2456.

174   M. Ren, C.D.S. Brites, S.S. Bao, R.A.S. Ferreira, L.M. Zheng, L.D. Carlos, *J. Mat. Chem. C*, 2015, **3**, 8480-8484.

175   P.B. Tsitovich, A.M. Kosswattaarachchi, M.R. Crawley, T.Y. Tittiris, T.R. Cook, J.R. Morrow, *Chem. Eur. J.*, 2017, **23**, 15327-15331.

176   J.H. Enemark, R.D. Feltham, *Coord. Chem. Rev.*, 1974, **13**, 339-406.

177   N. Levin, N.O. Codesido, E. Bill, T. Weyhermüller, A.P. Segantin Gaspari, R.S. Da Silva, J.A. Olabe, L.D. Slep, *Inorg. Chem.*, 2016, **55**, 7808-7810.

178   N. Levin, J. Perdoménico, E. Bill, T. Weyhermüller, L.D. Slep, *Dalton Trans.*, 2017, **46**, 16058-16064.

179   W.J. Yi, X.C. Yu, B. Wang, J. Zhang, Q.Y. Yu, X.D. Zhou, X.Q. Yu, *Chem. Commun.*, 2014, **50**, 6454-6457.

180   S. Maiti, I. Fortunati, A. Sen, L.J. Prins, *Chem. Commun.*, 2018, **54**, 4818-4821.

181   S. Garcia Martin, L.J. Prins, *Chem. Commun.*, 2016, **52**, 9387-9390.

References.

[1]   J.L. Atwood, J.W. Steed (Eds.), Encyclopedia of Supramolecular Chemistry, Marcel Dekker Inc., NY U.S.A., (2004) ISBN: 0-8247-5056-X.

Journal Name   **ARTICLE**

[2] R.M. Izatt (Ed.),Macrocyclic and Supramolecular Chemistry - How Izatt-Christensen Award Winners Shaped the Field, John Wiley & Sons, UK, (2019), ISBN: 1119053846.

[3] Q. He, G.I. Vargas-Zúñiga, S.H. Kim, S.K. Kim, J.L. Sessler, Chem. Rev. (2019) in press.

[4] S.M. Pinto, V. Tomé, M.J.F. Calvete, M.M.C.A. Castro, E. Tóth, C.F.G.C. Geraldes, Coord. Chem. Rev. 390 (2019) 1-31.

[5] A.C. Harnden, D. Parker, N.J. Rogers, Coord. Chem. Rev. 383 (2019) 30-42.

[6] F. Mancin, P. Scrimin, P. Tecilla, Chem. Commun. 48 (2012) 5545-5559.

[7] T. Joshi, M. Kubeil, A. Nsubuga, G. Singh, G. Gasser, H. Stephan, ChemPlusChem 83 (2018) 1-12.

[8] T. Joshi, B. Graham, L. Spiccia, Acc. Chem. Res. 48 (2015) 2366-2379.

[9] L.F. Lindoy, K.-M. Park, S.S. Lee, Chem. Soc. Rev. 42 (2013) 1713-1727.

[10] K. Gloe (Ed.), Macrocyclic Chemistry: Current Trends and Future Perspectives, Springer Netherlands, Dordrecht, 2005. ISBN: 1-4020-3364-8.

[11] P. Chaudhuri, K. Wieghardt, Prog. Inorg. Chem., S.J. Lippard (Ed.), John Wiley & Sons, 2007, pp 329-436.

[12] A.J. Blake, I.A. Fallis, S. Parsons, S.A. Ross, M. Schröder, J. Chem. Soc., Dalton Trans. (1996) 525-532.

[13] A.J. Blake, J.P. Danks, W.-S. Li, V. Lippolis, M. Schröder, J. Chem. Soc., Dalton Trans. (2000) 3034-3040.

[14] L. Tei, A.J. Blake, V. Lippolis, C. Wilson, M. Schröder, Dalton Trans. (2003) 204-210.

[15] M. Mameli, M.C. Aragoni, M. Arca, M. Atzori, A. Bencini, C. Bazzicalupi, A.J. Blake, C. Caltagirone, F.A. Devillanova, A. Garau, M.B. Hursthouse, F. Isaia, V. Lippolis, B. Valtancoli, Inorg. Chem. 48 (2009) 9236-9249.

[16] Y. Mikata, Y. Nodomi, A. Kizu, H. Konno, Dalton Trans. 43 (2014) 1684-1690.

[17] M. Aguado Tetilla, M.C. Aragoni, M. Arca, C. Caltagirone, C. Bazzicalupi, A. Bencini, A. Garau, F. Isaia, A. Laguna, V. Lippolis, V. Meli, Chem. Commun. 47 (2011) 3805-3807.

[18] A. Bencini, V. Lippolis, B. Valtancoli, Inorg. Chim. Acta 417 (2014) 38-58.

[19] A. Bencini, F. Caddeo, C. Caltagirone, A. Garau, M.B. Hursthouse, F. Isaia, S. Lampis, V. Lippolis, F. Lopez, V. Meli, M. Monduzzi, M.C. Mostallino, S. Murgia, S. Puccioni, J. Schmidt, P.P. Secci, Y. Talmon, *Org. Biom. Chem.* 11 (2013) 7751-7759.

[20] P. Benndorf, S. Schmitt, R. Köppe, P. Oña-Burgoas, A. Scheurer, K. Meyer, P.W. Roesky, Angew. Chem. Int. Ed. Engl. 51 (2012) 5006-5010.

[21] a) I. Castro-Rodriguez, H. Nakai, L. N. Zakharov, A. L. Rheingold, K. Meyer, Science 305 (2004) 1757-1759; b) I. Castro- Rodriguez, K. Meyer, J. Am. Chem. Soc. 127 (2005) 11242-11243.

[22] J.P. Cross, P.G. Sammes, J. Lumin. 110 (2004) 101-111.

[23] H. Nakai, T. Goto, K. Kitagawa, K. Nonaka, T. Matsumoto, S. Ogo, Chem. Commun. 50 (2014) 15737-15739.

[24] H. Nakai, K. Kitigawa. H. Nakamori, T. Tokunaga, T. Matsumoto, K. Nozaki, S. Ogo, Angew. Chem. Int. Ed. Engl. 52 (2013) 8722-8725.

[25] H. Nakai, J. Seo, K. Kitagawa, T. Goto, T. Matsumoto, S. Ogo, Dalton Trans., 45 (2016) 9492-9496.

[26] H. Nakai, M. Kuyama, J. Seo, T. Goto, T. Matsumoto, S. Ogo, Dalton Trans. 46 (2017) 9126-9130.

[27] S.J. Butler, B.K. McMahon, R. Pal, D. Parker, J.W. Walton, Chem. Eur. J. 19 (2013) 9511-9517.

[28] B.K. McMahon, D. Parker, RSC Adv. 4 (2014) 37649-37654.

[29] E.R. Neil, M.A. Fox, R. Pal, D. Parker, Dalton Trans. 45 (2016) 8355-8366.

[30] M. Roger, M. Regueiro-Figueroa, C.B. Azzeddine, V. Patinec, C.S. Bonnet, C. Platas-Iglesias, R. Tripier, Eur. J. Inorg. Chem. (2014) 1072-1081.

[31] Z. Li, Z.-R. Geng, C. Zhang, X.-B. Wang, Z.-L. Wang, Biosensors and Bioelectronic, 72 (2015) 1-9.

[32] X. Zeng, C. Bornholdt, D. Over, O. Reinaud, Org. Lett. 20 (2011) 5660-5663.

[33] D. Over, X. Zeng, C. Bernholdt, J. Marrot, O. Reinaud, Inorg. Chem., 52 (2013) 14089-14095.

[34] A. Brown, T. Bunchuay, C.G. Crane, N.G. White, A.L. Thompson, P.D. Beer, Chem. Eur. J. 24 (2018) 10434-10442.

[35] T. Mori, K. Okamoto, H. Endo, J.P. Hill, S. Shinoda, M. Matsukura, H. Tsukube, Y. Suzuki, Y. Kanekiyo, K. Ariga, J. Am. Chem. Soc. 132 (2010) 12868-12870.

[36] T. Mori, K. Okamoto, H. Endo, K. Sakakibara, J.P. Hill, S. Shinoda, M. Matsukura, H. Tsukube, Y. Suzuki, Y. Kanekiyo, K. Ariga, Nanoscale Res. Letter. 6 (2011) 304.

[37] C. Bazzicalupi, A. Bencini, E. Faggi, A. Garau, C. Giorgi, V. Lippolis, A. Perra, B. Valtancoli, Dalton Trans. (2006) 1409-1418.

[38] C. Bazzicalupi, A. Bencini, C. Giorgi, B. Valtancoli, V. Lippolis, A. Perra, *Inorg. Chem.*, 50 (2011) 7202-7216.

[39] E. Arturoni, C. Bazzicalupi, A. Bencini, C. Caltagirone, A. Danesi, A. Garau, C. Giorgi, V. Lippolis, B. Valtancoli, Inorg. Chem. 47 (2008) 6551-6563.

[40] C. Bazzicalupi, A. Bencini, S. Puccioni, B. Valtancoli, P. Gratteri, A. Garau, V. Lippolis, Chem. Commun., 48 (2012) 139-141.

[41] F. Bartoli, A. Bencini, A. Garau, C. Giorgi, V. Lippolis, A. Lunghi, F. Totti, B. Valtancoli, Chem. Eur. J. 22 (2016) 14890-14901.

[42] Z. Zeng, A.A.J. Torriero, A.M. Bond, L. Spiccia, Chem. Eur. J., 16 (2010) 9154-9163.

[43] M. Formica, G. Ambrosi, V. Fusi, L. Giorgi, M. Arca, A. Garau, A. Pintus, V. Lippolis, New J. Chem., 42 (2018) 7869-7883.

[44] A. Bencini, C. Coluccini, A. Garau, C. Giorgi, V. Lippolis, L. Messori, D. Pasini, S. Puccioni, Chem. Commun., 48 (2012) 10428-10430.

[45] M.J. Ruedas-Rama, E.A.H. Hall, Anal. Chem. 80 (2008) 8260-8268.

[46] C. Pezzato, S. Maiti, J.L.-Y. Chen, A. Cazzolaro, C. Gobbo, L.J. Prins, Chem. Commun. 51 (2015) 9922-9931.

[47] L. Prins, *Acc. Chem. Res.*, 48 (2015) 1920-1928.

[48] R. Bonomi, A. Cazzolaro, A. Sansone, P. Scrimin, L.J. Prins, Angew. Chem. Int. Ed. Engl., 50 (2011) 2307-2312.

[49] G. Pieters, A. Cazzolaro, R. Bonomi, L.J. Prins, Chem. Commun., 48 (2012) 1916–1918.

[50] G. Pieters, C. Pezzato, L. J. Prins, Langmuir 29 (2013) 7180-7185.

[51] U. H. F. Bunz and V. M. Rotello, Angew. Chem., Int. Ed., 49 (2010) 3268-3279.

[52] C. Pezzato, B. Lee, K. Severin, L.J. Prins, Chem. Commun., 49 (2013) 469-471.

[53] C. Pezzato, D. Zaramella, M. Martinelli, G. Pieters, M.A. Pagano, L.J. Prins, Org. Biomol. Chem. 13 (2015) 1198-1203.

[54] C. Pezzato, L.J. Prins, Nature Commun. 6 (2015) 7790-Manca ultima pagina).

[55] F. della Sala, S. Maiti, A. Bonanni, P. Scrimin, L.J. Prins, Angew, Chem. Int. Ed. Engl., 57 (2018) 1611-1615.

[56] S. Maiti, C. Pezzato, S.G. Martin, L.J. Prins, J. Am. Chem. Soc., 36 (2014) 11288-11291.

[57] S. Maiti, L.J. Prins, Chem. Commun. 51 (2015) 5714-5716.

[58] G. Zaupa, C. Mora, R. Bonomi, L.J. Prins, P. Scrimin, Chem. Eur. J. 17 (2011) 4879-4889.

[59] C. Pezzato, J.L-Y. Chen, P. Galzerano, M. Salvi, L.J. Prins, Org. Biom. Chem. 14 (2016) 6811-6820.

[60] P. Cragg, *Supramolecular chemistry: from biological inspiration to biomedical applications,* Springer Science+Business Media, Dordrecht, 2007, ISBN 978-90-481-2582-1.

[61] E. Kimura, E. Kikuta, J. Biol. Inorg. Chem. 5 (2000) 139-155.

[62] S. Aoki, E. Kimura J Biotechnol. 90 (2002) 129-155.

[63] E. Kuah, S. Toh, J. Lee, Q. Ma, Z. Gao, *Chem. Eur. J.* 2016, **22**, 8494-8430.

[64] I. Bertini, H. Gray, E.I. Stiefel, J.S. Valentine, Eds. *Biological Inorganic Chemistry* University Science Books, Mill Valley, CA, 2007, ISBN 978-1891389436.

[65] W.N. Lipscomb, N. Sträter, *Chem. Rev.,* 1996, **96**, 2375-2434.

[66] J. Chin 1 (1997) 514-521.

[67] F. Mancin, P. Scrimin, P. Tecilla, U. Tonellato, Coord. Chem. Rev. 253 (2009) 2150-2165.

[68] S. Mikkola, T. Lönnberg, H. Lönnberg, Beilstein J. Org. Chem.,14 (2018) 803-837.

[69] E.L. Legg, J.N. Burstyn, Coord. Chem. Rev. 173 (1998) 133-165.

[70] F. Mancin, L.J. Prins, P. Pengo, L. Pasquato, P. Tecilla, P. Scrimin, Molecules 21 (2016) 1014.

[71] J.R. Morrow, O. Iranzo, Curr. Op. Chem. Biol. 8 (2004) 192–200.

[72] X. Zhang, Y. Zhu, H. Gao, C. Zhao, Inorg. Chem., 53 (2014) 11903-11912.

[73] E.L. Hegg, S. Mortimore, C.-L. Cheung, J.E. Huyett, J.N. Burstyn, Inorg. Chem. 38 (1999) 2961-2968.

[74] K.M. Deck, T.A. Tseng, J.N Burstyn, Inorg Chem. 41 (2002) 669-677.

[75] K.A. Deal, J.N. Burstyn, Inorg. Chem. 35 (1996) 2792-2798.

[76] F.H. Fry, P. Jensen, C.M. Kepert, L. Spiccia, Inorg. Chem. 42 (2003) 5637-5644.

[77] F.H. Fry, A.J. Fischmann, M.J. Belousoff, L. Spiccia, J. Bruegger, Inorg. Chem. 44 (2005) 941-950.

[78] M.J. Belousoff, M.B. Duriska, B. Graham, S.R. Batten, B. Moubaraki, K.S. Murray, L. Spiccia, Inorg. Chem. 45 (2006) 3746-3755.

[79] T.-S.A. Tseng, J.N. Burstyn, Chem. Commun. 2008, 6209-6211.

[80] E.L. Hegg, J.N. Burstyn, Inorg. Chem. 35 (1996) 7474–7481.

[81] E.D. Horowitz, S. Lilavivat, B.W. Holladay, M.W. Germann, N.V. Hud, J. Am. Chem. Soc. 131 (2009) 5831–5838.

[82] P. Blondeau, M. Segura, R. Pérez-Fernández, J. de Mendoza, Chem. Soc. Rev. 26 (2007) 198–210.

[83] R. Savio, Chem. Eur. J., 21 (2015) 10960-10971.

[84] D.E. Wilcox, Chem. Rev. 96 (1996) 2435–2458.

[85] L. Tjioe, T. Joshi, J.L. Brugger, B. Graham, L. Spiccia, Inorg. Chem. 50 (2011) 621–635.

[86] L. Tjioe, T. Joshi, C.M. Forsyth, B. Moubaraki, K.S. Murray, J. Brugger, B. Graham, L. Spiccia, Inorg. Chem. 51 (2012) 939-953.

[87] L. Tjioe, A. Meininger, T. Joshi, L. Spiccia, B. Graham, *Inorg. Chem.* 50 (2011) 4327-4339.

[88] R. Salvio, R. Cacciapaglia, L. Mandolini, J. Org. Chem. 76 (2011) 5438-5443.

[89] M. Soler, E. Figueras, J. Serrano-Plana, M. Gonzalez-Bartulos, A. Massaguer, A. Company, M.A. Martínez, J. Malina, V. Brabec, L. Feliu, M. Planas, X. Ribas, M. Costas, Inorg. Chem. 54 (2015) 10542–10558.

[90] X. Zhang, X. Liu, D. L. Philips, C. Zhao, Dalton Trans, 45 (2016) 1593-1603.

[91] R. Savio, S. Volpi, R. Cacciapaglia, A. Casnati, L. Mandolini, F. Sansone J. Org. Chem. 80 (2015) 5887-5893.

[92] R. Savio, S. Volpi, R. Cacciapaglia, F. Sansone, L. Mandolini, A. Casnati J. Org. Chem. 81 (2016) 4728-4735.

[93] O. Iranzo, A. Y. Kovalevsky, J.R. Morrow, J.P. Richard, J. Am. Chem. Soc. 125 (2003) 1988-1993.

[94] C.S. Rossiter, R.A. Mathews, J.R. Morrow, Inorg. Chem., 25 (2005) 9397-9404.

[95] C.S. Rossiter, R.A. Mathews, J.R. Morrow, J.P. Richard, Dalton Trans. 2007, 3804-3811.

[96] X. Sheng, X.-M. Lu, J.-J. Zhang, Y.-T. Chen, G.-Y. Lu, Y. Shao, F. Liu, Q. Xu J. Org. Chem. 72 (2007) 1799-1802.

[97] D. Wanhon, A.-M. Lebuis, J. Chin, Angew Chem Int Ed Engl. 34 (1995) 2412-2414.

[98] N.H. Williams, W. Cheung, J. Chin, J. Am. Chem. Soc. 120 (1998) 8079-8087.

[99] N.H. Williams, A.-M. Lebuis, J. Chin, J. Am. Chem. Soc., 121 (1999) 3341-3348.

[100] M. J. Young, J. Chin, J. Am. Chem. Soc. 117 (1995) 10577-10578.

[101] K.P. McCue, D.A. Voss, Jr., C. Marks, J.R. Morrow, J. Chem. Soc., Dalton Trans. (1998) 2961-2963.

[102] K.P. McCue, J.R. Morrow, Inorg. Chem., 38 (1999) 6136-6142.

[103] L.J. Farrugia, P.A. Lovatt, R.D. Peacok, J. Chem. Soc., Dalton Trans. (1997) 911-912.

[104] F.H. Fry, L. Spiccia, P. Jensen, B. Moubaraki, K.S. Murray, E.R.T. Tiekink, Inorg Chem 42 (2003) 5594-5693.

[105] J. Qian, W. Gu, H. Liu, F. Gao, L. Feng, S. Yan, D. Liao, P. Cheng. Dalton Trans. (2007) 1060-1067.

[106] D. Montagner, V. Gandin, C. Marzano, A. Erxleben, J. Inorg. Biochem. 145 (2015) 101-107.

[107] M. Arca, A. Bencini, E. Berni, C. Caltagirone, F.A. Devillanova, F, Isaia, A. Garau, C. Giorgi, V. Lippolis, A. Perra, L. Tei, B. Valtancoli, Inorg. Chem. 42 (2003) 6929-6939.

[108] X. Sheng, X. Guo, X.-M. Lu, Y. Shao, F. Liu, Q. Xu, Bioconjugate Chem., 19 (2009) 490-498.

[109] P. Rossi, F. Felluga, P. Tecilla, F. Formaggio, M. Crisma, C. Tomiolo, P. Scrimin J. Am. Chem. Soc. 121 (1999) 6948-6949.

[110] C. Sissi, P. Rossi, F. Felluga, F. Formaggio, M. Palumbo, P. Tecilla, C. Toniolo, P. Scrimin, J. Am. Chem. Soc., 123 (2001) 3169–3170.

[111] J.P. Richard, J.R. Morrow, Chem. Commun. 2003, 22832-2833.

[112] O. Iranzo, T. Elmer, J.P. Richard, J.R. Morrow, Inorg. Chem., 42 (2003) 7737-7746.

[113] O. Iranzo, J.P. Richard, J.R. Morrow, Inorg. Chem., 43 (2004) 1743-1750.

[114] T. Humphry, S. Iuer, O. Iranzo, J.R. Morrow, J.P. Richard, P. Paneth, A.C. Hengge, J. Am. Chem. Soc. 130 (2008) 17858-17866.

[115] M.-Y. Yang, O. Iranzo, J.P. Richard, J.R. Morrow, J. Am. Chem. Soc. 125 (2005) 1064-1065.

[116] H. Gao, Z. Ke, N.J. DeYonker, J. Wang, H. Xu, Z.-W. Mao, D.L. Lee, C. Zhao, J. Am. Chem. Soc. 133 (2011) 2904-2915.

[117] R. Cao, P. Muller, S. J. Lippard, J. Am. Chem. Soc. 132 (2010) 17366-17369.

[118] A. Scarso, U. Scheffer, M. Göbel, Q.B. Broxterman, B. Kaptein, F. Formaggio, C. Toniolo, P. Scrimin, Proc. Natl. Acad. Sci. 99 (2002) 5144-5149.

[119] A. Scarso, G. Zaupa, F.D. Houillon. L.J. Prins, P. Scrimin, J. Org. Chem. 72 (2007) 376-385.

[120] P. Rossi, P. Tecilla, L. Nalzer, P. Scrimin, Chem. Eur. J., 10 (2004) 4163-4170.

[121] M.J. Hostetler, S.J. Green, J.J. Stokes, R.W. Murray, J. Am. Chem. Soc. 118 (1996) 4212– 4213.

[122] F. Manea, F.B. Houillon, L. Pasquato, P. Scrimin, Angew. Chem., Int. Ed. Eng. 43 (2004) 6165– 6169.

[123] M. Diez-Castellnou, F. Mancin, P. Scrimin, J. Am. Chem. Soc. 136 (2014) 1158-1161.

[124] J.L.-Y. Chen, C. Pezzato, P. Scrimin, L.P. Prins, Chem. Eur. J. 22 (2016) 7028-7032.

[125] M. Martin, F. Manea, R. Fiammengo, L.J. Prins, L. Pasquato, P. Scrimin, J. Am. Chem. Soc. 129 (2007) 6982-6983.

[126] G. Zaupa, L. J. Prins, P. Scrimin, J. Am. Chem. Soc., 130 (2008) 5699-5709.

[127] G. Zaupa, LJ. Prins, P. Scrimin, Bioorg. Med. Chem. Lett. 19 (2009) 3816-3820.

[128] C.M. Hartshorn, J.R. Deschamps, A. Singh, E.L. Chang, React. Funct. Polym., 55 (2003) 219-229.

[129] G.M. Bonora, S. Drioli, F. Felluga, F. Mancin, P. Rossi, P. Scrimin, P. Tecilla, Tetrahedron Lett. 44 (2003) 535-538.

[130] B.R. Bodsgard, J.N. Burstyn, Chem. Commun. 2001, 647-648.

[131] B.R. Bodsgard, R.W. Clark, A.W. Ehrbar, J.N. Burstyn, Dalton Trans. 2009, 2365-2373.

[132] A.J. Amoroso, I.A. Fallis, S.J.A. Pope, Coord. Chem. Rev. 340 (2017) 198-219.

[133] A.J. Amoroso, S.J.A. Pope, Chem. Soc. Rev. 44 (2015) 4723-4742.

[134] S.J. Butler, M. Delbianco, L. Lamarque, B.K. McMahon, E.R. Neil, R. Pal, D. Parker, J.W. Walton, J.M. Zwier, Dalton Trans. 44 (2015) 4791-4803.

[135] E.J. New, D. Parker, D.G. Smith, J.W. Walton, Curr. Opinion in Chem. Biol., 14 (2010) 238-246.

[136] S. Shuvaev, M. Starck, D. Parker, Chem. Eur. J. 23 (2017) 9974-9989.

[137] E. Terreno, D.D. Castelli, A. Viale, S. Aime, Chem. Rev. 110 (2010) 3019-3042.

[138] J.M. Zwier, H. Bazin, L. Lamarque, G. Mathis, Inorg. Chem., 53 (2014) 1854-1866.

[139] M. Delbianco, V. Sadovnikova, E. Bourrier, G. Mathis, L. Lamarque, J.M. Zwier, D. Parker, Ang. Chem. Intern. Ed. Engl 53 (2014) 10718-10722.

[140] M. Soulié, F. Latzko, E. Bourrier, V. Placide, S.J. Butler, R. Pal, J.W. Walton, P.L. Baldeck , B. Le Guennic, C. Andraud, J.M. Zwier, L. Lamarque, D. Parker, O. Maury, Chem. Eur. J., 20 (2014) 8636-8646.

[141] J.W. Walton, A. Bourdolle, S.J. Butler, M. Soulie, M. Delbianco, B.K. McMahon, R. Pal, H. Puschmann, J.M. Zwier, L. Lamarque, O. Maury, C. Andraud, D. Parker, Chem. Commun. 49 (2013) 1600-1602.

[142] M. Starck, R. Pal, D. Parker, Chem. Eur. J., 22 (2016) 570-580.

[143] N.H. Evans, R. Carr, M. Delbianco, R. Pal, D.S. Yufit, D. Parker, Dalton Trans. 42 (2013) 15610-15616.

[144] J.W. Walton, R. Carr, N.H. Evans, A.M. Funk, A.M. Kenwright, D. Parker, D.S. Yufit, M. Botta, S. De Pinto, K.L. Wong, Inorg. Chem. 51 (2012) 8042-8056.

[145] E.R. Neil, M.A. Fox, R. Pal, D.S. Yufit, D. Parker, Dalton Trans., 43 (2014) 5490-5504.

[146] E.R. Neil, M.A. Fox, R. Pal, L.O. Pålsson, B.A. O'Sullivan, D. Parker, Dalton Trans. 44 (2015) 14937-14951.

[147] A.T. Frawley, R. Pal, D. Parker, Chem. Commun. 52 (2016) 13349-13352.

[148] H. Nakai, K. Kitagawa, J. Seo, T. Matsumoto, S. Ogo, Dalton Trans., 45 (2016) 11620-11623.

[149] A.T. Bui, A. Grichine, S. Brasselet, A. Duperray, C. Andraud, O. Maury, Chem. Eur. J., 21 (2015) 17757-17761.

[150] A.T. Bui, A. Grichine, A. Duperray, P. Lidon, F. Riobé, C. Andraud, O. Maury, J. Am. Chem. Soc. 139 (2017) 7693-7696.

[151] T.I. Kostelnik, C. Orvig, Chem. Rev. 119 (2019) 902-956.

[152] E.W. Price, C. Orvig, Chem. Soc. Rev. 43 (2014) 260-290.

[153] C.F. Ramogida, C. Orvig, Chem. Commun., 49 (2013) 4720-4739.

[154] J. Notni, J. Šimeček, P. Hermann and H.J. Wester, Chem. Eur. J. 17 (2011) 14718-14722.

[155] J. Šimeček, H.J. Wester, J. Notni, Dalton Trans. 41 (2012) 13803-13806.

[156] D. Reich, A. Wurzer, M. Wirtz, V. Stiegler, P. Spatz, J. Pollmann, H.J. Wester, J. Notni, Chem. Commun. 52 (2017) 2586-2589.

[157] K. Pant, D. Gröger, R. Bergmann, J. Pietzsch, J. Steinbach, B. Graham, L. Spiccia, F. Berthon, B. Czarny, L. Devel, V. Dive, H. Stephan, R. Haag, Biocon. Chem. 26 (2015) 906-918.

[158] J. Guo, H. Hong, G. Chen, S. Shi, T.R. Nayak, C.P. Theuer, T.E. Barnhart, W. Cai, S. Gong, ACS Ap. Mat. Interf., 6 (2014) 21769-21779.

[159] J. Guo, H. Hong, G. Chen, S. Shi, Q. Zheng, Y. Zhang, C.P. Theuer, T.E. Barnhart, W. Cai, S. Gong, Biomat. 34 (2013) 8323-8332.

[160] Y. Xiao, H. Hong, A. Javadi, J.W. Engle, W. Xu, Y. Yang, Y. Zhang, T.E. Barnhart, W. Cai, S. Gong, Biomat. 33 (2012) 3071-3082.

[161] H. Hong, K. Yang, Y. Zhang, J.W. Engle, L. Feng, Y. Yang, T.R. Nayak, S. Goel, J. Bean, C.P. Theuer, T.E. Barnhart, Z. Liu, W. Cai, ACS Nano 6 (2012) 2361-2370.

[162] H. Hong, Y. Zhang, J.W. Engle, T.R. Nayak, C.P. Theuer, R.J. Nickles, T.E. Barnhart, W. Cai, Biomat. 33 (2012) 4147-4156.

[163] S. Shi, C. Xu, K. Yang, S. \Goel, H.F. Valdovinos, H. Luo, E.B. Ehlerding, C.G. England, L. Cheng, F. Chen, R.J. Nickles, Z. Liu, W. Cai, Ang. Chem. Int. Ed. 56 (2017) 2889-2892.

[164] F. Chen, H. Hong, Y. Zhang, H.F. Valdovinos, S. Shi, G.S. Kwon, C.P. Theuer, T.E. Barnhart, W. Cai, ACS Nano 7 (2013) 9027-9039.

[165] M.A. Wuillemin, W.T. Stuber, T. Fox, M.J. Reber, D. Brühwiler, R. Alberto, H. Braband, Dalton Trans. 43 (2014) 4260-4263.

[166] X. Yang, H. Hong, J.J. Grailer, I.J. Rowland, A. Javadi, S.A. Hurley, Y. Xiao, Y. Yang, Y. Zhang, R.J. Nickles, W. Cai, D.A. Steeber, S. Gong, Biomat. 32 (2011) 4151-4160.

[167] J.A. Barreto, M. Matterna, B. Graham, H. Stephan, L. Spiccia, New J. Chem., 35 (2011) 2705-2712.

[168] K. Pombo-García, K. Zarschler, J.A. Barreto, J. Hesse, L. Spiccia, B. Graham, H. Stephan, RSC Adv. 3 (2013) 22443-22454.

[169] H.S. Chong, H.A. Song, C.S. Kang, T. Le, X. Sun, M. Dadwal, H. Lee, X. Lan, Y. Chen, A. Dai, Chem. Commun. 47 (2011) 5584-5586.

[170] C.S. Kang, X. Sun, F. Jia, H.A. Song, Y. Chen, M. Lewis and H.S. Chong, Biocon. Chem. 23 (2012) 1775-1782.

[171] K.S. Pedersen, G. Lorusso, J.J. Morales, T. Weyhermüller, S. Piligkos, S.K. Singh, D. Larsen, M. Schau-Magnussen, G. Rajaraman, M. Evangelisti, J. Bendix, Ang. Chem. Int. Ed. 53 (2014) 2394-2397.

[172] P.B. Tsitovich, J.M. Cox, J.B. Benedict, J.R. Morrow, Inorg. Chem. 55 (2016) 700-716.

[173] A.E. Thorarinsdottir, A.I. Gaudette, T.D. Harris, Chem. Sci. 8 (2017) 2448-2456.

[174] M. Ren, C.D.S. Brites, S.S. Bao, R.A.S. Ferreira, L.M. Zheng, L.D. Carlos, J. Mat. Chem. C 3 (2015) 8480-8484.

[175] P.B. Tsitovich, A.M. Kosswattaarachchi, M.R. Crawley, T.Y. Tittiris, T.R. Cook, J.R. Morrow, Chem. Eur. J. 23 (2017) 15327-15331.

[176] J.H. Enemark, R.D. Feltham, Coord. Chem. Rev. 13 (1974) 339-406.

[177] N. Levin, N.O. Codesido, E. Bill, T. Weyhermüller, A.P. Segantin Gaspari, R.S. Da Silva, J.A. Olabe, L.D. Slep, Inorg. Chem. 55 (2016) 7808-7810.

[178] N. Levin, J. Perdoménico, E. Bill, T. Weyhermüller, L.D. Slep, Dalton Trans. 46 (2017) 16058-16064.

[179] W.J. Yi, X.C. Yu, B. Wang, J. Zhang, Q.Y. Yu, X.D. Zhou, X.Q. Yu, Chem. Commun. 50 (2014) 6454-6457.

[180] S. Maiti, I. Fortunati, A. Sen, L.J. Prins, Chem. Commun. 54 (2018) 4818-4821.

[181] S. Garcia Martin, L.J. Prins, Chem. Commun. 52 (2016) 9387-9390.

[182] H. Feuchter, G. Ortiz, Y. Rousselin, A. Bessmertnykh-Lemeune, S. Brandés, Cryst. Growth Des., 17 (2017) 3665-3676